8. SITE 739[1]

Shipboard Scientific Party[2]

HOLE 739A

Date occupied: 18 January 1988

Date departed: 18 January 1988

Time on hole: 7 hr

Position: 67°16.57′S, 75°04.91′E

Bottom felt (rig floor; m, drill-pipe measurement): 422.9

Distance between rig floor and sea level (m): 10.5

Water depth (drill-pipe measurement from sea level, m): 412.4

Total depth (rig floor, m): 428.5

Penetration (m): 5.6

Number of cores: 2

Total length of cored section (m): 5.6

Total core recovered (m): 5.73

Core recovery (%): 102

Oldest sediment core:
Depth sub-bottom (m): 5.6
Nature: sand-silt-clay
Earliest age: Quaternary
Measured velocity (km/s): 2.263

HOLE 739B

Date occupied: 18 January 1988

Date departed: 19 January 1988

Time on hole: 7 hr, 15 min

Position: 67°16.57′S, 75°04.91′E

Bottom felt (rig floor; m, drill-pipe measurement): 422.9

Distance between rig floor and sea level (m): 10.5

Water depth (drill-pipe measurement from sea level, m): 412.4

Total depth (rig floor, m): 430.1

Penetration (m): 7.2

Number of cores: 3

Total length of cored section (m): 7.2

Total core recovered (m): 1.92

Core recovery (%): 26

Oldest sediment core:
Depth sub-bottom (m): 3.10
Nature: clayey silt
Earliest age: Quaternary

HOLE 739C

Date occupied: 19 January 1988

Date departed: 23 January 1988

Time on hole: 4 days, 3 hr

Position: 67°16.57′S, 75°04.91′E

Bottom felt (rig floor; m, drill-pipe measurement): 422.9

Distance between rig floor and sea level (m): 10.5

Water depth (drill-pipe measurement from sea level, m): 412.4

Total depth (rig floor, m): 909.7

Penetration (m): 486.8

Number of cores: 62

Total length of cored section (m): 486.8

Total core recovered (m): 168.5

Core recovery (%): 34

Oldest sediment core:
Depth sub-bottom (m): 486.8
Nature: diamictite
Earliest age: Eocene–early Oligocene
Measured velocity (km/s): 2.164

Principal results: A thick sequence of glacial sediments ranging in age from late Eocene–early Oligocene to Quaternary was drilled on the shelf of East Antarctica in the outer part of Prydz Bay at Site 739 (67°16.57′S, 75°04.91′E) in 412.4 m of water. The drill hole is the first attempt to drill through the glacial sequence in East Antarctica, and the recovery is the first record of late Paleogene ice cover on the shelf. Although early Oligocene glacial sediments have been cored in the western Ross Sea, the onset of glaciation may well have been controlled by the uplift of the Transantarctic Mountains, which form the margin of East Antarctica immediately to the west. Prydz Bay is distant from such influences and, therefore, was expected to reflect the development of the East Antarctic ice sheet proper.

Coring commenced on 18 January 1988 with two unsuccessful attempts using the advanced piston corer (APC) and the extended core barrel (XCB) that each obtained just a few meters of the extremely hard surface layers. A third attempt with rotary drilling eventually penetrated to a depth of 486.8 m below seafloor (mbsf). However, recovery was only about 34%, falling to just a few percent in the upper 106 m. Nonglacial sediments were probably washed away during coring.

The recovered sequence is remarkably uniform, consisting almost exclusively of generally pebbly sandy mudstones (diamictons and diamictites). This succession was divided into five lithologic units. The top unit (0–15 mbsf) consists of a normally consolidated diamicton with diatoms of late Pliocene to Quaternary age. It was possibly highly disturbed by scouring of icebergs. Unit II (15–170 mbsf) is a very hard, compacted diamicton that is totally devoid of structures. This unit comprises a flat-lying sequence forming the banks of the outer shelf. The lower part of Unit II, between 100 and 170 mbsf, contains 1%–2% organic carbon and diatoms that indicate an early Pliocene to late Miocene age. Unit III (170–260 mbsf) consists of stratified diamictite horizons with diatoms. The stratification is commonly contorted, suggesting slumping or limited redeposition of melt-out tills by debris flows down the paleoshelf/paleoslope. At

[1] Barron, J., Larsen, B., et al., 1989. *Proc. ODP, Init. Repts.*, 119: College Station, TX (Ocean Drilling Program).

[2] Shipboard Scientific Party is as given in the list of Participants preceding the contents.

193 mbsf, the unit contains a claystone that is mostly gravel free and has up to 30% diatoms of late Eocene to early Oligocene age. Unit IV (260–313 mbsf) is a massive diamictite with 1%–2% calcium carbonate. Units III and IV comprise the innermost part of a thick prograding sequence that forms the outer part of the Prydz Bay shelf. The lower unit, from 313 mbsf to the bottom of the hole, is a massive, slightly indurated, but still friable, diamictite. The diamictite is mostly unfossiliferous and, as yet, is undated. The entire succession appears to have been deposited mainly by the raining-out of basal debris from a floating ice front, close to the grounding line at the shelf break, of an extended Lambert Glacier.

The diamictite sediments recovered afford poor biostratigraphic control throughout most of the sequence because of the occurrence of thick intervals barren of microfossils, the absence of zonal marker species, and the sporadic occurrence of reworked species. Diatoms are the most persistent of the recovered fossil groups, enabling recognition of the Quaternary down to 17 mbsf, the lower Pliocene between 111 and 127 mbsf, the upper Miocene between 142 and 168 mbsf, and the lower Oligocene between 178 and 318 mbsf. A hiatus probably lies between the lower Oligocene and the upper Miocene interval. The lowermost age determination of Site 739, at 378 mbsf, is from a nannoplankton species with ranges from middle Eocene to Oligocene.

The physical-properties data seem to indicate a thin cover of normally consolidated glacial sediments covering a thick sequence of overconsolidated sediments. The degree of overconsolidation appears to decrease downhole, and the lower 150 to 200 mbsf apparently has experienced no history of excess loading. Cyclic variations in all physical properties appear to be partly a function of lithology and bear evidence of glacial fluctuations with variations in distance to the grounding line.

The result of the glacial activity is a prograding sequence consisting of waterlain tills and glaciomarine sediments seaward of the old shelf break, and much thinner lodgement tills forming the banks on the shelf. Site 739 is the first record of a shelf-marginal succession dominated for a prolonged period of time by a major glacier complex. This may be typical of the greater part of the glacial sedimentation of the continental shelf of Antarctica and other high-latitude shelves.

The main conclusion of the investigation of Site 739 is that a major glacier complex reached Prydz Bay as early as the early Oligocene, with the ice front beyond that of the present day by at least 140 km. This suggests full-scale ice sheet development over East Antarctica in early Oligocene time and possibly earlier. The glacial record extends through the lower Oligocene, upper Miocene to lower Pliocene, possibly the upper Pliocene, and Quaternary. No trace of oil or gas was recorded at the site.

BACKGROUND AND OBJECTIVES

Site 739 (target Site PB6) lies on the shelf of East Antarctica in the central Prydz Bay (67°16.57′S, 75°04.91′E) in 412.4 m of water. The site is approximately 30 km from the shelf edge, 200 km from land, and 140 km from the Amery Ice Shelf. The site area is covered by pack ice for 11 months of the year and very little geological data are available from the area.

The Lambert Glacier, which feeds the Amery Ice Shelf at the head of Prydz Bay, drains 22% of the East Antarctic ice sheet. The glacier follows the line of the Lambert Graben, which extends 700 km inland and probably is of Permian or Early Cretaceous age. The present ice drainage basin is believed to be long-lived because of the structural control. Evidence for the occurrence of thick sequences of sediments in Prydz Bay has been demonstrated by seismic investigations by Stagg (1985) and Mizukoshi et al. (1988). Part of this sequence probably reflects stages of continental-scale glaciations and the preglacial environments on East Antarctica.

The morphology of Prydz Bay (Fig. 1) is similar to other former glaciated shelves, with deep erosional troughs in the inner shelf, from which broad banks decrease in depth toward the outer shelf, and the wide transverse trough from the ice to the shelf break, the Prydz Channel of Quilty (1985). In addition, some of the sparse sediment samples from the area (Udinstev, 1975) suggest a former cover of ice in the bay. Glaciomarine and meltwater sediments possibly mark periods with less extensive ice cover than that of the present. Thus, the glacially influenced sequence in Prydz Bay, in principle, is probably similar to the one sampled in the CIROS-1 drill hole in the western Ross Sea (Barrett et al., in press). The onset of glacial conditions in Prydz Bay would supposedly cause a major shift in the pattern of sedimentation.

Site 739 is on seismic line PB-21 of Stagg (1985; Fig. 2). A clear unconformity lies beneath an approximately 100-m-thick cover of presumed young glacial tills, forming the Four Ladies Bank. Below this cover, a 35–50-km-wide band of inclined reflectors is recognized in all of the seismic lines across the outer part of the shelf. The reflectors are chiefly parallel to the present-day shelf slope. This suggests that the reflectors represent a prograding sequence related to the mouth of the broad "Prydz Channel." This sequence forms the topmost part of a trough mouth fan, as described from other high-latitude shelves by Vorren et al. (1989). As a working hypothesis, we assumed that the innermost part of the prograding unit represented the major shift in sedimentation pattern caused by the first glaciation reaching the paleoshelf edge. The base of the prograding unit seems to be an angular unconformity, because the lower unit is less inclined.

Our objective at Site 739 was to sample and possibly date the upper covering unit, the innermost part of the prograding sequence, and the upper part of the underlying sequence in order to date the onset of glaciation in Prydz Bay. We expected that the sedimentary sequence would show a record of variation in climate and relative sea level. Very high seismic velocities from the seafloor suggest rather hard sediment, probably a compacted glacial till from near the surface. The geographical setting and the character of the seismic trace of the seafloor suggest extensive scouring by icebergs.

SITE GEOPHYSICS

Site Survey

A brief geophysical survey was conducted in the vicinity of Site 739 (Fig. 3). Ocean Drilling Program (ODP) survey line 119-04 was done with standard geophysical gear (see "Explanatory Notes" chapter, this volume) and with Transit satellite and dead-reckoning navigation, because Global Positioning System satellite information was not available. Three crossings of the site were made to augment the Australian Bureau of Mineral Resources six-channel seismic-reflection line (PB-21) that was previously recorded near Site 739.

The first survey line crossed the site area from northeast to southwest, about 45° to the anticipated east-west trend of the nearby, buried paleoshelf edge. A tentative location for Site 739 was selected using this seismic line. The ship then headed due east to the beginning of the third line, which ran northwest and parallel to PB-21. The third line, like the first, showed that the seaward-dipping reflections of the outer shelf areas are part of a prograding sequence rather than part of a local closed structural uplift. The beacon for Site 739 (shotpoint 944) was dropped over the dipping reflections beneath the third seismic line. A final traverse was recorded heading due east across Site 739 to confirm the continuity and flat relative dips of the reflectors along strike.

A sonobuoy was dropped along the final traverse about 1.5 km before crossing the site and was recorded to a total offset of about 6 km. The seismic gear was recovered, and the ship returned to the beacon to commence drilling. The seismic results are discussed in the "Seismic Stratigraphy" section, this chapter.

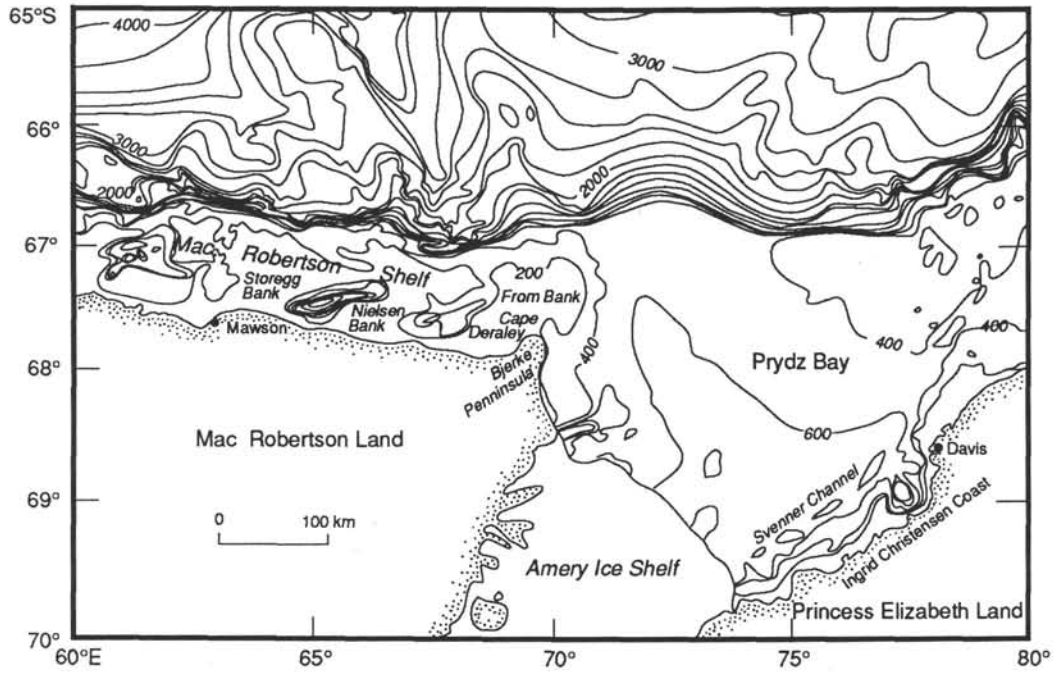

Figure 1. Bathymetry of the Prydz Bay region, after Stagg (1985).

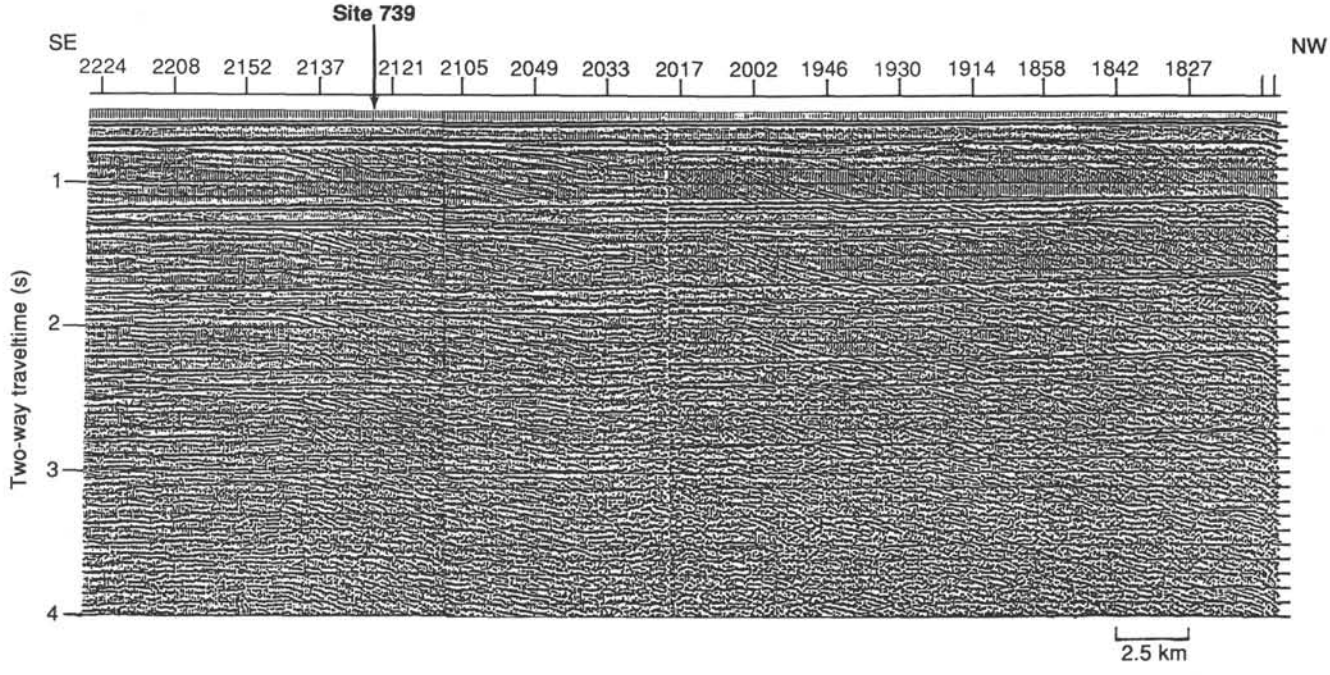

Figure 2. Seismic section across the outer part of the Prydz Bay shelf. The shelf break is at the right margin of the figure. The prograding unit is below the covering unit to the northwest of position 33.2137 (2 km southeast of the site). Seismic section from Stagg (1985).

Sonobuoy Data

The sonobuoy was deployed prior to reaching Site 739 to acquire velocity and stratigraphic data from wide-angle reflection and refraction arrivals through the sedimentary section beneath the site. Similar deployments had provided valuable real-time velocity data at Sites 736 through 738.

The sonobuoy, although successfully deployed, recorded only weak seismic arrivals because of high noise levels in the water column and poor penetration of seismic energy beneath the hard seafloor. High noise levels in the water column were caused by two the ships (*JOIDES Resolution* and service vessel *Maersk Master*) being within 6 km of the sonobuoy and by seismic reverberations from numerous seafloor multiple reflections in the relatively shallow (412.4 m) water. Wide-angle reflections from five horizons and refraction arrivals from the tops of three layers were identified on the sonobuoy record. Wide-angle reflections for horizons AA to DD can be clearly identified to hori-

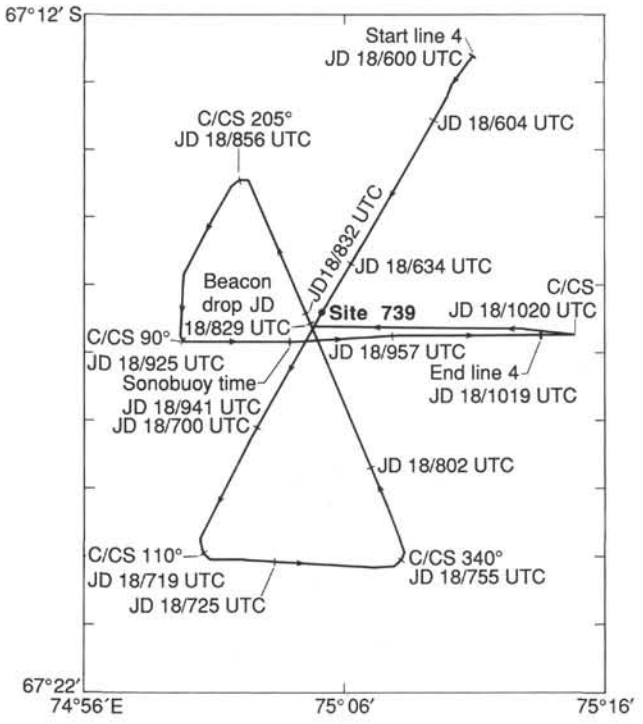

Figure 3. Index map of seismic lines recorded during site survey for Site 739.

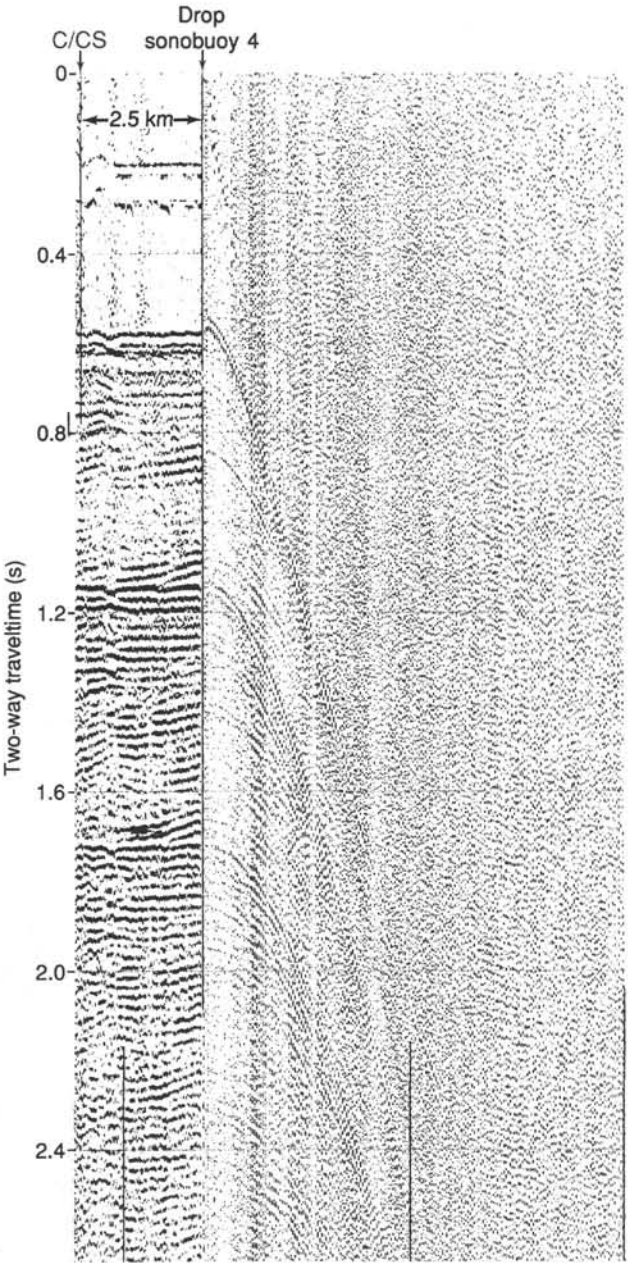

Figure 4. Vertical-incident seismic and sonobuoy seismic record for sonobuoy station 4. Site 739 is about 1.5 km east of where the sonobuoy was deployed. See Figure 3 for location.

zontal offsets of 1.3–1.7 km, where they are either overprinted by strong refraction arrivals or terminate (Figs. 4 and 5). Minor corrections (−46 m/s) were added to rms and refraction velocities to correct for a questionable direct arrival (*D*-wave; see sonobuoy error discussion in the "Underway Geophysics" chapter, this volume). The sonobuoy interval velocities and refraction velocities are given in Table 1.

The sonobuoy results indicate that rocks with high interval and refraction velocities (1.77–2.05 km/s) lie directly beneath the seafloor within a 124-m-thick layer above reflector BB (Fig. 6). Downhole logs ("Logging" section, this chapter) indicate that these rocks have *in-situ* velocities of about 2.05 km/s and are 110 m thick. Strata between horizons BB and DD (124–603 mbsf; Fig. 4) lie within the seaward prograding sequence and, along the sonobuoy line, have apparent interval velocities of 2.28–2.57 km/s. Refraction velocities are 2.12 km/s within layer BB-CC (124–307 mbsf) and 2.82 km/s within layer DD-EE (603–844 mbsf).

The apparent velocity inversion from 2.57 to 2.30 km/s at horizon DD may be due in part to uncorrected effects of dip for horizon DD and to the thinning (about 70 m over 1.5 km) of the sedimentary section directly above DD. The inversion would be smaller or nonexistent after these corrections. Horizon EE is a strong reflector at large horizontal ranges (up to 5.5 km); however, EE cannot be traced in the vertical-incident seismic profiles because EE lies within the seafloor multiple. The apparent dip of EE cannot be determined.

Refraction arrivals for horizon AA and within horizon BB-CC are linear over offset ranges of 1.5 to 2.7 km, after which they merge with a weak, curved refraction arrival seemingly associated with a layer between DD and EE. The distinct linear refraction arrivals indicate that velocities increase abruptly. Curved arrivals imply that velocities increase gradually with increasing depth. A refraction is not seen breaking away from horizon EE which suggests either that velocities do not increase abruptly at EE or that velocities decrease at EE.

In summary, the sedimentary section at Site 739 is characterized by highly indurated sediment with high refraction velocities (2.05–2.82 km/s) and interval velocities (1.77–2.57 km/s) within 844 m of the seafloor. Comparison of these preliminary sonobuoy interval velocities with downhole measurements indicate agreement within 5%–15% (compare with Fig. 29, "Logging" section). Refraction velocities are consistent with downhole measurements. Strong linear refractions in the upper 300 mbsf indicate distinct layers (highly compacted diamictite), whereas moderate to weak curved refractions at greater depth suggest a normal increase in velocity with depth (diamictons with a different lithology or compaction history).

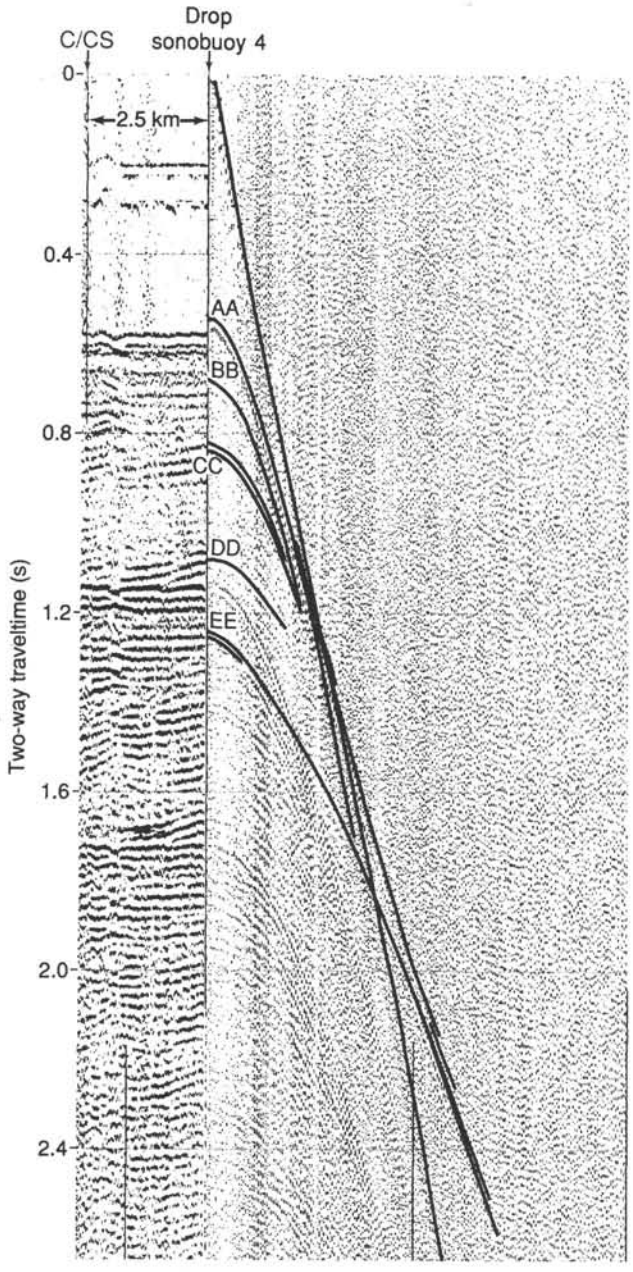

Figure 5. Vertical-incident seismic and sonobuoy seismic record for Site 739 showing wide-angle reflection and refraction interpretations. Letters denote layers given in Table 1. See Figure 3 for location.

OPERATIONS

The transit to Site 739 began shortly after we were notified that the contract term for *Maersk Master*, and thus the drillship's tenure in ice country, had been shortened because of funding limitations. Satellite ice maps and reports from Davis Station were encouraging, but not any more than those from 10 days earlier. *Maersk Master* had been sent ahead at full speed as soon as ice conditions at Site 738 permitted. She had instructions to scout for a route through or around the expected pack ice and to determine which of the proposed Prydz Bay operating areas was sufficiently clear for drilling. Reports from the lead vessel were increasingly encouraging, as she radioed ice-free conditions from 150 nmi ahead. Finally, *Maersk Master* reported from the first (and highest priority) location, target Site PB-6, that the entire area was clear, with only widely scattered bergs. The pack ice present a week earlier had disappeared completely.

The operating area was approached from the northeast, and profiling began about 4 nmi before the proposed drill site.

Table 1. Preliminary results for sonobuoy 4, Site 739.

Horizon[a]	Vrms (km/s)	Vint (km/s)	Ti (s)	Zi (km)	Vrfr (km/s)	To (s)
AA	1.450	1.77	0.57	0.412	2.05	0.399
BB	1.519	2.28	0.71	0.536	2.12	[c]0.446
CC	1.686	2.57	0.87	0.719	nr	—
DD	1.906	2.30	1.10	1.015	nr	—
EE	1.974	—	[b]1.31	1.256	2.82	[c]0.869

Note: Vrms = rms velocity for horizon; Vint = interval velocity computed using Vrms, Ti, and Dix equation (e.g., Vint between horizons AA and BB is 1.77 km/s); Ti = vertical incidence reflection time (two-way) to horizon; Zi = total depth from sea level to horizon computed from Vint and Ti (water depth = 412 m); Vrfr = refraction velocity associated with horizon (e.g., Vrfr at top of horizon EE is 3.21 km/s); To = intercept time for refractor associated with horizon; nr = no refractor observed.

[a] Letters of horizons do not correlate between drill sites and do not correspond to prior stratigraphic analyses.

[b] Time determined from time-squared vs. distance-squared graph.

[c] These refractions appear to be from layers within BB-CC and DD-EE.

Site 739—Outer Prydz Bay

Hole 739A

The precision depth recorder registered a water depth of only 421 m, and the initial pipe trip consisted primarily of the bottom-hole assembly (BHA) and top drive. The APC assembly was deployed, and a seafloor piston core was taken. Full-stroke indication was obtained, and a 4.6-m core of sticky gray clay was recovered (Table 2). The core liner was shattered, however, and the material in the core catcher was quite firm. Core 119-739A-2H attempted to deepen the hole with the APC, but only 1 m of core was recovered, and the cutter shoe was found to be bent. Because Prydz Bay is a glacial area, boulders and dropstones were expected. The indications of hard material prompted the decision to move over 20 m and start a new hole.

Hole 739B

The second APC spud-in attempt fared worse than the first, with an incomplete stroke that shook the drillship. Surprisingly, the core barrel was recovered intact with the shoe undamaged. Recovery was only 1.9 m of clay in another shattered core liner. The underlying material was obviously too hard for the APC, and because we still thought that it was boulders or gravel, the coring mode was switched to the XCB system. Core 119-739B-2X encountered hard drilling at the bottom of the APC interval, and penetration came to a near halt. With only a few meters of the outer core barrel supported by clay, only 3000 to 4000 lb could be applied to the bit with slow rotation. Two short cores were attempted, representing 5.3 m of steady penetration in 3 hr of rotation. Total recovery was 2 cm of sandy clay. The XCB cutting shoe showed considerable wear after the second core. Although the still-unidentified material could be drilled, it apparently did not consist of discrete rocks and was too hard for the XCB. A round trip was made for the rotary core barrel (RCB) BHA.

Hole 739C

The ship was offset again, this time 10 m in the opposite direction from the beacon and only 20 m from the original Hole 739A spud-in. Surprisingly, about 13 m of relatively soft mate-

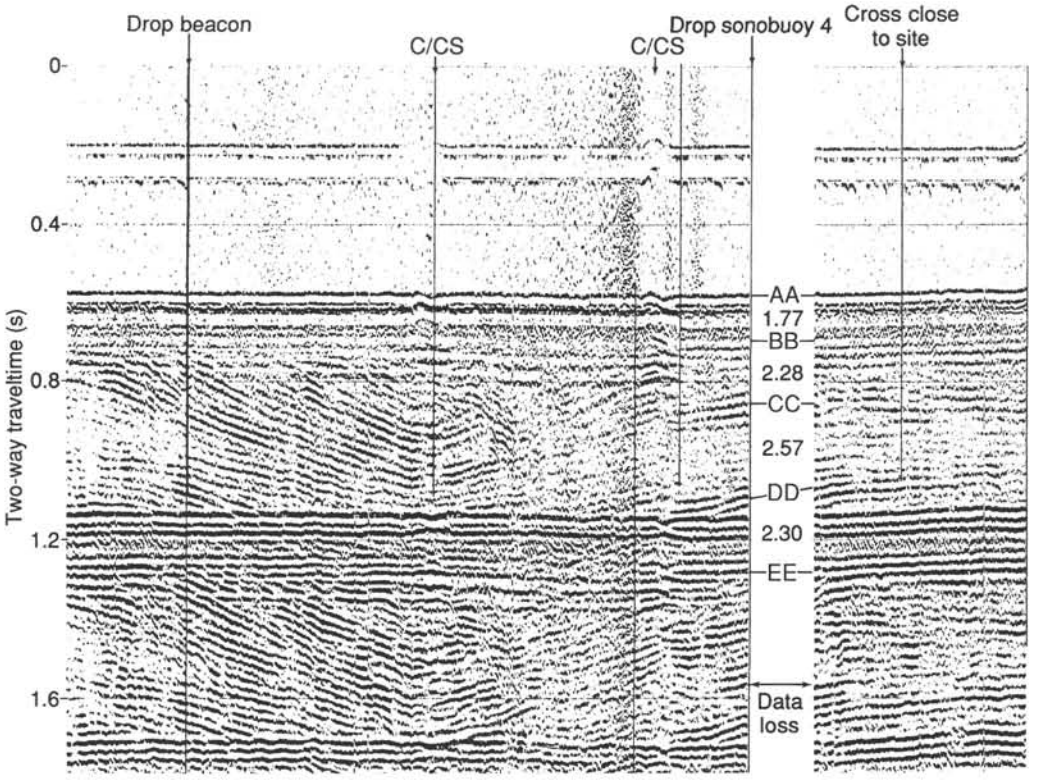

Figure 6. Vertical-incident seismic profile across Site 739 showing depths derived from sonobuoy interval velocities to reflection horizons.

rial was penetrated before hard drilling was encountered. Only about 1.3 m of clay and till was recovered from the interval. The hard substrate again drilled evenly but very slowly with the available bit weight. Finally, in Core 119-739C-4R, from 24–28 mbsf, the mystery material was recovered and identified as diamictite, glacially derived sediment that has been highly overcompacted by the weight of a continental glacier/ice shelf. The sediment was so hard that it required cutting with the diamond saw in the laboratory.

The rate of penetration increased with depth as more drill-collar weight could be laterally supported and applied to the formation at the bit. The degree of compaction of the sediment also decreased with depth, and the material was easier to drill. Core recovery remained low, apparently because numerous cobbles and boulders of hard igneous and metamorphic rock jammed the core catchers and the throat of the bit and also seemed to roll under the bit, thereby destroying the core before it could be formed. To increase core recovery, the core interval was reduced to half the usual 9.7-m length. Recovery was enhanced and, because of the minimal wireline time in the shallow water, the cost in operating time was small.

Core recovery returned to near normal by 200 mbsf, and the operation returned to full core intervals. The glacial material persisted, however, with its abrasive sand, pebbles, and cobbles. Core recovery again fell off below 300 mbsf and continued a decreasing trend with depth that was not materially improved by returning to half cores. The core catchers jammed repeatedly, even with high circulation rates, and increased "biscuiting" was noted in the core that was recovered. Obstruction of the core-bit throat was suspected, and the bit deplugger was used (without success). The abrasive formation apparently had worn the bit cones to the point where they were trimming core that was too large to pass through the bit throat and core catcher.

Coring was discontinued at 487 mbsf when icebergs approached and, for the second time on Site 739, forced a "short" trip to just below the seafloor. With poor core recovery and little prospect of reaching the desired marine sediments within the 500-m penetration limit imposed by the JOIDES Safety Panel, there was little justification for spending additional operating time at Site 739.

When *Maersk Master* had cleared the iceberg threat, the bit was run back to total depth, the hole was filled with special mud, and the bit was released for logging. Because of the extraordinarily firm near-surface sediment, the end of the pipe was pulled to just 54 mbsf. A seismic stratigraphic log of excellent quality was then recorded from apparent fill at about 14 m above total depth to 25 mbsf (with the pipe raised in the derrick).

The drill string was then run back into the hole, and the hole was plugged with cement. All pipe was recovered by 0545 hr, 23 January, and *JOIDES Resolution* again proceeded southward.

LITHOSTRATIGRAPHY AND SEDIMENTOLOGY

The succession at Site 739 has been divided into five lithologic units, ranging in age from late Eocene or early Oligocene to Quaternary, with a possible major hiatus from early Oligocene to late Miocene time (Table 3). However, recovery was poor, and several major lithologic changes evidenced from logging are not represented in the cores. The upper Unit I (0–24.1 mbsf) consists of a normally consolidated diamicton (gravelly sandy silty clay; see "Explanatory Notes" chapter concerning terminology) with up to 30% diatoms of late Pliocene to Quaternary age. Unit II (24.1–173.6 mbsf) is an indurated diamictite, totally devoid of structures, with diatoms at a few levels, and is of late Miocene to early Pliocene age. Unit III (173.6–267.2 mbsf) in-

Table 2. Coring summary, Site 739.

Core no.	Date (Jan. 1988)	Time	Depth top (mbsf)	Depth bottom (mbsf)	Length cored (m)	Length recovered (m)	Recovery (%)
119-739A-							
1H	18	1820	0.0	4.6	4.6	4.65	101.0
2H	18	1845	4.6	5.6	1.0	1.08	108.0
					5.6	5.73	
119-739B-							
1H	18	2005	0.0	1.9	1.9	1.90	100.0
2X	18	2130	1.9	3.1	1.2	0.02	1.7
3X	19	0045	3.1	7.2	4.1	0.00	0.0
					7.2	1.92	
119-739C-							
1R	19	0555	0.0	9.5	9.5	1.20	12.6
2R	19	0955	9.5	19.0	9.5	0.06	0.6
3R	19	1135	19.0	24.1	5.1	0.02	0.4
4R	19	1410	24.1	28.7	4.6	5.03	109.0
5R	19	1800	28.7	38.3	9.6	3.51	36.5
6R	19	2010	38.3	48.0	9.7	0.00	0.0
7R	19	2245	48.0	57.6	9.6	0.02	0.2
8R	20	0100	57.6	67.3	9.7	0.05	0.5
9R	20	0310	67.3	76.9	9.6	0.31	3.2
10R	20	0415	76.9	86.6	9.7	0.10	1.0
11R	20	0600	86.6	96.3	9.7	0.06	0.6
12R	20	0705	96.3	105.9	9.6	0.08	0.8
13R	20	0815	105.9	115.5	9.6	1.74	18.1
14R	20	1030	115.5	125.2	9.7	4.49	46.3
15R	20	1200	125.2	130.3	5.1	1.50	29.4
16R	20	1335	130.3	135.0	4.7	4.43	94.2
17R	20	1500	135.0	140.0	5.0	5.13	102.6
18R	20	1600	140.0	144.7	4.7	3.49	74.2
19R	20	1700	144.7	149.7	5.0	3.82	76.4
20R	20	1800	149.7	154.3	4.6	3.42	74.3
21R	20	1945	154.3	159.3	5.0	4.40	88.0
22R	20	2050	159.3	164.0	4.7	5.04	107.0
23R	20	2250	164.0	169.0	5.0	3.12	62.4
24R	21	0300	169.0	173.6	4.6	0.16	3.5
25R	21	0410	173.6	183.2	9.6	1.35	14.0
26R	21	0455	183.2	192.9	9.7	4.84	49.9
27R	21	0540	192.9	202.5	9.6	0.95	9.9
28R	21	0640	202.5	212.2	9.7	7.06	72.8
29R	21	0730	212.2	221.8	9.6	7.37	76.8
30R	21	0815	221.8	231.4	9.6	8.44	87.9
31R	21	0850	231.4	241.1	9.7	6.60	68.0
32R	21	0915	241.1	250.7	9.6	1.15	12.0
33R	21	0950	250.7	260.4	9.7	8.60	88.6
34R	21	1020	260.4	270.0	9.6	7.03	73.2
35R	21	1045	270.0	279.7	9.7	5.41	55.8
36R	21	1125	279.7	289.3	9.6	7.60	79.1
37R	21	1200	289.3	298.9	9.6	1.04	10.8
38R	21	1240	298.9	308.6	9.7	4.83	49.8
39R	21	1320	308.6	318.2	9.6	5.01	52.2
40R	21	1400	318.2	327.8	9.6	1.67	17.4
41R	21	1505	327.8	337.5	9.7	4.81	49.6
42R	21	1545	337.5	347.1	9.6	3.02	31.4
43R	21	1625	347.1	356.8	9.7	1.76	18.1
44R	21	1705	356.8	366.5	9.7	2.95	30.4
45R	21	1735	366.5	376.2	9.7	0.26	2.7
46R	21	1820	376.2	385.9	9.7	2.23	23.0
47R	21	1910	385.9	395.6	9.7	0.98	10.1
48R	21	2000	395.6	405.2	9.6	2.49	25.9
49R	21	2100	405.2	414.9	9.7	0.06	0.6
50R	21	2220	414.9	424.5	9.6	2.13	22.2
51R	21	2330	424.5	434.2	9.7	2.23	23.0
52R	22	0005	434.2	439.2	5.0	2.39	47.8
53R	22	0040	439.2	443.9	4.7	1.54	32.7
54R	22	0115	443.9	448.9	5.0	1.90	38.0
55R	22	0155	448.9	453.5	4.6	2.18	47.4
56R	22	0235	453.5	458.5	5.0	0.95	19.0
57R	22	0305	458.5	463.2	4.7	0.99	21.0
58R	22	0355	463.2	468.2	5.0	3.13	62.6
59R	22	0455	468.2	472.9	4.7	0.76	16.2
60R	22	0610	472.9	477.9	5.0	1.46	29.2
61R	22	0800	477.9	482.6	4.7	0.02	0.4
62R	22	1015	482.6	486.8	4.2	0.13	3.1
					486.8	168.50	

cludes two stratified diamictite horizons (Subunits IIIA and IIIC) with diatoms, separated by a mainly gravel-free diatomaceous sandy silty claystone (Subunit IIIB); this unit might be of a late Eocene or early Oligocene age. Units IV (267.2–315.7 mbsf) and V (315.7–486.8 mbsf) are massive, slightly indurated but friable diamictites. Unit IV is fossiliferous and has a similar age range to Unit III, but Unit V is mostly unfossiliferous and is as yet undated (Table 3 and Fig. 7).

The entire succession appears to have been deposited close to the grounding line of an extended ancestor of the present-day Lambert Glacier, mainly as a result of raining out of basal debris from the floating ice shelf or glacier tongue. Some slumping and minor debris-flow activity are evident in the more stratified units. The succession is interpreted as a largely prograding sequence at the shelf edge, although the upper part may have been deposited on the shelf itself, as the glacier built the shelf outward. Major hiatuses and unrecovered intervals are probably associated with periods of advance of ice and erosion of sediment.

Smear slide data (Fig. 8) were obtained at least once from most cores, and the sand-silt-clay size fractions, as well as the proportions of minerals and biogenic material, were estimated. Smear slide analysis did not allow the relative proportions of quartz and feldspar to be accurately determined, because many of the feldspar grains were uncleaved or untwinned, angular to subangular in shape, and unweathered. The proportions of quartz and feldspar are therefore best treated in combination. Visual core description provided rough data on the gravel content (Fig. 9). Smear slide analysis does not allow accurate quantification of the sand fraction, which commonly is underestimated. All these data are presented in the "barrel sheets." A few samples were run on a Lasentec Lab-Tec 100 particle-size analyzer, but the sand fraction was again seriously underestimated.

Visual core descriptions also included estimations of gravel shapes, based on sample sizes that range from about 25 to 50 clasts. At two levels in Unit II and one level in Unit III, horizontal "slices" were examined for grain orientation fabrics. Both grain shape and orientation studies can facilitate the interpretation of the mode of origin of the diamictites; however, no true directional component was obtainable.

Calcium carbonate and organic carbon determinations were also made aboard ship using a chemical titration method (by coulometer, see "Organic Geochemistry" section, this chapter).

Drilling Disturbance

The varying degree of compaction and clast size in the sediments gave rise to considerable variation in drilling disturbance features. All of the Hole 739C cores were obtained by RCB drilling; the overall drilling recovery statistics are given in the "Operations" section of this chapter.

Unit I, the normally consolidated diamicton, suffered from soupy (flowed) recovery and some downhole contamination of the first section in each core. The highly compacted diamictites of Unit II were relatively undisturbed by coring, but the larger clasts commonly were completely isolated from their matrix. Other clasts are embedded in a drilling paste. Special fracturing that probably exploits pre-existing structural fabrics is very commonly developed in parts of Subunits IIIA and IIIB. Below Core 119-739C-35R, biscuiting becomes common; below Core 119-739C-42R rotary-drilling conical shear features are manifested as thin (5 mm), dark and vague bands with convex-upward, bowed cross sections in the split cores. The grain size in the bands is no different from that in the adjacent sediments.

Most of the missing parts of the core are considered to be sand layers, washed out during coring; boulders in an easily disaggregated matrix also were not recovered, except for fragments (see "Operations" section).

Table 3. Summary of lithostratigraphy at Site 739.

Age	Unit	Depth (mbsf)	Thickness (m)	Core interval	Lithology	Sedimentary structures
Quaternary	I	0–24.1	24.1	739A-1H to -2H 739B-1H to -2X 739C-1R to -3R	Diamicton and pebbly sand-silt-clay with 1%–10% gravel and up to 30% diatoms.	Structures not in evidence because of drilling disturbance. Poor recovery.
				Contact not observed—no recovery interval		
late Miocene–?Quaternary	II	24.1–173.6	149.5	739C-4R to -24R	Massive diamictite; mainly 10%–20% gravel, up to 10% diatoms.	Structureless with only slight variations in gravel content.
				Contact not observed—no recovery interval		
late Eocene–early Oligocene	IIIA	173.6–192.9	16.7	739C-25R to -26R	Stratified diamictite; gravel content mainly 1%–3%, some diatoms.	Diffuse bedding, slickensides on faults, some slumping.
				Contact not observed—no recovery interval		
	IIIB	192.9–198.1	7.8	739C-27R-1 to -27R-CC	Sandy silty claystone; 30% diatoms.	Structures not in evidence; core mostly broken by drilling.
				Contact not observed—no recovery interval		
	IIIC	198.1–267.2	69.1	739C-28R-1 to -34R-3, 84 cm	Stratified diamictite; gravel content mainly 3%–10%.	Wispy bedding, slumps, load structures, rhythmic laminations, burrows, and faulted with slickensides near top.
				Sharp erosional contact		
	IV	267.2–315.7	48.5	739C-34R-3, 84 cm, to -39R-4, 30 cm	Massive diamictite; gravel content mainly 5%–10%; diatoms up to 15%.	Structureless, except for minor laminae highly disrupted by drilling.
				Transitional contact		
?middle Eocene/Oligocene	V	315.7–486.8	171.1	739C-39R-4, 30 cm, to -62R-CC	Massive diamictite with calcareous cement in horizons about 10 cm thick; gravel content mainly 1%–3%; unfossiliferous.	Structureless, badly broken in large part by drilling.

Lithologic Summary

Unit I

Cores 119-739A-1H through 119-739A-2H; depth, 0–5.6 mbsf.
Cores 119-739B-1H through 119-739B-2X; depth, 0–7.2 mbsf.
Cores 119-739C-1R through 119-739C-3R; depth, 0–24.1 mbsf.
Age: Quaternary.

Unit I consists of diamicton and sand-silt-clay with a varying diatom content. The whole unit is unlithified and unstratified, and the components are poorly sorted. The color of the sediment ranges from olive (5Y 5/3) to dark gray (5Y 4/1) and very dark grayish brown (2.5Y 3/2).

The only age obtained for this unit is late Pliocene or younger from Core 119-739C-2R. No data are available for the boundary with Unit II. The diamicton proportion from 0–3 mbsf (Sections 119-739A-1H-1 to 119-739A-1H-2) contains up to 10% gravel; the sand-silt-clay from 5.6 mbsf (Sections 119-739A-1H-3 to 119-739A-2H-CC) contains between about 1% and 2%. The gravel clasts are predominantly subangular, but include all shapes from rounded to angular. They consist mainly of metamorphic rock fragments, including gneisses with amphibole and garnet, biotite gneisses, and garnetiferous mica schists.

The major components, based on smear slide analysis, are quartz (30% to 60%), feldspar (5% to 25%), and clay (10% to 20%). The minerals appear to be in a relatively fresh state. The diatom content of Unit I ranges from 5% to 35%. Radiolarians occur either as traces or range from 3% to 5%. In Section 119-739A-1H-1 the sediment is sprinkled with sparse echinoderm fragments (about 1 mm in diameter).

Unit I is relatively homogeneous. The sediment is soft and sticky, and most of the sections were highly deformed by drilling. Approximately the first 1.5 m (from 0 cm in Section 119-739A-1H-1 to 150 cm in Section 119-739A-1H-3 and from 0 to 150 cm in Section 119-739B-1H-1) of the unit is highly disturbed. From 0 cm in Section 119-739C-1R-1 to 11 cm in Section 119-739C-1R-CC the recovered sediment is soupy and thus, is devoid of any structures. Large boulders were found in the lower part of this unit, and only fragments were recovered in the core catcher. Given the size of some of the fragments, they probably represent a more bouldery diamictite than what was recovered.

The carbonate content in Unit I ranges from 0.1%–0.3%, with 0.35%–0.45% organic carbon ("Organic Geochemistry" section).

Unit II

Sections 119-739C-4R-1 through 119-739C-24R-CC; depth, 24.1–173.6 mbsf.
Age: late Miocene to early Pliocene or younger.

Unit II is characterized by massive, poorly sorted diamictite. Neither the top nor the base of the unit was recovered. The top is taken as the first recovered harder interval. The upper part of the unit (24–106 mbsf) is only poorly recovered (Cores 119-739C-6R to 119-739C-12R). The diamictite is dark colored throughout, with the dominant color codes black (5Y 2.5/1) and very dark gray (5Y 3/1). No sedimentary structures are present in the diamictite, which is compacted, but slightly friable, and not cemented (Fig. 9).

The age determined for this unit is imprecise. Based on diatoms in Cores 119-739C-13R and 119-739C-14R, an early Pliocene age is suggested. Cores 119-739C-4R to 119-739C-12R are either barren or contain sparse species. Diatoms recovered from Cores 119-739C-17R through 119-739C-19R and 119-739C-22R are late Miocene in age.

Although the sediment has a homogeneous appearance throughout the unit, some minor fluctuations in the grain-size distribution are evident. Excluding the gravel content, smear slide analyses indicate that most of the sediment belongs to the sand-silt-clay class. However, some smaller intervals consist of clayey silt or silty clay, each with a minor and fluctuating sand component. The gravel content of the diamictite ranges from 5% to 20%, with an apparent trend to a lower maximum value in the lowermost part of the unit (159–170 mbsf; Cores 119-739C-22R to 119-739C-24R). The majority of the gravel clasts have diameters of about 1 cm, but there are always several larger

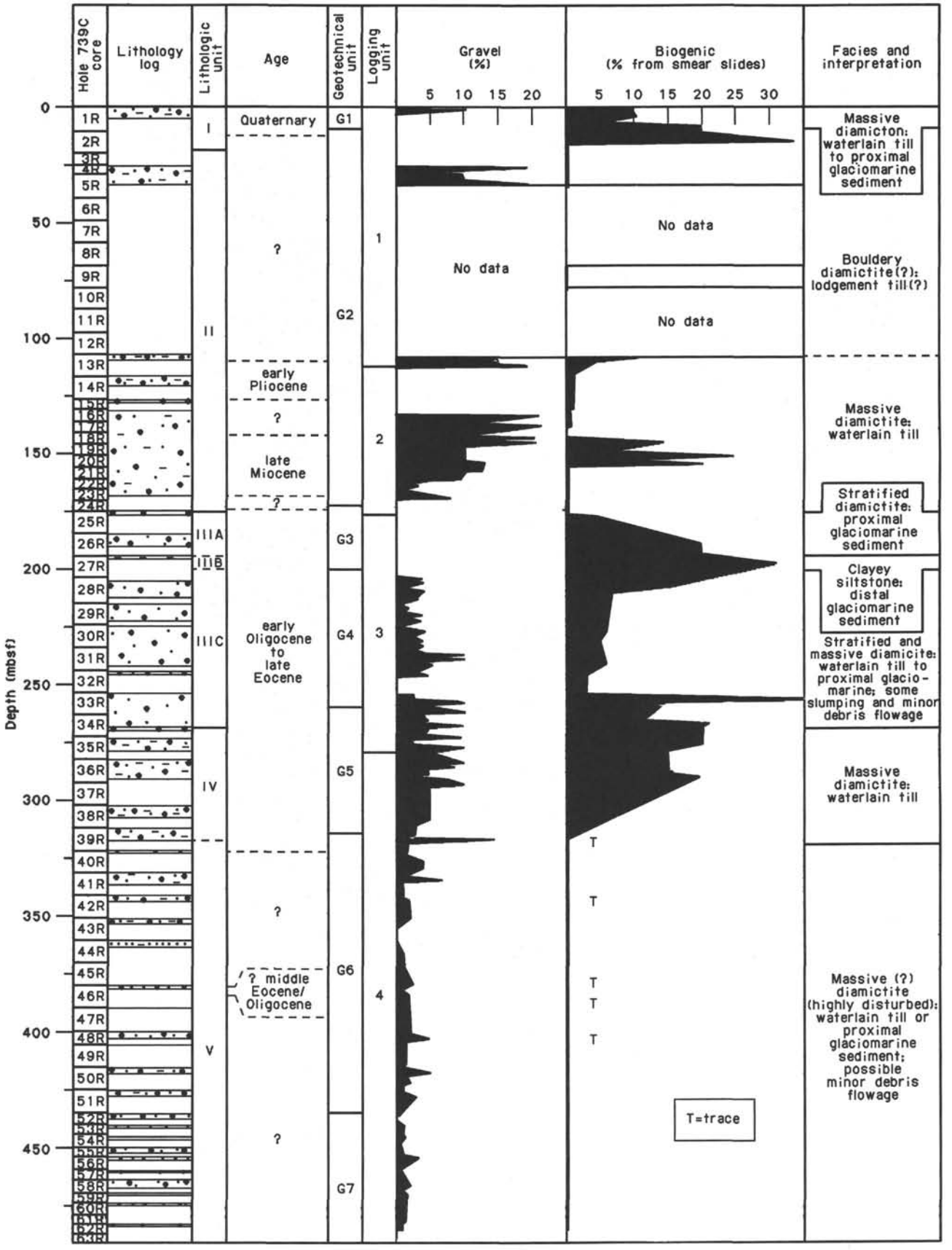

Figure 7. Summary lithologic log of recovered intervals and interpretation. For geotechnical and downhole logging units, see "Physical Properties" and "Logging" sections, respectively (this chapter).

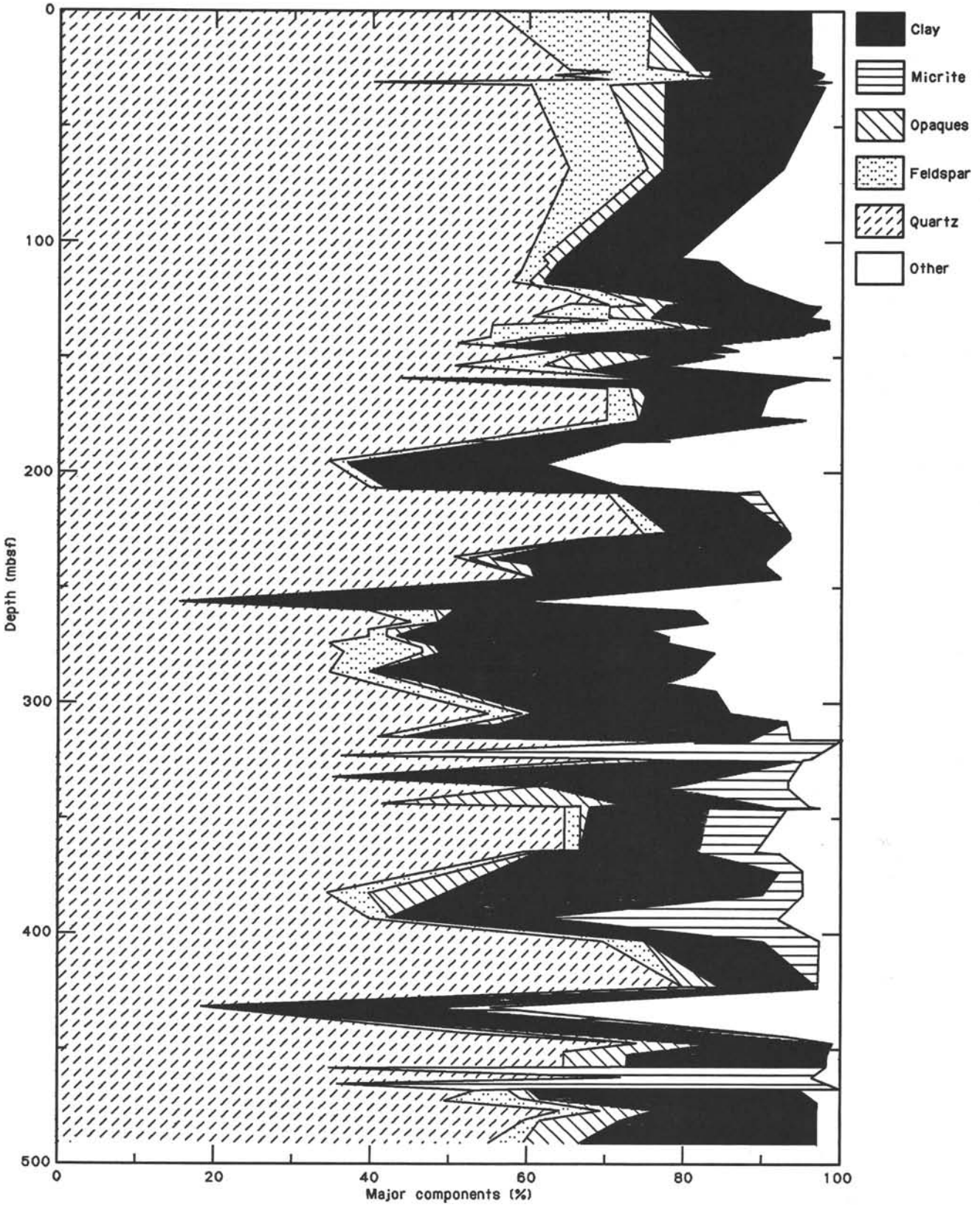

Figure 8. Summary diagram of smear slide compositional data, Hole 739C. The quartz and feldspar values independently are unreliable because it proved impossible to distinguish the two minerals in smear slides where the latter were fresh and unclaved.

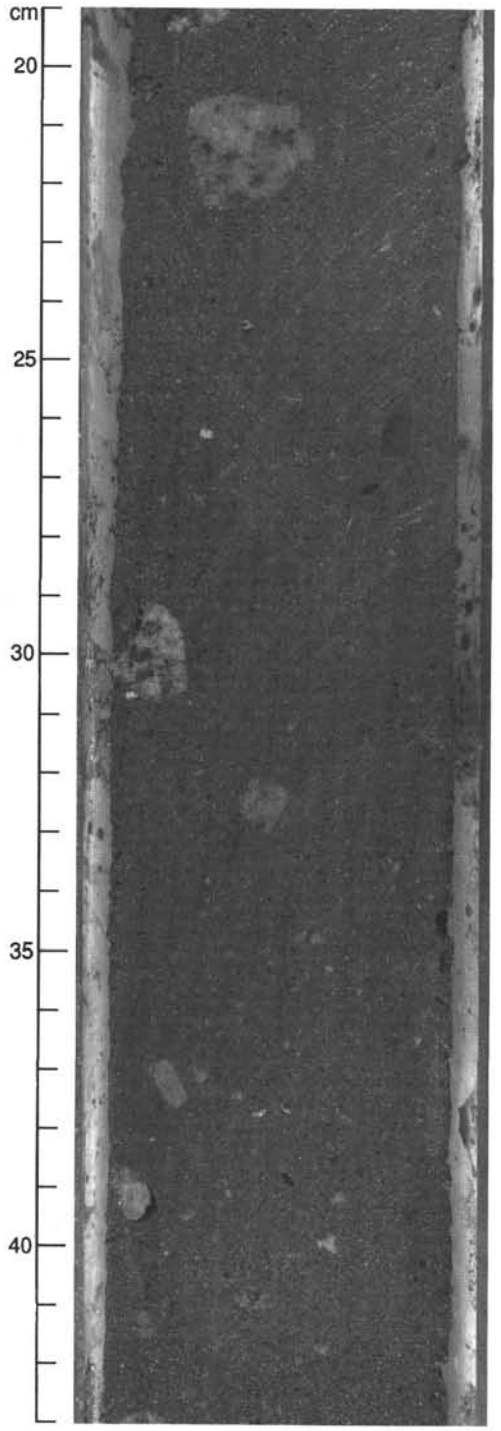

Figure 9. Typical massive diamictite, with assorted gneissic clasts, in lithologic Unit II; Section 119-739C-4R-3, 19–43 cm.

clasts of several centimeters in diameter in each core. Some clasts exceed the diameter of the core. The largest extends up to 20 cm downcore (14.6–14.9 mbsf, Section 119-739C-18R-1). Such large clasts possibly are responsible for the negligible recovery from 40 to 106 mbsf (Cores 119-739C-5R to 119-739C-15R), especially in the light of sharp distinctive fluctuations in the downhole logging records (see "Logging" section).

Clast-shape analyses (for details see the barrel sheets) show that most of the gravel is subangular to subrounded (averaging about 35% in both classes) whereas angular and rounded gravels each average only about 15%. In some intervals (e.g., 125–126.5 mbsf, Core 119-739C-15R) the larger clasts tend to be subrounded or rounded whereas the smaller clasts are angular to subangular. The clasts have no significant preferred orientation, as determined from studies of elongate grains in two horizontal slices in this unit (Fig. 10) and from visual core descriptions. Only at 164–167 mbsf, from 4 to 7 cm in Section 119-739C-23R-1, do elongate clasts show long-axis orientation at a high angle to the slight bedding.

The composition of the gravel includes a great variety of rock types. However, igneous and metamorphic rocks prevail. The most abundant are several types of gneisses. Granites, amphibolites, mica schists, and coaly shales are also common. Only a few other clasts of sedimentary origin were found, and they are composed of sandstone and quartzite. Quartz and feldspar dominate the monomineralic gravel components, but some grains of garnet and biotite are also present. Most of the clasts are fresh and unaltered, but a few grains showed signs of weathering (e.g., 150–153 mbsf, Core 119-739C-20R).

From 106 to 148 mbsf (Cores 119-739C-13R to 119-739C-19R) the diamictite contains up to 25% diatoms. A minor lithology at 147 mbsf (Core 119-739C-19R) consists of a clayey silt with 25% diatoms. This olive (5Y 3/2) sediment forms wispy layers and mottles that are up to 5 cm thick, with diffuse boundaries. The clayey silt is better sorted than the host diamictite; it contains less clay, only minor sand, and a single pebble. In addition, at about 164 mbsf (10–20 cm in Section 119-739C-22R-CC) the sediment is somewhat better sorted, consisting of an olive gray (10Y 3/1) sand that is relatively free of clay and silt.

The carbonate content in Unit II ranges from 0.1% to 0.8%, with 0.36%–2.08% organic carbon. Although there are no obvious lithologic grounds for subdividing Unit II, chemical and downhole logging data suggest that an abrupt change occurs at about 106 mbsf. The bulk of the sequence above this depth, which was so poorly recovered, may be rich in boulders and interbedded sands, a conclusion supported by drilling problems and the retrieval of only fragmented boulders. Also, above 106 mbsf there is $<0.4\%$ organic carbon, whereas below it the organic carbon content is typically from 1% to 1.8%.

Unit III

Section 119-739C-25R-1 through Sample 119-739C-34R-3, 84 cm; depth, 173.6–267.2 mbsf.
Age: early Oligocene to late Eocene.

Unit III is divided into three subunits (Table 3) according to the presence or absence of bedding and the nature of the bedding. The age of the unit is based on the core-catcher sample of Core 119-739C-25R. Subunit IIIA is characterized by diffuse bedding and slickensides on fault planes, Subunit IIIB is structureless except for faint to wispy bedding, and Subunit IIIC shows well-defined wispy bedding, slumps, load structures, rhythmic laminations, and burrows. The lower boundary of Unit III is sharp and erosional (Table 3); all other boundaries lie within intervals of no recovery, but they probably are gradational. The boundary with Unit II coincides with marked changes in the downhole logging properties (see "Logging" section) and physical properties (see "Physical Properties" section) and is also represented by a major biostratigraphic hiatus (see "Biostratigraphy" section, this chapter).

Carbonate percentages range from 0.6% to 1.9%, with 0.26% to 0.77% organic carbon.

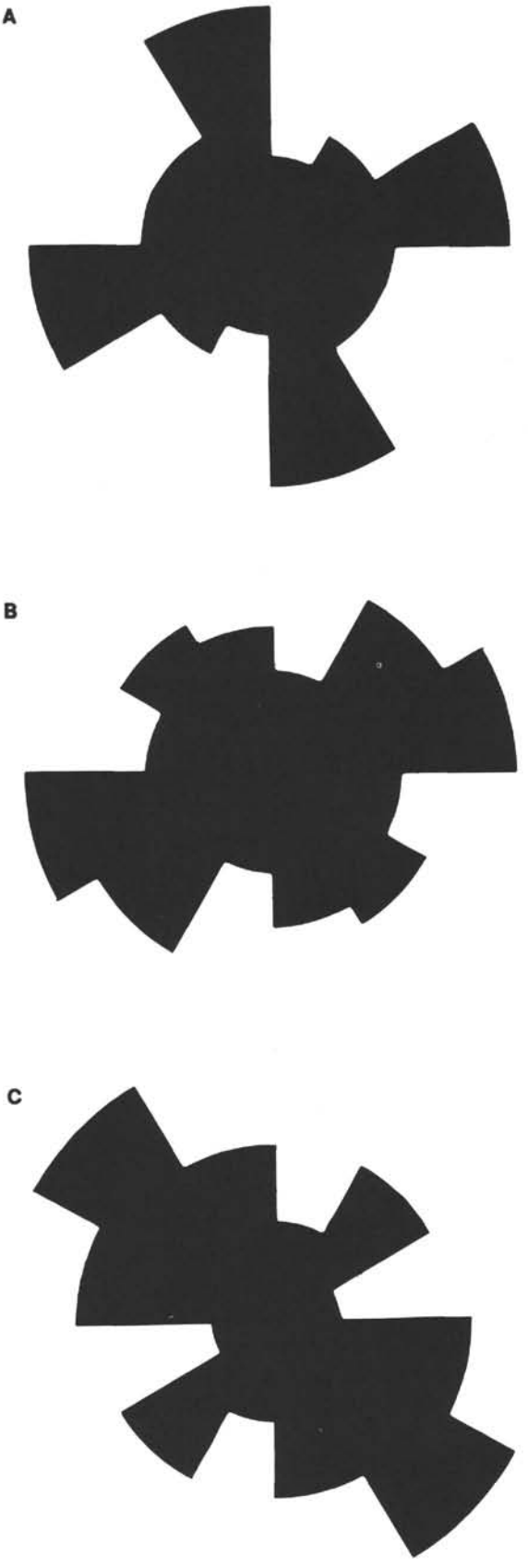

Figure 10. Rose diagrams showing orientation of elongate grains determined on horizontal cut surfaces in lithologic Units II (**A.** 122 cm in Section 119-739C-4R-1; **B.** 20 cm in Section 119-739C-16R-2) and III (**C.** about 70 cm in Section 119-739C-34R-2).

Subunit IIIA

Sections 119-739C-25R-1 through 119-739C-26R-CC; depth, 173.6–192.9 mbsf.
Age: early Oligocene to late Eocene.

The gravel content of the sediments declines markedly between Cores 119-739C-24R and 119-739C-25R, coincident with a paleontological break (Fig. 7) and an increase in carbonate from about 0.5% to >1.2%. Subunit IIIA lies directly below that change, and it consists of moderately well to weakly stratified diamictite and sand-silt-claystone. The bedding is vague and is marked principally by color changes spaced at 10–100 cm, between the dark olive gray (5Y 5/1) of the bulk of sediment and olive gray (5Y 3/1) 3–20-mm-wide laminae. The former lithology is similar to the diamictite but with <1% gravel, generally at sizes less than 5 mm, whereas the paler laminae are diatom rich and finer grained. There is no evidence of seafloor current activity associated with the layers. In smear slides the total range in sediment components is measured as 74%–52% quartz and feldspar grains, 15%–20% clay, 3%–5% accessory minerals, and 6%–20% diatoms. Intraclasts of diamictite are found in the lower parts of the unit along with graded bedding and possible burrowing.

Inclinations of up to 60° are observed on the bedding, which is attenuated (wispy) and commonly shows small soft-sediment deformation offsets resulting from slumping. In some beds an imbrication of small gravel particles or inclined trains of gravel parallel the inclined bedding. A related feature is the many breaks in the core that parallel the inclined bedding (see the core photograph of Section 119-739-26R-2), which have slickensides oriented approximately downdip.

Subunit IIIB

Sections 119-739C-27R-1 through 119-739C-27R-CC; depth, 192.9–198.1 mbsf.
Age: early Oligocene to late Eocene.

This subunit, which has an unusual fracture pattern, lies within an interval of poor core recovery (<10% of the recorded interval; Table 3). It consists of very dark gray (5Y 3/1) diatomaceous sandy-silty claystone with very minor gravel (granule size and coarser). The gravel component is <1% and is confined to the upper 9 cm of the subunit. It consists predominantly of angular to subangular quartz granules, without any systematic variation in concentration. Also present are very rare pebbles up to 1.2 cm in diameter of reworked olive gray (5Y 4/2) diamictite containing <1% gravel.

Subunit IIIB differs from Subunits IIIA and IIIC by its lack of bedding structures, low percentage of gravel, fine-grained nature, and confinement to a single stratigraphic interval. The claystone is massive, poorly sorted and nonstratified, with large quartz grains scattered sporadically throughout the rock. Irregular light and dark streaks occur in the lower 70–80 cm of Section 119-739C-27R-1; the variation in color depends mainly on sand content. Smear slide examination indicates that the claystone is composed of quartz and clay with minor feldspar and amphibole. Biogenic components are chiefly diatoms (up to 30%) with minor amounts of sponge spicules (2%), silicoflagellates (1%), and broken pieces of mollusk shells.

Subunit IIIC

Section 119-739C-28R-1 through Sample 119-739C-34R-3, 84 cm; depth, 198.1–267.2 mbsf.
Age: early Oligocene to late Eocene.

The boundary between Subunits IIIB and IIIC is placed midway in the nonrecovered interval between Cores 119-739C-27R and 119-739C-28R. Subunit IIIC consists of alternating beds of massive, weakly stratified and nonstratified diamictite that are

partly disrupted by slumping. A few minor laminated siltstone horizons are also present. The unit is slightly indurated.

The massive diamictite (varying from a "silty clay" or "clayey silt" with sand and minor gravel to "sand-silt-clay" with minor gravel) lacks bedding and appears macroscopically to be homogeneous, except for slight variations in the sand and gravel content. The color is mainly very dark gray (5Y 3/1) to dark greenish gray (5Y 4/1) and black (5Y 2.5/1). Beds of massive diamictite range from decimeters to meters in thickness. Shell fragments and complete shells, including scaphopods, are thinly dispersed throughout these beds. Burrowlike structures, a few of which are partially filled with pyrite, are also present. The gravel content reaches up to 10%, and the largest clast measures 12.5 cm downcore.

The stratified diamictite is similar to massive diamictite except that it has lighter greenish gray (10Y 4/1) layers interbedded with the dominant very dark gray (5Y 3/1) and black (5Y 2.5/1) lithology. These layers are of millimeter to centimeter scale, diffuse, wispy as well as well-defined features that lie at various angles to horizontal (Fig. 11). They also show signs of slumping at several levels, but only rarely are the layers broken or disaggregated. A few layers consist of paler sand and are up to 5 mm thick. Pyritization is associated with some inclined bedding. Contacts with the massive diamictite beds are both sharp and gradational, and some contacts show soft-sediment loading. At 273.5 mbsf (55–110 cm in Section 119-739C-35R-3) a greenish silty clay (10Y 4/1) with 40% diatoms is interfolded with the more clast-rich sediment. Both complete and broken shell fragments, including scaphopods, are scattered through the stratified diamictites; usually up to 15% diatoms is present. At about 222–231 mbsf (Core 119-739C-30R) there are some small (< 5 mm), sharply-defined lenses of darker, more clay-rich material, possibly burrows. Mottling is probably due to bioturbation. Most of the gravel in the stratified diamictites is < 1 cm in diameter, but the largest reaches 4 cm. A good dropstone structure, with disrupted laminae below the clast and draped lamination over the top, is present at 264.1 mbsf (Section 119-739C-34R-3; Fig. 12). Few other convincing dropstone structures were observed owing to the slumped nature of the sediment.

The diamictites contain a varied assemblage of clasts, but the clasts are predominantly of metamorphic and igneous basement, including vein quartz, quartzite, granite, garnetiferous gneiss, biotite-(?)pyroxene-quartz-feldspar-(?)cordierite gneiss, fine-grained mafic gneiss, felsite, and amphibolite schist. There is also a minor sedimentary component, including coal and light brown limestone. Some of the mafic gneiss clasts are weathered. The shape of the clasts varies from rounded to angular, with the following typical ranges: 5%–16% angular, 15%–28% subangular, 53%–67% subrounded, and 4%–14% rounded.

A minor lithology, laminated clayey silt, occurs at five intervals up to 5 cm thick between 261 and 264.3 mbsf (Core 119-739C-34R). The laminae are < 1 mm thick and have minor local pyrite development. They are planar or wavy, and appear to be of a rhythmic character (Fig. 12).

Smear slide analyses on the finer fraction of the diamictites gave the following size fraction ranges: 10%–30% sand, 40%–55% silt, and 15%–40% clay. The principal sediment components are 40%–75% quartz, 1%–2% feldspar, 15%–35% clay, and 3%–15% diatoms. There are also minor amounts of carbonate, amphibole, palagonite, opaque and accessory minerals, sponge spicules, silicoflagellates, and calcareous nannofossils. The clast-poor greenish horizon consists of 5% sand, 40% silt, and 55% clay size fractions, with a composition of 10% quartz, 2% feldspar, 45% clay, and 40% diatoms. A sample from a laminated horizon was 5% sand, 50% silt, and 45% clay; the composition is similar to that of the diamictite.

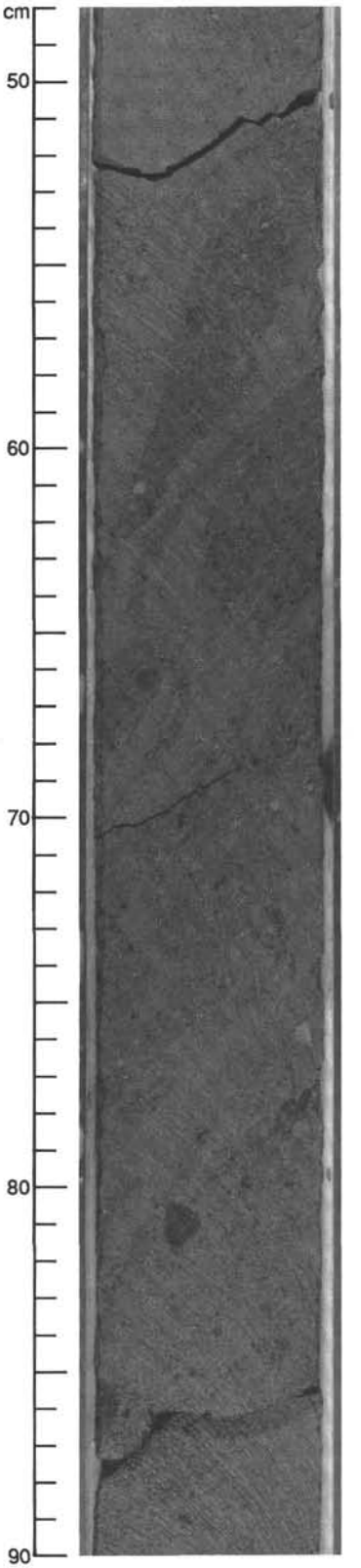

Figure 11. Stratified diamictite of lithologic Subunit IIIC, showing the slumped and wispy nature of the bedding; Section 119-739C-33R-3, 48–90 cm.

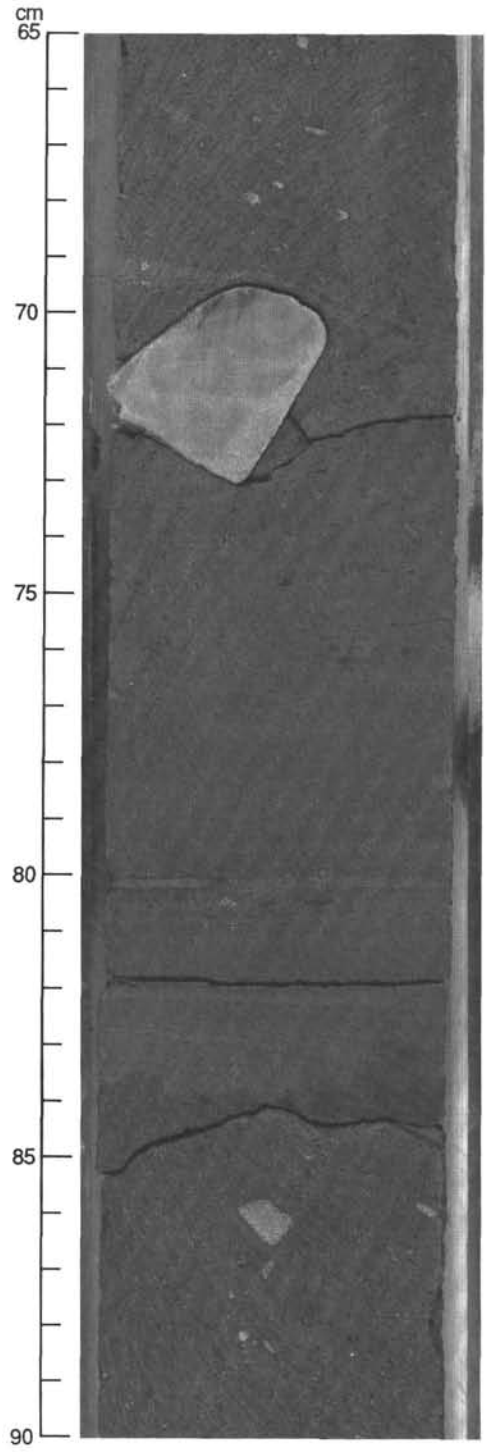

Figure 12. Features from top to bottom at the base of lithologic Subunit IIIC in Section 119-739C-34R-3, 65–90 cm: (1) stratified diamictite with a dropstone of quartzite at 71 cm, (2) bedded to laminated clayey siltstone, and (3) sharp, irregular contact with massive diamictite of Unit IV at 84 cm. Note the pyritiferous layer at 80 cm and the draped diamictite.

Unit IV

Samples 119-739C-34R-3, 84 cm, through 119-739C-39R-4, 30 cm; depth, 267.2–315.7 mbsf.
Age: early Oligocene to late Eocene.

Unit IV consists of massive diamictite. It has a sharp erosional upper boundary and is separated from Unit V based on the presence of carbonate, the amount of biogenic components, and the percentage of gravel. The boundary is gradational.

Unit IV consists of very dark gray (5Y 3/1), massive, poorly sorted diamictite containing scattered granules and pebbles up to 5 cm in diameter. Lithologically, the diamictite is composed of silty clay, sandy-silty clay, and silty-sandy clay. Analysis of clast lithologies indicates that the granules are composed mainly of quartz, whereas the pebbles are lithologically more variable and include granite, various types of gneiss, pyroxenite, and diamictite. Although most of the clasts are fresh, some mafic metamorphic clasts show the effects of weathering. The majority of the clasts are subangular to subrounded, with only minor angular and rounded types. However, clast size influences roundness in that smaller clasts are generally more angular. The percentage of gravel varies throughout the unit from 1% to 10%, with an average of 3%. Fluctuations between 5% and 10% are typical within single sections.

The sand content is also variable (10%–30%). Paler colored sandy pockets and lenses and fine (1-mm-thick) laminae in 10-cm-thick zones are locally developed within this unit. Rare pyrite grains, wispy undulating bedding, and faint diffuse laminations are also found. Shell fragments 1–3 mm long occur sporadically throughout Unit IV, but are especially common from 265 to 267.4 mbsf (Sections 119-739C-34R-4 and 119-739C-34R-5). Small, intact mollusk (gastropod) shells were recovered from this part of the succession. Very localized, rare mottling and bioturbation occur in the upper part of the unit.

Smear slide examination shows that the diamictite is composed mainly of quartz and clay, with minor amounts of relatively fresh feldspar and ferromagnesian minerals. Although most of the quartz grains are angular to subangular, a few well-rounded sand-size grains occur. The biogenic component is dominated by diatoms, ranging from trace amounts to 20%. However, the diatom content decreases downcore through the unit, and only trace amounts are recorded from 308.6 to 313.2 mbsf (Sections 119-739C-39R-1 to 119-739C-39R-4). In addition, there are minor to trace amounts of silicoflagellates, radiolarians, and nannofossils in Unit IV. The nannofossils, however, appear to be confined to the very bottom of the unit.

The carbonate content of Unit IV ranges from 0.7% to 1.8%, with 0.64% to 0.95% organic carbon.

Unit V

Sample 119-739C-39R-4, 30 cm, through Section 119-739C-62R-CC; depth, 315.7–486.8 mbsf.
Age: middle Eocene(?) to early Oligocene.

Unit V consists of very dark gray (5Y 3/1), dark gray (2.5Y 4/1), "yellowish gray" (7.5Y 3/1; color name unavailable), dark greenish gray (10Y 4/1), and dark olive gray (5Y 3/2) massive, nonstratified poorly sorted diamictite. This unit contains few fossils, and the lowest recovery of diatoms in this hole is from the core-catcher sample of Core 119-739-39R; these give an age of late Eocene to early Oligocene. The lowest nannofossils occur in Sample 119-739C-46R-1, 43 cm, and give an age of middle Eocene to Oligocene.

Lithologically, the diamictite is composed of sandy-silty clay and clayey-silty sand. The amount of clay and sand varies almost continuously throughout the unit, and this variation is reflected some in color changes. Clay-rich zones tend to be darker and greener in contrast to the paler sand-rich zones. The major differences between this unit and the overlying Unit IV are (1) the introduction of carbonate-rich intervals, (2) the paucity of microfossils, and (3) the lower percentage of gravel and the composition of the clasts. Carbonate is present in the form of micrite and microsparite. It is concentrated in a number of pale layers, which are 5–20 cm thick (e.g., Fig. 13). Smear slide examination shows that the micrite occurs as well-formed, typi-

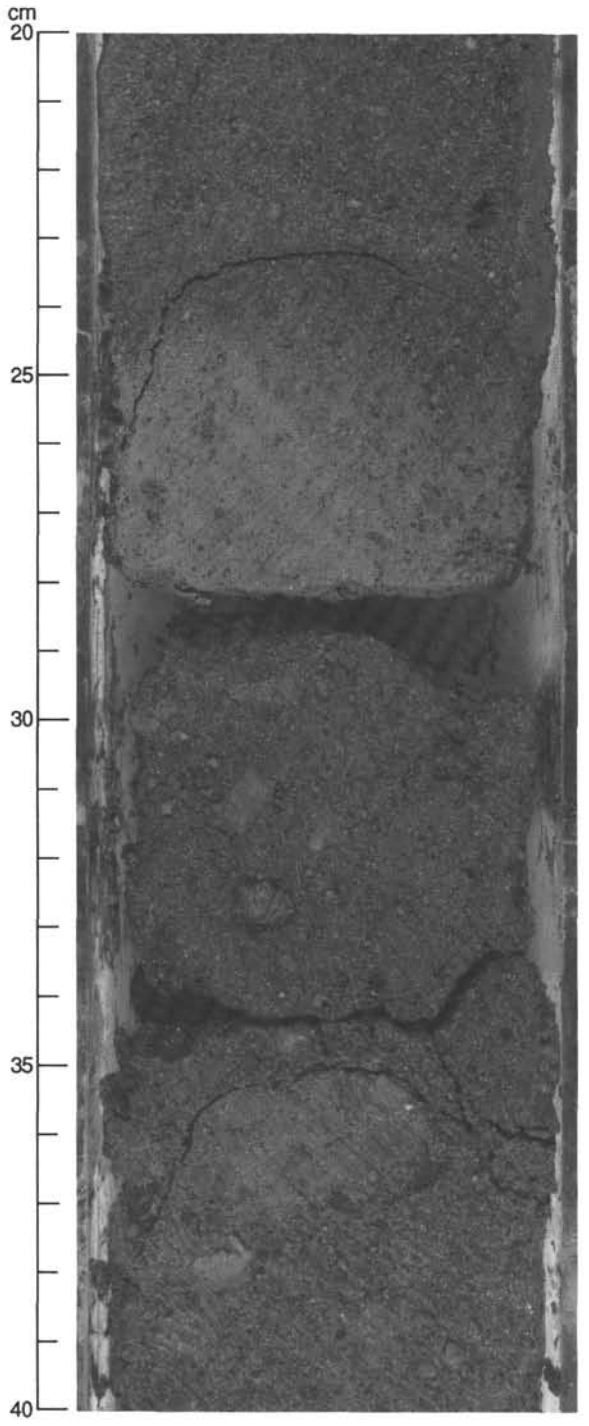

Figure 13. Massive, friable diamictite near the top of lithologic Unit IV in Hole 739C. The diffuse pale patch at 25–28 cm contains a high proportion of calcite cement, but the rest of the core is uncemented. Section 119-739C-40R-1, 20–40 cm.

cally euhedral, grains that may be authigenic. These form aggregates of similar-size grains scattered throughout the samples. The appearance of the micrite grains does not suggest an authigenic origin and probably resulted from transportation to the site of deposition.

Unit V is characterized by the presence of scattered, predominantly subrounded granules and pebbles up to 3.5 cm in diameter. Clast composition is more variable than in the overlying unit and includes quartz, gneiss, granite, felsite, quartz schist, quartzite, sulfide-bearing quartzite, diamictite, coal, shale, micaceous yellow sandstone, gray burrowed sandstone, and red sandstone. Gravel content is lower than in Unit IV, averaging around 1%, but with a range from 1% to 5%. There is some local segregation of large clasts, as well as of stringers and pockets of quartz granules. Some granules show alignment of the long-axis fabric at a high angle to the horizontal. This could be related to slumping (Subunit IIIC), although the only other evidence is a slump structure near the base of the unit at 454 mbsf (Section 119-739C-56R-1). Pyrite grains are disseminated throughout most of the unit and are especially common between 424.5 and 436.4 mbsf (Cores 119-739C-51R and 119-739C-52R).

Microfossils are rare in Unit V. Trace amounts of diatoms, nannofossils, and sponge spicules are confined to the upper part of the unit, above 395 mbsf (Core 119-739C-48R). Likewise, shell fragments were found only in the upper part of the unit, between 328 and 360 mbsf (Sections 119-739C-41R-1 and 119-739C-44R-2). Carbonate percentages range mainly from 0.4% to 2%, but two samples contained 18% and 23%, respectively. Organic carbon varies from 0.46% to 3%.

Diagenesis

Diagenetic processes have not extensively affected this rapidly deposited clastic sequence, even though the mineral content is extremely labile. Physical-properties data on porosity, compressional-wave velocity, and shear strength show several levels of overcompacted sediment that are probably related to periods of ice loading, with the added possibility of a now-eroded sediment overburden (see "Physical Properties" section). Culminations of compaction are detected at 9–130 (upper part of geotechnical unit G2), 167 (top of geotechnical unit G3), 255 (base of geotechnical unit G5), and 310 mbsf (base of geotechnical unit G6), in good correspondence with the lithologic unit boundaries. In these shallow compacted intervals no actual cementation is in evidence and the sediment is still relatively easily disaggregated. Mineralogical diagenetic changes were observed only at greater depths of approximately 360 mbsf (Core 119-739C-44R), with the appearance of probable neomorphic microspar and of clay "clots" as a precursor to lithification. This carbonate cementation appears to be confined to thin (15–20 cm), discrete, widely spaced horizons.

Interpretation

Because of the poor core recovery, Site 739 provides only an incomplete picture of the sedimentary history. The site is dominated by diamictons and diamictites of various types, which indicates that glacial processes were of paramount importance during the deposition of the recovered sediments. The terminology of glacial sediments is in a state of flux, particularly for the marine environment. Our usage is outlined in the "Explanatory Notes" chapter. The greater part of the sequence consists of massive diamicton, interpreted as waterlain till, deposited by continuous rain-out of basal glacial debris seaward of the grounding line of an ice mass (terminology following Barrett et al., in press, for the Ross Sea). Also present is stratified diamicton, which embraces proximal and distal glaciomarine sediments and reflects a decreasing glacial (ice-rafting) influence seaward and a concomitant increase in biogenic material.

None of the recovered sediments indicates full glacial retreat; such intervals were probably lost during coring. Furthermore, a number of hiatuses probably occur, but the lithologic evidence provides few clues as to their stratigraphic levels.

The interpretation of the sedimentary record indicates that for ice to reach Site 739, full-scale ice sheet development over East Antarctica had occurred by early Oligocene time and pos-

sibly earlier. The lithologic units are interpreted as follows and summarized in Figure 7.

Unit I: This soft, normally consolidated unit that caps the sequence at Site 739 is a massive diamicton. It is interpreted as a proximal glaciomarine sediment on the basis of its diatom content.

Unit II: The upper part of this unit, although poorly recovered, is believed to consist of bouldery and sandy deposits, based on drilling experience and the downhole logging character. However, this deposit is conceivably a lodgement till. The lower part of Unit II (below 106 mbsf) consists of a uniform, unstratified diamicton, interpreted as a waterlain till.

Unit III: This unit consists of two stratified diamictites (Subunits IIIA and IIIC) above and below a claystone (Subunit IIIB). Much of the unit is rich in fossils. Depending on gravel content, the sediment is inferred to have formed in proximal to distal glaciomarine settings. Slumping is evident from inclined stratification, and a few debris flows are indicated by massive diamictite beds with sharp bounding contacts.

Unit IV: The massive diamictite of this unit, with abundant biogenic material, is considered to be a waterlain till.

Unit V: This unit is a sediment similar to that of the overlying unit, although it was poorly recovered. It may also be a waterlain till, possibly slumped in part, but fluctuations in the downhole logging characteristics may indicate unrecovered sandier intervals.

BIOSTRATIGRAPHY

The diamictite sediments recovered at Prydz Bay Site 739 afford poor biostratigraphic control throughout most of the sequence (Fig. 14). Factors contributing to the uncertainty in age determinations include (1) the occurrence of several broad intervals barren of microfossils, (2) poor sediment recovery, (3) the absence of zonal marker species, and (4) sporadic occurrences of reworked specimens.

Diatoms are the most persistent of the recovered fossil groups, enabling recognition of the Quaternary down to 17 mbsf, the lower Pliocene between 111 and 127 mbsf, the upper Miocene between 142 and 168 mbsf, and the upper Eocene to lower Oligocene between 178 and 318 mbsf. A hiatus is tentatively placed between the upper Eocene to lower Oligocene and upper Miocene interval. Occurrence of rare, and probably *in-situ*, calcareous nannofossils support the late Eocene to early Oligocene determination for the lower part of the sequence. The lowermost age determination of Site 739, which occurs in Sample 119-739C-46R-1, 43 cm (378 mbsf), is from a calcareous nannofossil species that ranges from the middle Eocene to Oligocene. Reworking of Upper Cretaceous and younger calcareous nannofossils was also recognized. Planktonic foraminifers were not found below 38 mbsf, and benthic foraminifers are very rare below this depth. Quaternary radiolarians were observed down to 5 mbsf, but none were found any deeper. Palynomorphs are absent from all of the samples examined.

Calcareous Nannofossils

All of the core-catcher samples from Site 739 were examined for calcareous nannofossils, but little useful biostratigraphic information was provided by the recovered data.

Rare calcareous nannofossils of one or several species were found in the following samples: 119-739A-2H-CC, 119-739B-2X-CC, 119-739C-8R-CC, 119-739C-12R-CC, 119-739C-13R-CC, 119-739C-18R-CC, 119-739C-26R through 119-739C-30R-CC, 119-739C-33R through 119-739C-42R-CC, 119-739C-44R-CC, and 119-739C-46R-1, 43 cm. The calcareous nannofossils include the Pliocene *Reticulofenestra producta* and the following Eocene-Oligocene species: *Coccolithus formosus, Coccolithus pelagicus, Chiasmolithus altus, Chiasmolithus solitus, Cyclicargolithus floridanus, Isthmolithus recurvus, Neococcolithes dubius, Pontosphaera* sp., *Reticulofenestra bisecta, Reticulofenestra daviesii, Reticulofenestra samodurovii*, and *Reticulofenestra umbilica*. Two Late Cretaceous age species, *Arkhangelskiella cymbiformis* and *Cribrosphaerella ehrenbergii*, were found in Sample 119-739C-8R-CC.

The calcareous nannofossils present in the upper 150 mbsf are believed to be reworked from older sediments. Some calcareous nannofossils, such as *R. daviesii*, in the lower part of Hole 739C are probably *in situ*, and they may indicate a middle Eocene to Oligocene deposition of the diamictites.

The recognition of *R. producta*, a Pliocene species (Backman, 1980), at this site indicates that Pliocene calcareous nannofossils were deposited in the area. These species represent the youngest Cenozoic calcareous nannofossils recognized in Antarctica. This may have important paleoclimatic implications, because living calcareous nannoplankton are only known from relatively warm to temperate surface waters above the 2°C isotherm (Tappan, 1980).

Foraminifers

Planktonic Foraminifers

Foraminifers are rare or absent from the core-catcher samples examined at Site 739. *Neogloboquadrina pachyderma* and sporadic specimens of *Globigerina bulloides* are the only planktonic foraminifers observed, occurring down to Sample 119-739C-5R-CC (38.3 mbsf). This provides only a broad age determination of late Miocene to Holocene for this upper interval.

Benthic Foraminifers

Benthic foraminifers are abundant in the mud-line sample at Hole 739C, but occur in low abundance or are absent from the underlying glaciomarine sediments. The mud-line sample contains a diverse benthic assemblage consisting entirely of agglutinated species. The sample was stained with Rose Bengal to distinguish the living from the dead foraminiferal component. This method resulted in a living assemblage of approximately 30%–40% of the total population. The excellent preservation, even of extremely fragile species, and the high percentage of living specimens indicate that the material directly reflects the sediment/water interface. Tubular species are well represented by *Rhabdammina discreta, Hyperammina friabilis, Rhizammina algaeformis, Botellina labyrinthica*, and *Marsipella cylindrica*. The genus *Reophax* shows a high species diversity with *Reophax scorpiurus, Reophax bilocularis, Reophax distans, Reophax delicatulus, Reophax fusiformis*, and *Reophax dentaliniformis*. Common species are *Miliammina arenacea, Textularia earlandi, Saccammina difflugiformis, Psammosphaera fusca*, and *Cribrostomoides wiesneri*. A rare occurrence is observed of *Vanhoeffenella gaussi, Hormosina* sp., *Haplophragmoides* sp., and *Cystammina pauciloculata*. The tests of several nonselective arenaceous forms reflect the coarse nature of the local substrate.

The rich agglutinated surface assemblage was not found to be preserved downcore. The upper five core-catcher samples contain a few calcareous specimens related to *Globocassidulina subglobosa, Cassidulina crassa, Uvigerina* sp., *Astrononion* sp., *Cibicides lobatulus*, and *Angulogerina earlandi*. Below Core 119-739C-5R almost all of the samples are barren of foraminiferal species. Identification of the few specimens and fragments in the lower sequence is questionable.

Diatoms

Diatoms are present in about half the core-catcher samples examined from Holes 739A, 739B, and 739C, occurring consistently in the Quaternary, upper Miocene–lower Pliocene, and upper Eocene–lower Oligocene sediments recovered above Core

119-739C-40R (318.2 mbsf). Preservation, abundance, and diversity vary from sample to sample without an apparent stratigraphic trend.

Core-catcher samples examined from Cores 119-739A-1H, 119-739A-2H, 119-739B-1X, 119-739B-2X, and 119-739C-1R contain moderate to well-preserved and common to abundant diatoms. The assemblage consists of species characteristic of the Southern Ocean, including: *Nitzschia kerguelensis, Nitzschia angulata, Thalassiosira gracilis, Nitzschia curta, Thalassiosira lentiginosa*, and *Actinocyclus actinochilus*. The occurrence of *N. kerguelensis* as well as other *Nitzschia* spp. without the occurrence of *Actinocyclus ingens* or *Rhizosolenia barboi* allows placement of these samples into the uppermost Quaternary *Thalassiosira lengtiginosa* Zone.

The interval from Cores 119-739C-2R through 119-739C-10R contains sparse diatoms, with only Samples 119-739C-2R-CC, 119-739C-8R-CC, and 119-739C-10R-CC containing rare, poorly preserved specimens. The stratigraphic placement of these samples is tentative at best. The occurrence of *N. kerguelensis* in Sample 119-739C-2R-CC suggests a maximum age of late Pliocene. The occurrence of *Nitzschia praeinterfrigidaria* in Sample 119-739C-8R-CC suggests an age no older than early Pliocene, and the occurrence of *Thalassiosira gravida* in Sample 119-739C-10R-CC indicates an age of late Miocene or younger.

No sample was available from Core 119-739C-11R, and only a 2-cm interval was recovered from Core 119-739C-12R-CC. This latter sample contains a Quaternary assemblage that is considered to be downhole contamination. Supporting this conclusion is the occurrence of an early Pliocene diatom assemblage in Cores 119-739C-13R and 119-739C-14R. Species observed include *Rouxia peragalli, Nitzschia* cf. *cylindrus, Denticulopsis hustedtii, T. lentiginosa, R. barboi, Nitzschia praeacuta*, and *N. praeinterfrigidaria*. This assemblage suggests that this sample is equivalent to either the *Nitzschia praeinterfrigidaria/Nitzschia angulata* Zone or the uppermost part of the *Nitzschia reinholdii* Zone.

With the exception of *D. hustedtii* in Sample 119-739C-17R-CC, diatoms were not observed in Samples 119-739C-15R-CC through 119-739C-17R-CC. The occurrence of *D. hustedtii* in core-catcher Sample 119-739C-17R suggests a late Miocene age, but such an age determination is only tentative.

Samples 119-739C-18R-CC, 119-739C-19R-CC, and 119-739C-22R-CC contain few to common diatoms with poor to moderate preservation. These samples are placed in the upper Miocene *Denticulopsis hustedtii* Zone based on the occurrence of *D. hustedtii, Thalassiosira burckliana, Nitzschia porteri, Hemidiscus karstenii*, and *Rouxia californica*. This diatom assemblage is significant in that with the exception of *D. hustedtii* and *H. karstenii*, it is characteristic of lower latitudes, suggesting that thermal isolation of Antarctica did not commence until post-late Miocene.

Diatoms were not observed in Samples 119-739C-21R-3, 123 cm, or 119-739C-20R-CC. The occurrence of *D. hustedtii* in Sample 119-739C-23R-CC suggests that this sample may be stratigraphically equivalent to the sequence directly above it (i.e., Core 119-739C-22R).

Unfortunately, no sample was available from Core 119-739C-24R, and the diatom assemblage present in Core 119-739C-25R through the uppermost part of Core 119-739C-39R consists of a typical lower Oligocene–upper Eocene diatom assemblage. Thus, either a condensed sequence or a hiatus representing the upper Oligocene through upper Miocene occurs within the interval from Samples 119-739C-23R-CC to 119-739C-25R-CC.

The diatom assemblage observed in Cores 119-739C-25R to 119-739C-39R consists of rare to abundant diatoms with poor to good preservation. Preservation, abundance, and diversity vary from sample to sample. Stratigraphically useful species include *Pyxilla reticulata, Hemiaulus caracteristicus, Stephanopyxis grunowii, Pseudotriceratium chenevieri, Hemiaulus polycystinorum, Melosira architecturalis, Stephanopyxis turris* var. *cylindricus, Stephanopyxis turris, Goniothecium odontella, Kisseleviella carina, Pterotheca danica, Asteromphalus oligocenicus, Thalassiosira hydra, Coscinodiscus hajosiae, Pseudostictodiscus picus*, and *Trinacria excavata*. This assemblage is similar to that described from the South Tasman Rise, Deep Sea Drilling (DSDP) Sites 280 to 283 (Hajos, 1976) and from the Falkland Plateau (Gombos and Ciesielski, 1983). Although the majority of the stratigraphically useful species suggest a late Eocene to Oligocene age (see Schrader and Fenner, 1976; Hajos, 1976; Gombos and Ciesielski, 1983; and Fenner, 1978), the occurrence of *T. hydra, A. oligocenicus*, and the common occurrence of the silicoflagellate *Dictyocha deflandrei* indicate an early Oligocene age. However, the absence of *Rhizosolenia gravida* and *Rhizosolenia antarctica*, two zonal indicators for the lowermost Oligocene, makes this age assignment tentative at the present time.

Sample 119-739C-39R-CC is the lowermost sample in which diatoms were observed. The assemblage present in this sample is similar to that previously described and suggests a late Eocene/early Oligocene age. Examined core-catcher samples from below this sample are barren of diatoms.

Radiolarians

Well-preserved Pleistocene radiolarians were observed in Samples 119-739A-1H-CC, 119-739A-2H-CC, 119-739B-1H-CC, and 119-739C-1R-CC. All remaining core-catcher samples examined were barren of radiolarians. Pleistocene forms are rare, and only 10 species, dominated by *Antarctissa strelkovi* and *Botryopera triloba*, were recognized. All species are diagnostic of a Quaternary age, and no precise zonation can be proposed.

Palynomorphs

Selected samples from Site 739 were processed for palynomorphs but were found to be barren. Overall, the organic content of samples examined was very low.

PALEOMAGNETICS

Three holes were drilled at Site 739. Discrete paleomagnetic samples were collected from Holes 739A and 739C. Of the four samples from Core 119-739A-1H, three samples from Section 119-739A-1R-1 showed normal polarity and the remaining Sample 119-739A-1R-2, 7–9 cm, showed reverse polarity. One hundred thirty-eight discrete oriented paleomagnetic samples were collected from Hole 739C. The samples examined consist of glacial debris of approximately equal amounts of sand, silt, and clay, with 5%–20% gravel (see "Lithostratigraphy and Sedimentology" section). The random orientation of the gravels and coarse sands in this type of deposit typically makes it useless for magnetic stratigraphy. Nevertheless, the natural remanent magnetization (NRM) was measured on each of these samples using the shipboard Molspin magnetometer. Because the cores from Hole 739C were collected using rotary drilling, the samples were azimuthally unoriented; therefore, only inclination and intensity results are shown in Figure 15 (declination omitted). Discrete sample susceptibility measurements were made for comparison with the magnetic intensities measured for these samples. The results of these measurements are shown in Figure 15.

Alternating field (AF) demagnetization studies were conducted on representative samples to assess magnetic stability. The results of these stability tests are shown in Figure 16. The pilot samples studied display very large components of unstable magnetization. In the case of Sample 119-739C-14R-2, 8–10 cm, approximately 80% of the magnetization was lost on demagnetization to only 5 mT. Similarly, Sample 119-739C-13R-2, 18–20 cm, lost 80% of its magnetization by 10 mT (no data are avail-

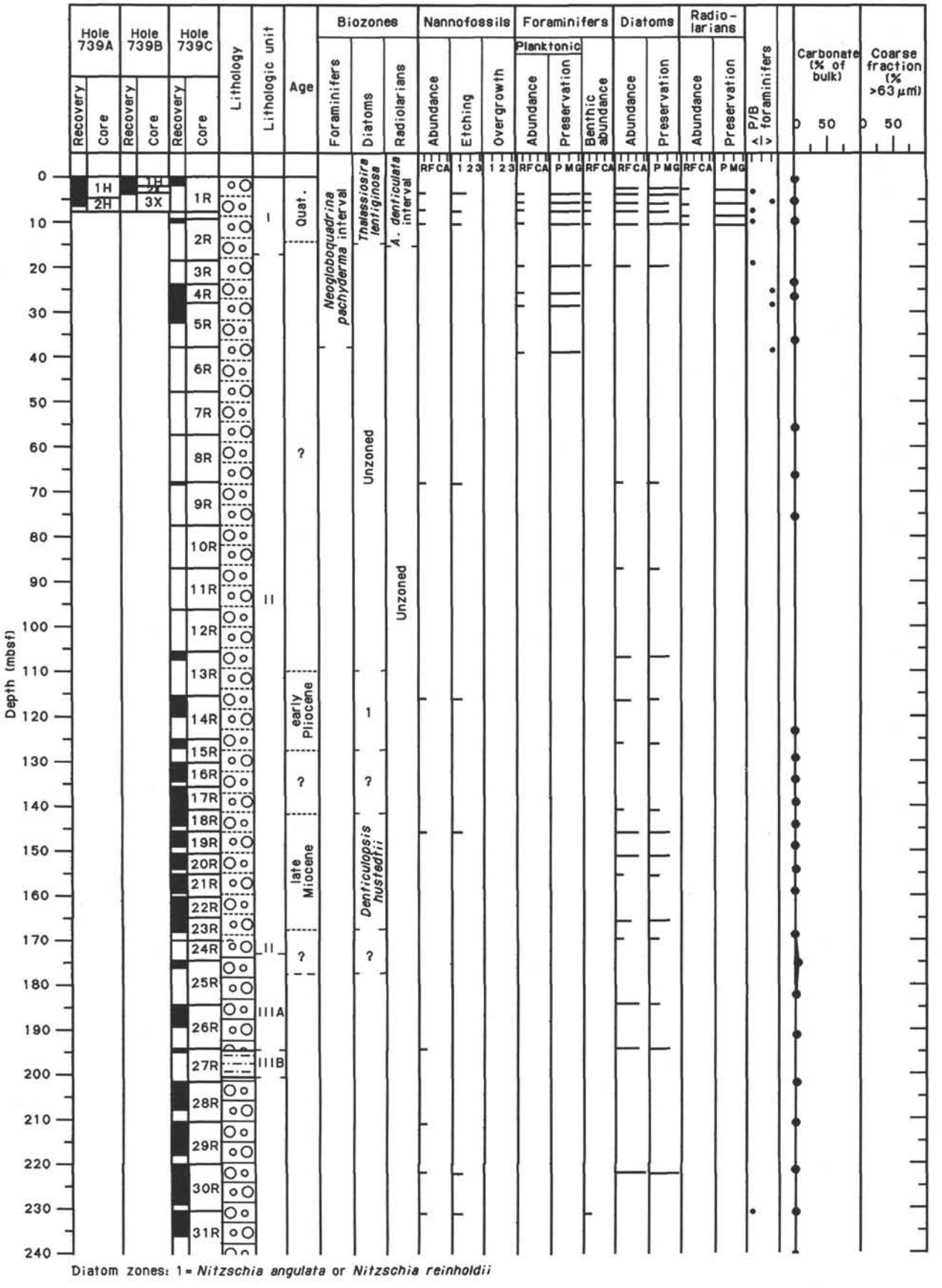

Figure 14. Biostratigraphic summary, Site 739.

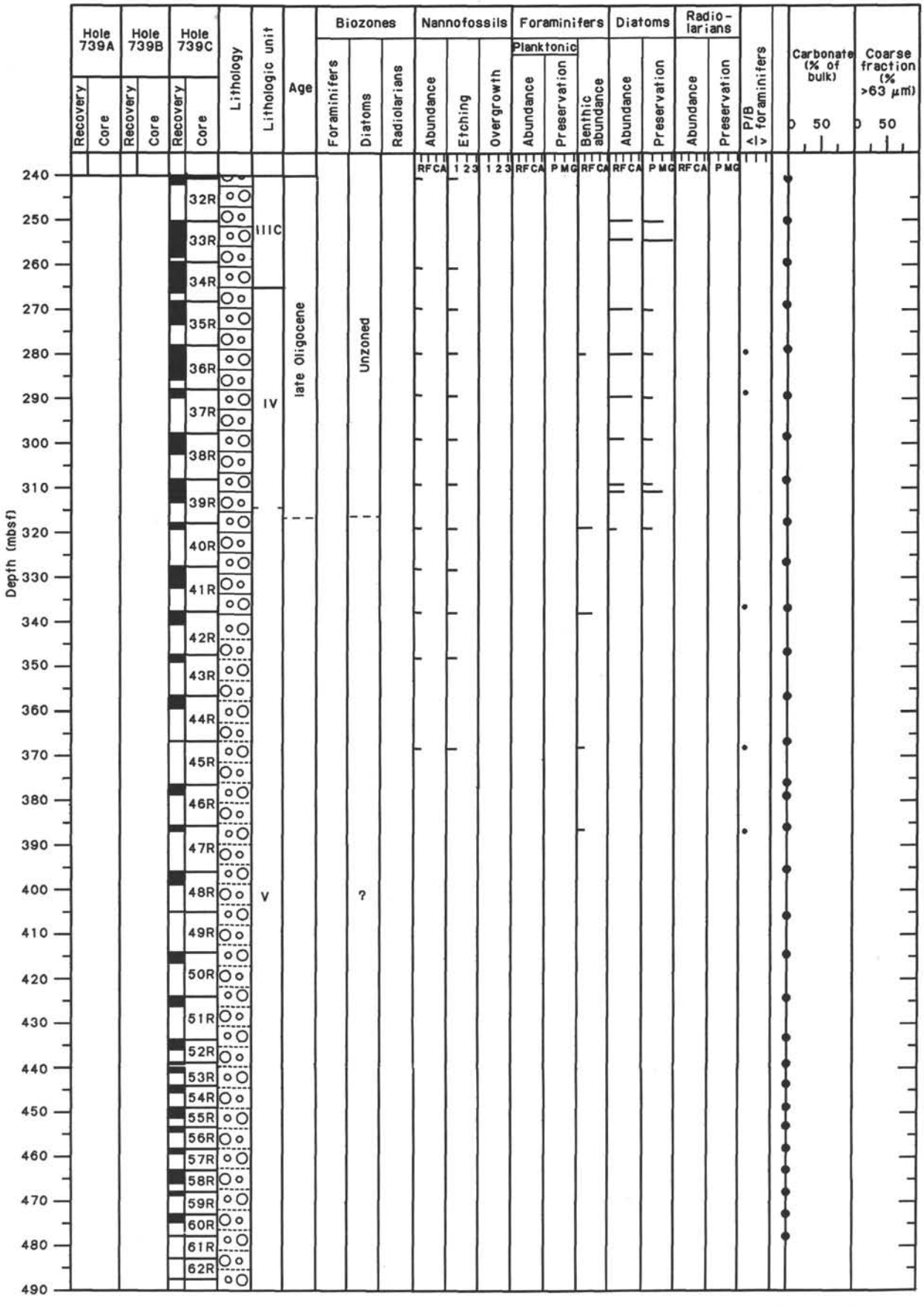

Figure 14 (continued).

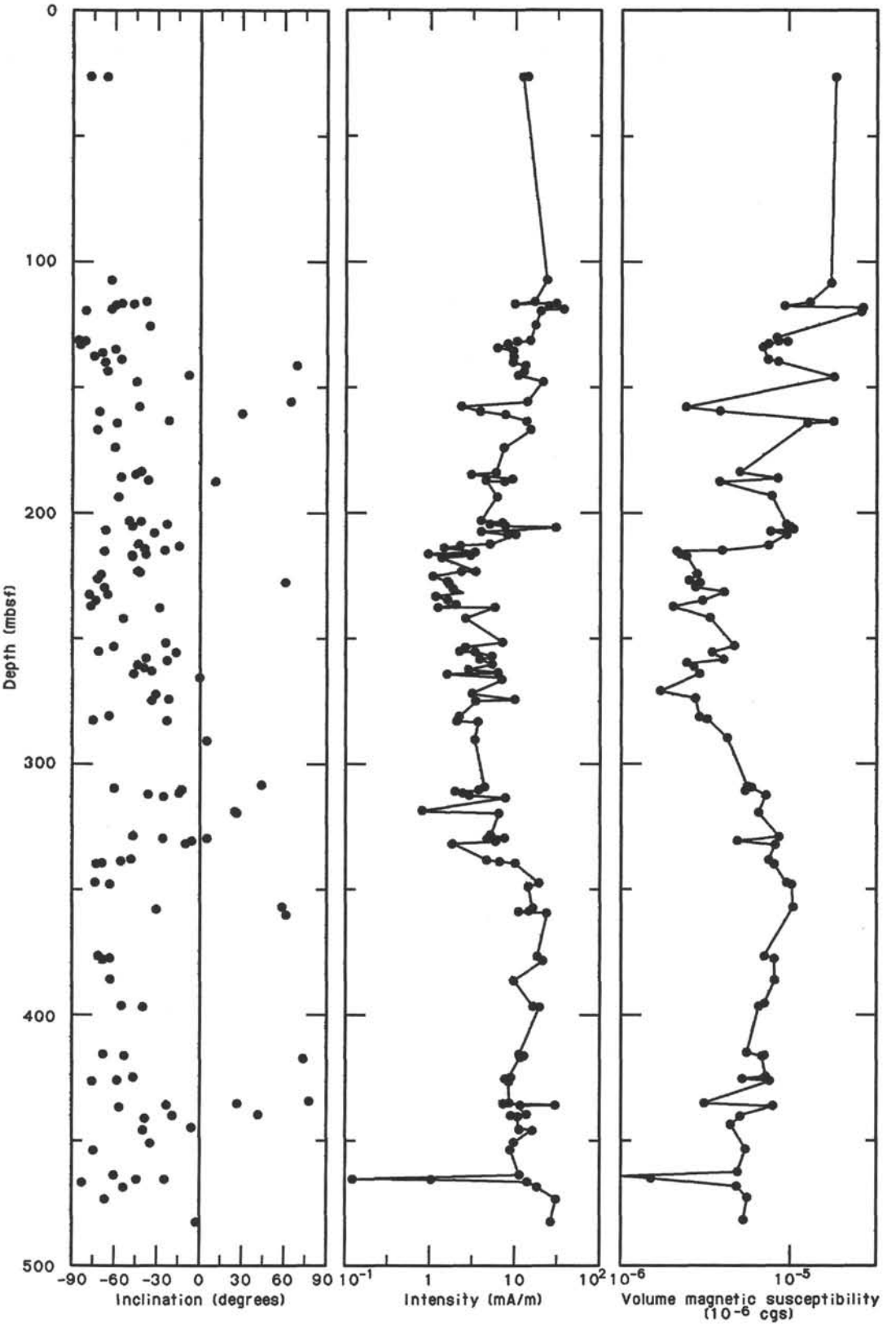

Figure 15. Stratigraphic plot of discrete sample measurements of NRM inclination, intensity, and volume magnetic susceptibility for sediments from Hole 739C. Magnetic intensity and magnetic susceptibility are strongly correlated in these sediments.

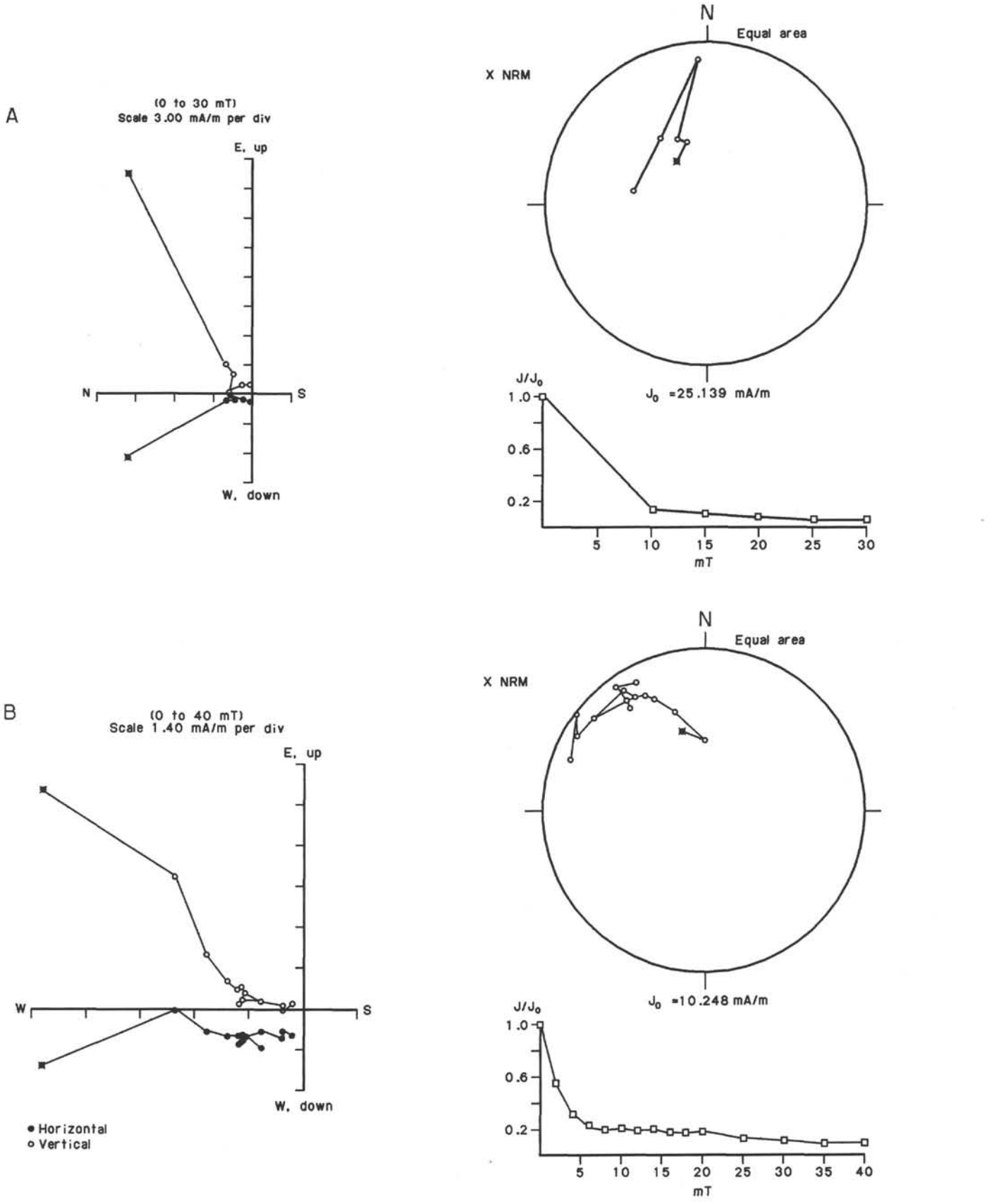

Figure 16. Plotted magnetic stability measurements for two samples from Hole 739C. These samples show low coercivities and low directional stability. **A.** Sample 119-739C-13R-2, 18–20 cm. **B.** Sample 119-737C-14R-2, 8–10 cm.

able for 5 mT). These samples are characterized by low coercivities and by very unstable directional behavior, displaying tens of degrees of directional change on demagnetization to 40 mT. This type of behavior is fairly typical of a coarse-grained sediment that contains large amounts of multidomain magnetic carriers and of coarse-grained conglomerates that incorporate large amounts of randomly oriented rock fragments.

The measured inclinations are dominantly negative (normal polarity in the Southern Hemisphere). They vary considerably, from approximately 0° to 85°, with the mean at about 45°. Most of the few reversals of inclination can not be reliably verified as polarity changes, because only one sample of inverse inclination was measured.

The most interesting observation regarding the magnetic properties measured in the samples from Hole 739C is that long-term oscillations in magnetic intensity are present in the stratigraphic sequence. The magnetization is near its peak at 100 mbsf, from where it gradually decays downward in the hole to a minimum NRM intensity at approximately 225 mbsf. The intensity gradually increases with depth, with a maximum value at approximately 360 mbsf. These oscillations in intensity could reflect actual changes of the Earth's magnetic field with time, or they could reflect variations in the amounts of magnetic minerals supplied to the sediments. In order to better evaluate these magnetic fluctuations, magnetic susceptibility measurements were made on discrete samples from this hole. The results are plotted stratigraphically in Figure 15. At this site the correlation between NRM intensity and magnetic susceptibility is truly remarkable. The same oscillations are present in each record, and remarkably sharp peaks in the data can be identified and correlated at 115, 130, 160, 180, 210, 240, 325, 360, 420, and 465 mbsf in both profiles. The exact correlation between the records is interpreted as direct evidence that the magnetic intensity in these rocks fluctuates as a direct function of the amount of magnetic minerals present in the rock, instead of reflecting changes in the Earth's magnetic field. The degree of similarity between these measurements of two different magnetic properties is unusually strong and definitely provides evidence for the sedimentologic control of NRM intensities within these sediments.

SEDIMENTATION RATES

The 487 m of diamictite cored at Site 739 lacks the biostratigraphic control necessary for an accurate determination of sedimentation rates. Poor core recovery and the absence of index species inhibit the recognition of hiatuses that probably exist in this interval, given the proximity to the Antarctic coastline and the glacial nature of the sediments. A minimum sedimentation rate of 19 m/m.y. is estimated for the Neogene sequence (upper 165 mbsf). This is based on recognition of uppermost Quaternary diatoms down to 9.5 mbsf, a maximum age of 5.3 Ma determined from a lower Pliocene diatom assemblage occurring down to Sample 119-739C-14R-CC (125 mbsf), and a maximum age of 8.25 Ma for Sample 119-739C-22R-CC (139 mbsf), based on the presence of an upper Miocene diatom assemblage.

Diatoms and calcareous nannofossils recovered in the underlying middle Eocene to lower Oligocene sequence are long ranging and cannot be used to estimate the rate of sedimentation. Samples are barren of microfossils below 386 mbsf.

INORGANIC GEOCHEMISTRY

Three holes were cored in a water depth of 412.4 m at Site 739 on the continental shelf of East Antarctica in Prydz Bay. Sediments were rotary cored to a total depth of 486.8 mbsf in Hole 739C. Whole-round minicores 5 to 10 cm in length were obtained for the purpose of interstitial-water geochemical studies. As a result of poor core recovery in the upper part of the sedimentary section, only one interstitial-water sample was recovered in the first 100 mbsf. A total of 14 interstitial-water samples was obtained between 133 and 465 mbsf.

The core intervals sampled for interstitial waters at Site 739 are composed of glaciomarine sediments deposited in close proximity to the grounding line of an ancient glacier (see "Lithostratigraphy and Sedimentology" section). Four samples were taken in the upper Miocene to lower Pliocene indurated diamictite devoid of sedimentary structures (between 27 and 162 mbsf), four samples were taken in the lower Oligocene to upper Eocene stratified diamictites (between 175 and 263 mbsf), and seven samples were taken from massive, slightly indurated diamictite between 302 and 465 mbsf. Calcium carbonate content is less than 2% in nearly all of the sediment samples analyzed (see "Organic Geochemistry" section). Samples with higher calcium carbonate percentages (up to 23% calcium carbonate) do occur, but much of this material appears to have a detrital origin (see "Lithostratigraphy and Sedimentology" section). The organic carbon content of the interstitial-water minicores ranges between 0.39% and 1.86% (see "Organic Geochemistry" section).

Results

A total of 15 interstitial-water samples was taken from Hole 739C. This hole was cored with the RCB system, and, as a result, there is a greater probability for sediment disturbance and contamination of pore fluids than when the APC or XCB method is used. During the RCB coring process, drilling muds and surface seawater are often pumped into the hole for lubrication and cleaning purposes. The water used to prepare the drilling mud was analyzed and found to have the following composition:

Salinity	5.0 g/kg
Calcium	0.6 mmol/L
Silica	179 μmol/L
Phosphate	1 μmol/L
Ammonium	0 mmol/L

A surface seawater sample was also analyzed:

Chloride	527 mmol/L
Silica	41 μmol/L
Phosphate	1 μmol/L

Evidence for the presence of these contaminants in the interstitial-water samples may be indicated by abrupt changes in the concentration vs. depth profiles toward the contaminant values. In addition, charge-balance calculations were also performed on each of the interstitial-water samples to check for gross irregularities in the data. Sodium and potassium concentrations were calculated by multiplying the ratios of these cations to chloride for average seawater, using the values provided by Stumm and Morgan (1981), by the chloride concentration of each sample. None of the Site 739 samples have charge imbalances greater than 1.3%, implying that contamination levels are quite low and/or that the contaminant has a seawater composition.

Site 739 interstitial-water samples were analyzed for salinity, chloride, calcium, magnesium, silica, pH, alkalinity, sulfate, ammonium, and phosphate using the methods detailed in the "Explanatory Notes" chapter. Not all of the samples were large enough to allow the full compliment of analyses. All of the data obtained at Site 739 are presented in Table 4.

Salinity and Chloride

Total dissolved solid (salinity) and chloride concentrations exhibit considerable variability in the Site 739 interstitial waters (Fig. 17). Salinity and chloride concentrations generally tend to be lower near the bottom of Hole 739C than at the top. The mean salinity is 34.2 g/kg (standard deviation 0.8, n = 15), and

Table 4. Interstitial-water geochemical data for Hole 739C.

Core, section, interval (cm)	Depth (mbsf)	Volume (mL)	Salinity (g/kg)	Chloride (mmol/L)	Calcium (mmol/L)	Magnesium (mmol/L)	Mg^{2+}/Ca^{2+}	Silica (μmol/L)	pH	Alkalinity (mmol/L)	Sulfate (mmol/L)	Ammonium (mmol/L)	Phosphate (μmol/L)
4R-2, 145–150	27.05	2	36.2	562	19.5	42.6	2.2	136	—	—	26.7	0.14	—
16R-2, 140–150	133.20	3	35.5	565	17.9	40.6	2.3	140	—	—	17.7	0.46	1
19R-2, 140–150	147.60	3	34.4	554	15.6	37.7	2.4	482	—	—	13.6	0.69	—
22R-2, 140–150	162.20	3	35.2	560	14.3	42.4	3.0	237	—	—	17.4	0.69	—
25R-1, 122–130	174.82	9	34.0	563	14.6	38.8	2.6	489	7.9	3.85	11.9	0.90	0
28R-3, 140–150	206.90	7	34.5	552	13.9	36.6	2.6	412	8.1	3.60	10.8	1.05	—
31R-3, 140–150	235.80	17	34.4	551	14.0	37.3	2.7	592	7.8	4.12	9.4	1.03	1
34R-2, 140–150	263.30	33	34.0	558	14.1	36.0	2.6	615	7.9	3.99	8.4	1.09	0
38R-2, 140–150	301.80	12	33.8	553	13.9	35.0	2.5	485	7.9	3.38	8.4	1.08	0
41R-2, 140–150	330.70	5	33.8	551	13.2	35.8	2.7	98	—	—	10.8	0.91	0
44R-1, 140–150	358.20	5	34.4	561	13.8	33.1	2.4	94	—	—	10.5	1.03	0
48R-1, 140–150	397.00	11	33.5	552	13.4	33.1	2.5	106	8.1	2.15	8.1	0.94	0
50R-1, 140–150	416.30	10	33.0	546	13.8	31.8	2.3	175	8.0	3.02	8.1	0.76	0
54R-1, 140–150	445.30	9	33.5	553	13.8	28.3	2.0	98	8.2	2.22	6.0	1.01	0
58R-1, 140–150	464.60	4	33.5	556	14.4	26.1	1.8	79	—	—	6.0	1.01	0

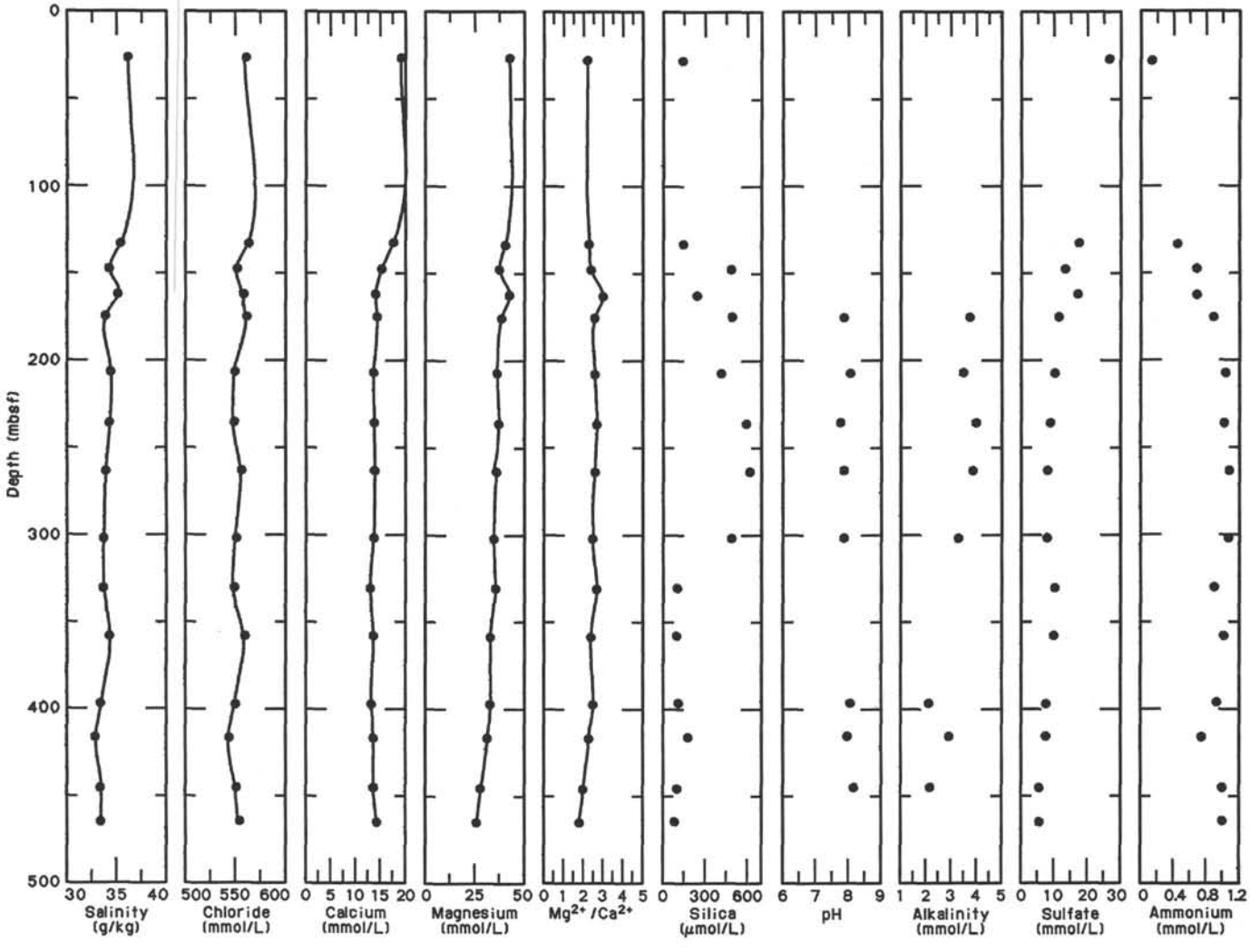

Figure 17. Salinity, chloride, calcium, magnesium, Mg^{2+}/Ca^{2+} ratio, silica, pH, alkalinity, sulfate, and ammonium interstitial-water profiles, Site 739.

the mean chloride concentration is 556 mmol/L (standard deviation 5, n = 15). Analytical errors account for approximately 25% of the salinity variation and 60% of the chloride variation. The contaminants noted in the preceding text should have the effect of lowering the salinity and chloride values; Sample 119-739C-54R-1, 140–150 cm, may have experienced some contamination, but its low sulfate concentration (8.1 mmol/L) does not support this possibility. The lack of data in the upper 100 mbsf makes interpretation of the data set difficult, but it seems clear that the chloride concentration in the mud-line sediments must be lower than in the samples we analyzed because of the low salinity of high-latitude bottom water. Much of the variation can

be accounted for by analytical error and low levels of contamination; the mean chloride concentration of Site 739 interstitial waters may be indicative of the higher salinity of Antarctic Bottom Water during the last major Pleistocene glaciation.

Calcium and Magnesium

Dissolved calcium concentrations at Site 739 indicate that calcium is being added to the interstitial waters between 27 and 133 mbsf (Fig. 17). Average surface seawater has a calcium concentration of around 10.2 mmol/L (Stumm and Morgan, 1981). At Site 739, the concentration of calcium is about twice as great as average surface seawater at 27 mbsf. The dissolved calcium concentration decreases rapidly between 133 and 206 mbsf, from where it shows little variation to a depth of 465 mbsf. Thus, there is a maximum in the calcium concentration vs. depth profile between the seafloor and 133 mbsf, which suggests that there is a shallow-level calcium source in the sediments at Site 739. This calcium source occurs in the same depth zone as the magnesium sink, indicating that the two processes may be related.

The concentration of magnesium in the Site 739 interstitial waters shows a general decreasing trend with increasing depth (Fig. 17). Considering that average surface seawater has a magnesium concentration of 53.7 mmol/L, the rapid decrease to a concentration of 42.6 mmol/L at 27 mbsf indicates that a significant amount of magnesium is precipitating below the sediment/water interface. This magnesium sink may occur near the lower boundary of lithologic Unit I (see "Lithostratigraphy and Sedimentology" section), a normally consolidated diamictite with up to 30% diatoms. Low dissolved silica concentrations in the interstitial-water samples below this depth indicate that magnesium silicates may be forming in this zone. Poor recovery between 27 and 133 mbsf precludes the interpretation of magnesium concentrations in this depth range. Interstitial-water magnesium concentrations again decrease rapidly between 133 and 206 mbsf. The sample at 162 mbsf (Sample 119-739C-22R-2, 140–150 cm) is an anomaly on many of the profiles in Figure 17, indicating that it may have been contaminated during the drilling process. Below 206 mbsf dissolved magnesium concentrations decrease gradually to the deepest sample analyzed at 465 mbsf. Physical-property studies indicate that there is an abrupt porosity increase at about 167 mbsf and a porosity decrease at about 309 mbsf. If dissolved magnesium is precipitating at deeper levels, the changes in the slope of the concentration profile may be a result of changes in the diffusion properties of the sediments because of porosity variations. The dissolved silica concentration drops sharply near 300 mbsf, once again implicating the formation of magnesium silicates as a possible sink for dissolved magnesium.

The concentration vs. depth profiles of magnesium and calcium for the Site 739 interstitial waters indicate nonconservative behavior for both elements and variations in the diffusion characteristics of the sediments (Fig. 17). The magnesium and calcium concentrations are poorly correlated ($r = 0.562$) in the set of interstitial-water samples obtained at Site 739 (see Fig. 18). With only one sample in the first 130 mbsf, the behavior of magnesium and calcium in Site 739 pore fluids is difficult to interpret. The three samples between 27 and 148 mbsf are linearly correlated, but the lack of data in this interval precludes any interpretation of this relationship. Magnesium is supplied to the interstitial waters by ocean bottom waters and is removed by water-rock reactions. Calcium is supplied to the interstitial waters by a sediment source in the upper 133 m of sediment. Abrupt changes in the slopes of the profiles between 133 and 206 mbsf may be related to changes in the diffusion characteristics of the sediments as a result of a porosity increase with increasing depth in this zone.

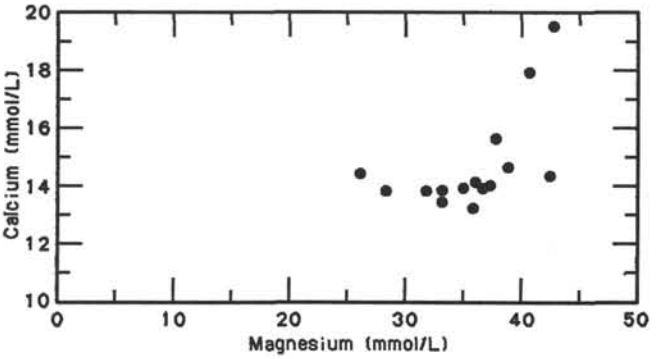

Figure 18. Calcium concentration vs. magnesium concentration for Site 739 interstitial waters.

Silica

A distinct maximum is present in the concentration vs. depth profile for dissolved silica in Site 739 interstitial waters (Fig. 17). Samples between 147 and 302 mbsf contain significantly more dissolved silica (mean = 512 μmol/L, s.d. = 76 μmol/L, n = 6) than the interstitial waters above (mean = 138 μmol/L, s.d. = 3 μmol/L, n = 2) and below (mean = 108 μmol/L, s.d. = 34 μmol/L, n = 6) this zone. Sample 119-739C-22R-2, 140–150 cm, was not included in these calculations because it appears to be slightly contaminated (as discussed for magnesium). The zone of high dissolved silica coincides with the zone of high and variable porosity and water content discovered by physical-property studies (see "Physical Properties" section). The only solid phase present in the sediments with a sufficiently high solubility to constitute a source of dissolved silica is the small amount of biogenic silica (i.e., diatom frustules) noted by the shipboard sedimentologists. The concentration of dissolved silica in the Site 739 interstitial waters does not appear to be high enough to precipitate diagenetic silica phases. The decrease in dissolved silica at about 300 mbsf may be due to the precipitation of less soluble solid silicates such as smectites. It is not yet clear whether there is a cause and effect relationship between the physical-property and chemical variations.

pH, Alkalinity, and Sulfate

Interpretation of the pH and alkalinity data obtained from Site 739 interstitial waters is severely hampered by the lack of sufficient samples in the first 170 mbsf (Fig. 17). The pH values do not vary significantly in the eight samples analyzed between 175 and 445 mbsf (mean = 8.0, s.d. = 0.1). There does appear to be a significant decrease in alkalinity in comparison of the samples between 175 and 302 mbsf (mean = 3.79, s.d. = 0.30, n = 5) and those below 397 mbsf (mean = 2.46, s.d. = 0.48, n = 3). The sample at 416 mbsf shows signs of contamination in several of the concentration vs. depth profiles. The shallower group of samples has alkalinities that are slightly elevated above that of typical seawater. The elevated alkalinities are probably due to the production of bicarbonate ions and bisulfide ions during sulfate reduction. The decrease in alkalinity below 302 mbsf may be a result of the formation of carbonate cements noted by the shipboard sedimentologists.

Sulfate concentrations in Site 739 interstitial waters are negatively correlated with sub-bottom depths ($r = -0.857$, n = 15) (Fig. 17). The steady decrease in sulfate concentrations with increasing depth is undoubtedly due to microbial sulfate reduction. No special precautions, other than refrigeration, were made to prevent the loss of sulfide from the samples. Apparently enough marine organic matter is present in these rocks to allow the production of anaerobic conditions below the seafloor. How-

ever, the amount of reactable organic matter is not sufficient to completely remove the available sulfate from the interstitial waters. Data in this depth zone are lacking, but the data in Figure 17 indicate that the sharpest decrease in sulfate concentrations occurs between 133 and 175 mbsf. Increases in sediment porosity, dissolved silica, and ammonium and decreases in dissolved calcium and magnesium also occur in this interval.

Ammonium and Phosphate

The concentration of ammonium in Site 739 interstitial waters is intimately related to the degradation of organic matter by bacterial sulfate reduction. Ammonium and sulfate concentrations are negatively correlated in this set of interstitial-water samples ($r = -0.903$, $n = 15$) (Fig. 17). The sediment zone from 133 to 207 mbsf appears to support the bulk of the microbial catabolism. This zone appears to have a higher organic carbon content (see "Organic Geochemistry" section) than the shallower sediments, and the greatest decrease in dissolved sulfate occurs within it. Ammonium concentrations increase rapidly between 133 and 207 mbsf and remain at high levels (i.e., around 1 mmol/L) down to 465 mbsf.

All of the Site 739 interstitial-water samples analyzed for phosphate were near or below the detection limit (around 2 mmol/L) of the spectrophotometer. Previous experience on Leg 119 indicated that most of the phosphate should be produced by microbial catabolism near the sediment/water interface. Unfortunately, the shallowest sample obtained in Hole 739C was at 27 mbsf, and no interpretations concerning phosphate are possible at this site.

ORGANIC GEOCHEMISTRY

Site 739 was drilled in Prydz Bay. Organic geochemistry was studied on squeeze cakes of the interstitial-water samples from Holes 739A, 739B, and 739C, as outlined in the "Explanatory Notes" chapter.

Hydrocarbon Gases

The headspace procedure was used approximately every 30 m to determine hydrocarbon gases. Most of the samples had methane near or below the mean laboratory air level of 3 ppm. No sample had more than 30 ppm methane. Ethane was not detected in any samples from Site 739. No gas pockets were observed at this site.

Carbon Analysis

Inorganic carbon was measured on most core-catcher samples and all of the interstitial-water squeeze-cake samples. Total carbon was measured on all of the interstitial-water squeeze cakes and most of the core-catcher samples. Total organic carbon (TOC) was calculated for all the samples for which total carbon was determined. See Table 5 and Figure 19 for tabular and graphic representations of the data.

The sediments at Site 739 are high in organic matter. The samples are generally above 0.5% TOC throughout Hole 739C. Between 100 and 170 mbsf, TOC values jump to over 1%. Unfortunately, Rock-Eval analysis was not performed aboard ship, as the instrument would not detect S3 peaks. Proposed onshore studies of biomarkers will help elucidate the organic carbon picture.

BIOLOGY AND OCEANOGRAPHY

Physical Characteristics of the Marine Ecosystem

Under an overcast sky, the east-northeast winds were brisk during three of the four days at Site 739, with the sky clearing and the winds switching to south on the fourth day (Table 6). A short twilight period of about 2 hr bridged the time between

Table 5. Total carbon, organic carbon, inorganic carbon, and carbonate carbon, Site 739.

Core, section, interval (cm)	Depth (mbsf)	Total carbon (%)	Inorganic carbon (%)	Organic carbon (%)	$CaCO_3$ (%)
119-739A-					
1H-CC, 0-1	4.22	0.22	0.02	0.20	0.2
2H-CC, 0-1	5.41	0.28	0.03	0.25	0.3
119-739B-					
1H-CC, 0-1	1.50	0.40	0.01	0.39	0.1
119-739C-					
1R-CC, 0-1	1.09	0.36	0.01	0.35	0.1
2R-CC, 0-1	9.50	0.49	0.04	0.45	0.3
4R-2, 145-150	27.05	0.49	0.06	0.43	0.5
4R-CC, 0-1	29.00	0.42	0.04	0.38	0.3
5R-CC, 0-1	32.16	0.42	0.06	0.36	0.5
8R-CC, 0-1	57.60	0.55	0.09	0.46	0.8
9R-CC, 0-1	67.30	0.65	0.07	0.58	0.6
10R-CC, 0-1	76.90	0.47	0.07	0.40	0.6
14R-CC, 0-1	119.78	0.94	0.01	0.93	0.1
16R-2, 140-150	133.20	1.42	0.08	1.34	0.7
16R-CC, 0-1	134.56	1.63	0.06	1.57	0.5
17R-CC, 0-1	140.10	2.14	0.06	2.08	0.5
18R-CC, 0-1	143.46	1.37	0.01	1.36	0.1
19R-2, 140-150	147.60	1.62	0.01	1.61	0.1
19R-CC, 0-1	148.48	1.28	0.01	1.27	0.1
20R-CC, 0-1	153.08	1.66	0.02	1.64	0.2
22R-2, 140-150	162.20	1.93	0.07	1.86	0.6
22R-CC, 0-1	164.13	0.86	0.01	0.85	0.1
24R-CC, 0-1	169.00	1.43	0.06	1.37	0.5
25R-1, 122-130	174.82	0.95	0.26	0.69	2.2
25R-CC, 0-1	174.90	1.12	0.07	1.05	0.6
26R-CC, 0-1	187.70	0.76	0.14	0.62	1.2
27R-CC, 0-1	193.70	0.59	0.14	0.45	1.2
28R-2, 50-51	204.50		0.14		1.2
28R-3, 140-150	206.90	0.71	0.07	0.64	0.6
28R-4, 27-28	207.27		0.09		0.8
28R-CC, 0-1	209.25	0.35	0.09	0.26	0.8
29R-2, 33-34	214.03		0.12		1.0
29R-4, 55-56	217.25		0.14		1.2
29R-CC, 0-1	219.33	0.89	0.17	0.72	1.4
30R-CC, 0-1	230.18	0.84	0.17	0.67	1.4
31R-2, 66-70	233.56		0.19		1.6
31R-3, 140-150	235.80	0.89	0.17	0.72	1.4
31R-4, 88-89	236.78		0.18		1.5
31R-CC, 0-1	237.78	0.94	0.17	0.77	1.4
32R-1, 18-23	241.28		0.18		1.5
32R-CC, 0-1	242.13	0.89	0.23	0.66	1.9
33R-2, 19-23	252.39		0.21		1.8
33R-4, 20-25	255.40		0.16		1.3
33R-CC, 0-1	259.14	0.78	0.20	0.58	1.7
34R-2, 37-38	262.27		0.18		1.5
34R-2, 140-150	263.30	0.71	0.16	0.55	1.3
34R-4, 59-60	265.49		0.20		1.7
34R-CC, 0-1	267.31	1.00	0.19	0.81	1.6
35R-2, 50-60	272.00		0.20		1.7
35R-4, 19-20	274.69		0.16		1.3
35R-CC, 0-1	275.25	0.84	0.16	0.68	1.3
36R-2, 60-64	281.80		0.18		1.5
36R-4, 140-144	285.60		0.20		1.7
36R-CC, 0-1	287.11	1.16	0.21	0.95	1.8
37R-1, 30-31	289.60		0.15		1.3
37R-CC, 0-1	290.30	0.90	0.18	0.72	1.5
38R-2, 14-15	300.54		0.15		1.3
38R-2, 140-150	301.80	1.05	0.18	0.87	1.5
38R-4, 20-30	303.66		0.14		1.2
38R-CC, 0-1	308.66	0.77	0.13	0.64	1.1
39R-2, 30-31	310.40		0.14		1.2
39R-3, 148-149	313.08		0.08		0.7
39R-CC, 0-1	313.42	0.78	0.09	0.69	0.8
40R-1, 50-51	318.70		0.11		0.9
40R-1, 127-128	319.47		0.12		1.0
40R-CC, 0-1	319.82	0.87	0.14	0.73	1.2
41R-2, 60-61	329.90		0.15		1.3
41R-2, 140-150	330.70	0.82	0.11	0.71	0.9
41R-3, 107-108	331.87		0.11		0.9
41R-CC, 0-1	332.30	0.89	0.19	0.70	1.6

Table 5 (continued).

Core, section, interval (cm)	Depth (mbsf)	Total carbon (%)	Inorganic carbon (%)	Organic carbon (%)	$CaCO_3$ (%)
119-739C-					
42R-1, 22-23	337.72		0.07		0.6
42R-2, 46-47	339.46		0.05		0.4
42R-CC, 0-1	340.30	0.60	0.14	0.46	1.2
43R-1, 14-15	347.24		2.15		17.9
43R-1, 18-19	347.28		0.14		1.2
43R-CC, 0-1	348.60	0.91	0.10	0.81	0.8
44R-1, 44-45	357.24		0.21		1.8
44R-1, 140-150	358.20	0.79	0.09	0.70	0.8
44R-2, 3-4	358.33		0.07		0.6
44R-2, 117-118	359.47		0.07		0.6
44R-CC, 0-1	359.71	0.65	0.20	0.45	1.7
45R-CC, 0-1	366.50	0.86	0.16	0.70	1.3
46R-1, 38-39	376.58		0.07		0.6
46R-2, 45-46	378.15		0.08		0.7
46R-CC, 0-1	378.25	1.95	0.38	1.57	3.2
47R-1, 22-23	386.12		0.15		1.3
47R-CC, 0-1	386.83	1.42	0.05	1.37	0.4
48R-1, 15-20	395.75		0.07		0.6
48R-1, 140-150	397.00	0.75	0.11	0.64	0.9
48R-2, 33-34	397.43		0.09		0.8
48R-CC, 0-1	398.04	0.69	0.15	0.54	1.3
49R-CC, 0-1	405.20	0.72	0.08	0.64	0.7
50R-1, 29-30	415.19		0.10		0.8
50R-2, 53-54	416.93		0.15		1.3
50R-CC, 0-1	416.99	0.86	0.13	0.73	1.1
51R-1, 26-27	424.76		0.07		0.6
51R-CC, 0-1	426.69	0.60	0.14	0.46	1.2
52R-1, 36-39	434.56		0.05		0.4
52R-CC, 0-1	436.46	0.75	0.12	0.63	1.0
53R-1, 94-103	440.14		0.10		0.8
53R-CC, 0-1	440.49	0.45	0.12	0.33	1.0
54R-1, 25-26	444.15		0.05		0.4
54R-1, 140-150	445.30	0.44	0.05	0.39	0.4
54R-CC, 0-1	445.40	0.39	0.02	0.37	0.2
55R-1, 98-100	449.88		0.08		0.7
55R-CC, 0-1	450.88	0.51	0.05	0.46	0.4
56R-1, 13-16	453.63		0.05		0.4
56R-CC, 0-1	454.15	0.55	0.05	0.50	0.4
57R-CC, 0-1	459.22	0.63	0.06	0.57	0.5
58R-1, 109-112	464.29		0.06		0.5
58R-CC, 0-1	466.09	0.53	0.03	0.50	0.3
59R-1, 55-65	468.75		0.06		0.5
59R-CC, 0-1	468.90	0.60	0.09	0.51	0.8
60R-1, 47-55	473.37		0.05		0.4
60R-CC, 0-1	474.30	3.18	0.21	2.97	1.8
61R-CC, 0-1	477.90	0.78	0.06	0.72	0.5
62R-CC, 0-1	482.60	0.64	0.05	0.59	0.4
62R-CC, 4-9	482.64		2.76		23.0

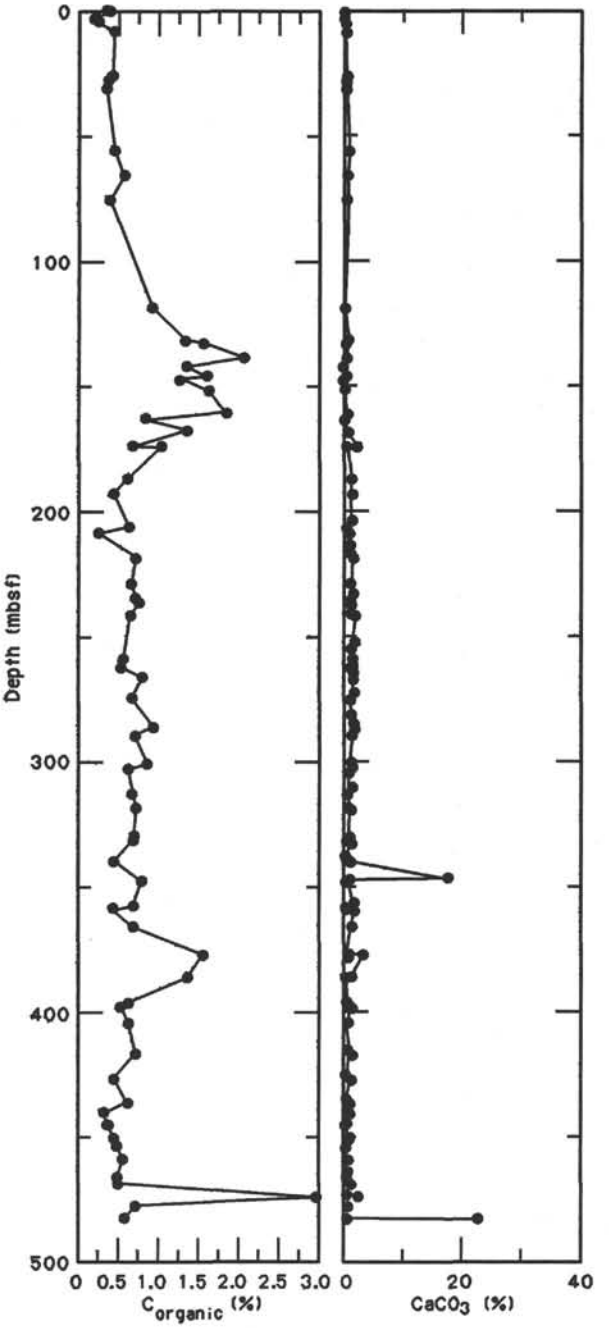

Figure 19. Inorganic carbon ($C_{organic}$) and percent calcium carbonate from squeeze-cake and core-catcher sediment samples, Site 739.

sunset and sunrise. The sea-surface temperature at the drill site ranged from −0.1° to +0.9°C, with 2- to 4-m waves at the air/sea interface. The mixed layer extended to about 20 m when Site 739 was first occupied and later dropped to 40 to 55 m (Figs. 20A–20D). Even larger internal waves may be indicated at the pycnocline interface between the mixed layer and subsurface water by the disparity between the downward and upward traces recorded by the self-contained SEACAT CTD (conductivity, temperature, and depth) unit (Fig. 20D). Internal waves can cycle phytoplankton into and out of different light regimes, and in this case even into and out of the euphotic zone (the depth illuminated by 1% of the incident light at the surface). The euphotic zone, which was estimated visually by the use of a Secchi disc, deepened (13.5, 16.2, 21.7, and 20.3 m), indicating increasing clarity of the surface water during occupation of the site.

Phytoplankton

A bucket water sample was taken 10 days previously (8 January 1988) during an attempted approach to the site (transit was blocked by an ice field). The diatoms retained in a hand-held 20-μm-mesh net are listed in Table 7. The phytoplankton was not abundant and was dominated by small ice-related diatoms, especially *Nitzschia subcurvata*. Many cells were empty; others appeared as single cells or in short chains.

At Site 739 the phytoplankton in the water column was sampled from 18 through 22 January 1988 from aboard *Maersk Master* with horizontal tows and vertical hauls of 35- and 64-μm-mesh nets and from water samples used for estimation of biomass by chlorophyll analysis and cell counts. Water was filtered to make permanent phytoplankton mounts for a quantitative shorebased study; other filters were used for the related pigment and chemical analyses. A three-tiered sediment trap (50, 100,

Table 6. Weather summary for *JOIDES Resolution* at Site 739 (67.3°S, 75.1°E).

Time (hr)/ date (Jan. 1988)	Winds (kt)	Sea-surface temperature (°C)	Waves (m)	Sky
18/23 to 21/32	E-NE to E 18–26	0.5–0.1	2–3, increasing to 3–4 late in the period	Overcast with occasional heavy snowshowers. Pressure slowly decreasing, then rising late in the period
			Maximum: 1.5 (12 hr, 20 Jan.) Minimum: −0.5 (18 hr, 18 Jan., and 00 hr, 19 Jan.)	
21/04 to 22/12	E-SE to SE 22–28, decreasing to 15–20 late in the period	0.2–0.9	3–4, decreasing to 1–2 late in the period	Decreasing cloudiness from overcast to clear over the period
			Maximum: 2.1 (12 hr, 22 Jan.) Minimum: 0.6 (06 hr, 22 Jan.)	
22/22 to 23/02	S 8–12	0.4	2–4	Clear
			Maximum: 0.8 (00 hr, 23 Jan.)	

and 200 m) was deployed for approximately 24 hr to obtain four recoveries for later analysis. In addition, the living material was examined aboard *Maersk Master* for autofluorescence of active chlorophyll. Preliminary microscopic examination of the flora and the life stages represented was performed aboard *JOIDES Resolution*; light micrographs (utilizing a strobe light source) documented key life stages of freshly collected, fixed material.

Preliminary analyses of discrete water samples showed that the chlorophyll maximum remained at 33 m while on site and was about five times the maximum at Site 738 on the southern Kerguelen Plateau. The species found in the plankton that had not been noted in the surface sample taken before occupation of Site 739 are listed in Table 8. The most striking features of the samples collected upon occupation of Site 739 are the numbers of ice-related diatoms, such as the small *N. subcurvata*, still found in the surface water and the overall abundance of *Corethron criophilum* and *Corethron inerme*.

The surface (0 to 40 m) net tows collected empty cells and cells whose contents did not fluoresce. Even after fixation, empty cells and chains of small species floated at the top of the net collections; especially notable were long *Chaetoceros* chains and empty *Corethron* cells, with some *Rhizosolenia alata* chains of small diameter. However, 4 days later (22 January), on the last day of occupation of the site, long, healthy chains—especially of *Chaetoceros, Eucampia, Thalassiosira*, and *Odontella*—were noted in the top 40 m. A few heavily silicified valves of *Thalassiosira tumida* were observed, suggesting that these valves had formed at or below 0°C (Fryxell, 1988). Because the two valves of a diatom form at different times, each locks in the conditions during valve morphogenesis. This same feature was also apparent with the two species of *Corethron*.

Phytoplankton from the 40- to 80-m net tows appeared healthy, with *Corethron* auxospores and cells with four to 64 microspores in evidence. Although microspores have been noted previously (e.g., Fryxell, in press), these collections offered an excellent overview of the sexual life stage, as well as the differences and similarities between *C. inerme* and *C. criophilum*. With both taxa, the first-formed valve after auxospore formation is the complex valve with claws, formed as hypotheca to the simpler vegetative valve that has only spines. The primary valves of both *C. criophilum* and *C. inerme* have curved spines, and during formation they fit into the rounded ends of the auxospores, with small domes that were shaped by the discarded vegetative (clawed) valve. *C. inerme* has more delicate spines that commonly are bent at other life stages as well. Apparently, these two sibling species, or forms, with their highly specialized elements, overlap in the timing of their auxospores, raising interesting biological questions as to their relationships.

In these mid-water tows, *Odontella weissflogii* was found with a resting spore in formation. The southern form of *Eucampia antarctica* (straight cells in broad girdle view, but flexed in narrow girdle view) occurred only as single cells or doublets, with no winter forms seen. Large diameter (35-μm) cells of *R. alata*, with small, broad processes, were present in long chains. The occurrence of this form is in contrast to the thin (7 μm diameter) valves in the surface mixed layer. In deeper water, many *Leptocylindrus mediterraneus* cells were present along with what has been considered an epiphytic flagellate, *Solenicola setigera*; this cosmopolitan pair is often seen in abundance at the ice edge. Although they are considered to be symbionts, evidence is mounting that one is a lifestage of the other (Fryxell, in press). Scattered weak fluorescence was noted in the external epiphytic cells. Fecal pellets were found to be abundant in this depth interval, commonly with pigmented cells included. These were documented by color photography and epifluorescence.

Diatoms in Quaternary Sediments

The assemblage at the mud line reflects the more heavily silicified component of the plankton community, and it is dominated by the ribbon-colony-forming *Nitzschia* species with some resting spores (Table 9). However, fragments of other cells were also observed, such as claws from *Corethron*. A heavily silicified small centric diatom, *Thalassiosira* sp. cf. *gravida*, was abundant. Because *Thalassiosira gravida* is not as heavily silicified as the species found in the sediment and is not known to make resting spores in culture, this form has been selected for study. It was not seen in the plankton.

PHYSICAL PROPERTIES

Most of the published work on physical properties of high-latitude sediments covers surficial, relatively soft mud and sand (Clukey et al., 1978; Schwab and Lee, 1983). Exceptions are results from site surveys of exploration drilling locations, but these are usually confidential data, and little effort has been made to synthesize this information. Furthermore, almost all geotechnical studies of high-latitude continental shelf sediments have been in the Arctic. With the exception of a few studies of a more general character (e.g., Kurtz et al., 1979; Anderson et al., 1977, 1980), most of which concern sediments that can be reached by gravity and piston coring, essentially no systematic studies of

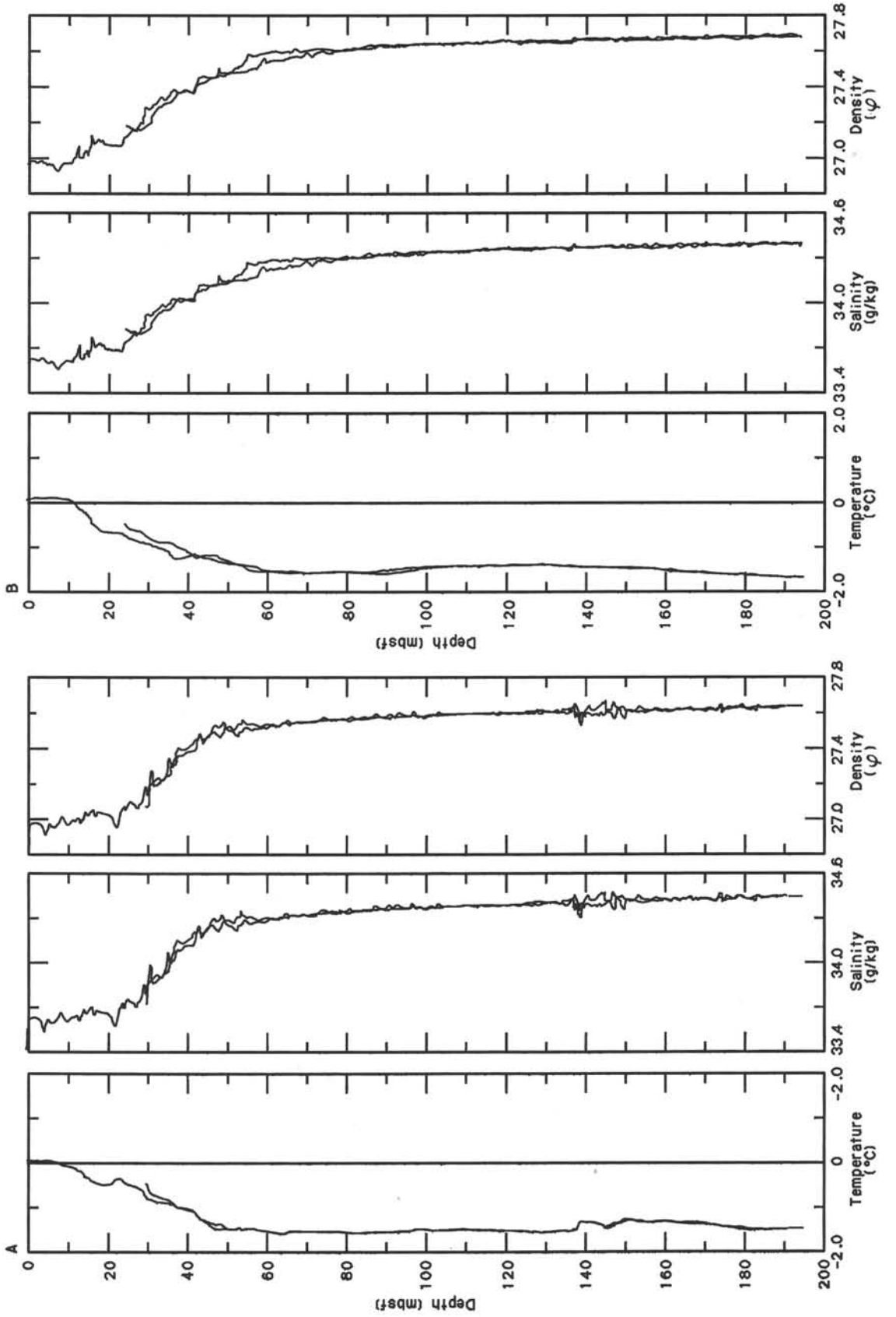
A
B
Depth (mbsf)
Temperature (°C)
Salinity (g/kg)
Density (φ)
0
20
40
60
80
100
120
140
160
180
200
-2.0
0
2.0
33.4
34.0
34.6
27.0
27.4
27.8

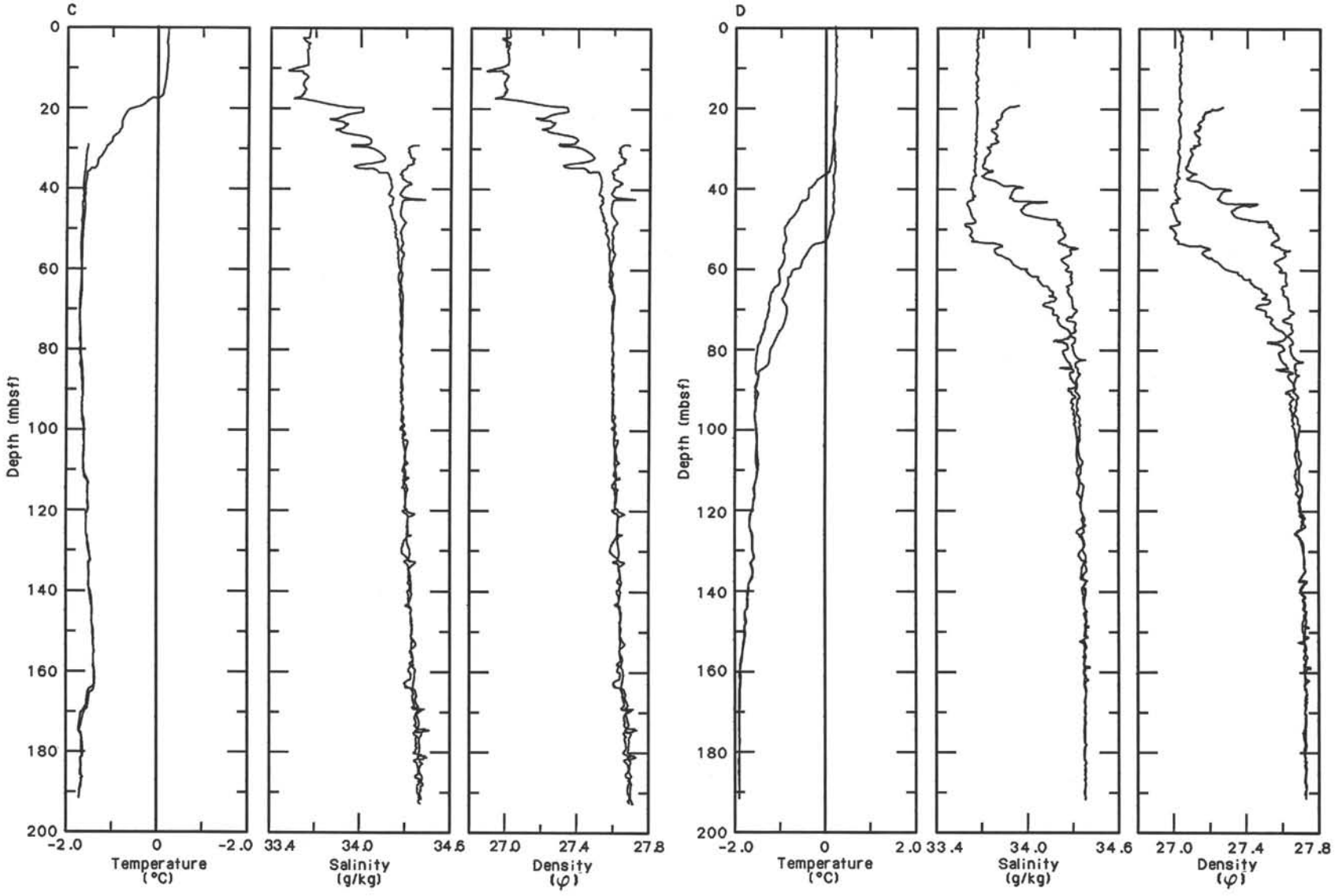

Figure 20. Conductivity, temperature, and depth (CTD) downgoing and upgoing traces recorded from the *Maersk Master* in the top 200 m of the water column in the vicinity of Site 739. The top 20–25 m of the downgoing traces are removed because of the noise that occurs until the SEACAT unit comes to *in-situ* equilibrium. The general agreement of the upgoing and downgoing traces, together with the offset of both temperature and salinity below 40 m, suggests a lag time in the instrument or that part of an internal wave was caught. **A.** CTD-4: 18 January 1988, operation 219, 1547–1559 hr (local time); 67°15.4′S, 75°00.5′E. **B.** CTD-5: 19 January 1988, operation 227, 1640–1654 hr (local time); 67°17.5′S, 75°04′E. **C.** CTD-6: 21 January 1988, operation 240, 1652–1703 hr (local time); 67°16.5′S, 75°01′E. **D.** CTD-7: 22 January 1988, operation 248, 1250–1300 hr (local time); 67°17′S, 75°05′E. The deepening of the mixed layer is apparent in CTD-7.

Table 7. Diatoms collected at 67.1°S, 75.3°E, in outer Prydz Bay at 1600 hr (local time), 8 January 1988.

[a]*Actinocyclus actinochilus*
Amphiprora sp.
Asteromphalus hyalinus
Chaetoceros bulbosus complex
Chaetoceros dichaeta
Chaetoceros flexuosus
Chaetoceros neglectus
Chaetoceros neogracile
Chaetoceros pendulus
Chaetoceros sp. cf *wighamii*
[a]*Corethron criophilum*
Corethron inerme?
[a]*Coscinodiscus oculoides*
[a]*Dactyliosolen antarcticus*
[a]*Eucampia antarctica* (vegetative, straight in broad girdle view but flexed dorsally/ventrally)
Nitzschia closterium
[a]*Nitzschia curta* (up to 45 μm long)
[a]*Nitzschia cylindrus* (two lengths, one is 40–60 μm long)
Nitzschia heimii
Nitzschia inflatula?
[a]*Nitzschia kerguelensis*
Nitzschia lecointei?
Nitzschia lineola?
Nitzschia spp. (ribbon colonies)
Nitzschia subcurvata
Nitzschia turgiduloides?
Odontella weissflogii (vegetative)
[a]*Porosira pseudodenticulata*
Rhizosolenia alata
[a]*Stellarima microtrias* (two stages: vegetative and heavier)
Thalassiosira gerloffii (valve)
Thalassiosira gravida
[a]*Thalassiosira lentiginosa*
Thalassiosira ritscheri
Thalassiosira sp.
Thalassiosira trifulta
Thalassiosira tumida (type variety)
Tropidoneis belgicae
Tropidoneis glacialis

Note: Bucket sample was filtered through a 20-μm-mesh net from quiet water in ice field, with sea-surface temperature +0.1°C. Also observed were fecal pellets, some full of pigmented cells; *Distephanus speculum*; and *Phaeocystis* in single cells and rosettes.

[a] Some life stages found in sediments at Site 739.

Table 8. Plankton collected in vertical hauls and horizontal tows of 35-μm-mesh nets deployed 18–22 January 1988 from *Maersk Master* in the Site 739 area.

Chaetoceros atlanticus
Chaetoceros castracanei
Chaetoceros convolutus
Chaetoceros curvisetus
Chaetoceros sp. cf. *dichaeta* (Hyalochaete)
Chaetoceros sp. cf. *wighamii* (with smooth resting spores)
Corethron inerme (diameters from 8 to 65 μm)
Dactyliosolen tenuijunctus
Haslea sp.
Leptocylindrus mediterraneous (with *Solenicola setigera* epiphyte)
Nitzschia obliquecostata
Porosira glacialis
Rhizosolenia alata
[a]*Rhizosolenia hebetata* f. *semispina*
Rhizosolenia chunii
[a]*Synedra reinboldii*

Note: Also observed were *Distephanus speculum*; *Phaeocystis* (biflagellates, rosettes, and gelatinous colonies); *Parvicorbicula socialis*, choanoflagellate, in colonies; acantharians and polychaete larvae; and fecal pellets, both pigmented and bleached, some with *Chaetoceros* sp. cf. *wighamii* resting spores.

[a] Also found in sediment at Site 739.

Table 9. Diatom species found in Sample 119-739C-1R-1, 0 cm, at the sediment/water interface.

Actinocylus actinochilus
[a]*Asteromphalus parvulus*
[a]*Chaetoceros* resting spore (spiny)
[a]*Chaetoceros* resting spore (smooth)
Corethron (claws, valves)
Coscinodiscus sp.
Dactyliosolen antarctica (bands)
Eucampia antarctica (winter form)
Navicula directa
[a]*Nitzschia angulata*
Nitzschia cylindrus
Nitzschia kerguelenisis
Nitzschia obliquecostata
[a]*Nitzschia pseudonana*
[a]*Nitzschia ritscherii*
[a]*Nitzschia separanda*
[a]*Nitzschia sublinearis*
Porosira pseudodenticulata
Rhizosolenia hebetata f. *semispina*
[a]*Rouxia* sp.?
Stellarima microtrias (heavy valves)
Synedra reinboldii
[a]*Thalassiosira gracilis*
[a]*Thalassiosira gracilis* var. *expecta*
[a]*Thalassiosira* sp. cf. *gravida* (heavily silicified)
Thalassiosira lentiginosa
[a]*Thalassiosira oliverana*

[a] Not noted in this season in the plankton.

Antarctic shelf sediment physical properties have been carried out. The only studies based on deeper samples are from DSDP Leg 28 in the Ross Sea (Hayes, Frakes, et al., 1975), during which relatively little physical-properties information was collected.

In consideration of the preceding, the physical-properties program at Site 739 was aimed at obtaining a better understanding of variations in geotechnical parameters of different sediment types on the Antarctic continental shelf. Of particular interest were diamictons of glacial and glaciomarine origin. Furthermore, the shipboard program will provide the necessary background information for a shorebased study of consolidation characteristics of the cored sediments. The repeated glaciations of the continental shelf are expected to have left an imprint on the downcore-measured physical properties.

Parameters measured were (1) index properties, (2) undrained shear strength and (3) compressional-wave velocity. Techniques and laboratory procedures employed are discussed in the "Explanatory Notes" chapter. Because the RCB-cored diamictites do not fill the core liners completely, continuous logging with the *P*-wave logger (PWL) and GRAPE could only be run on a few sections in the upper part of the drilled section in Holes 739A and 739B. For Hole 739C, GRAPE measurements were run as 2-min counts on the same discrete samples used for velocity measurements in the Hamilton Frame Velocimeter. Owing to time constraints, the overconsolidated and pebbly character of the sediment, and the fact that no heatflow measurements were carried out at Site 739, thermal conductivity was not measured.

Three holes were drilled at Site 739, of which Holes 739A and 739B recovered only 5.73 and 1.92 m, respectively. The one physical-properties data point from Hole 739B is from the sequence that was also cored in Hole 739A and, thus, is not included in the Site 739 data plots.

Results

The sediments cored at Site 739 show an overall trend clearly indicative of a post-depositional loading history different from

that of a pure increase in sediment overburden with depth. Mainly as a result of the unsorted character of the diamictons and diamictites cored (see "Lithostratigraphy and Sedimentology" section) and the relatively small sediment volumes involved in the physical-properties measurements, individual parameters show considerable scatter. This is particularly evident in the velocity data, where clasts of high-velocity metamorphic rocks may have a large effect. However, the main trends are well defined, and seven different geotechnical units (G1–G7) have been identified based on slope changes in the plotted data. The differences can be seen in downhole plots of all of the parameters, but they are most evident in the index properties, with the exception of grain density, which stays fairly constant throughout the hole (Fig. 21 and Table 10). Where core recovery at apparent unit boundaries is poor, the boundary is generally placed midway between the two closest data points. Downhole logging results were used to help define the unit boundaries (see "Logging" section). However, the ODP practice of adjusting recovered material upcore (in cores with less than 100% recovery) may result in up to 9 m of mismatch between laboratory and *in-situ* measurements. Within the constraints set by the core recovery, the geotechnical units show a good match with the lithologic units at this site, particularly where unconformities are involved.

All physical properties measured at this site are given in Figure 21 and Table 10. Table 11 gives the range and mean values for the physical properties within the different geotechnical units.

Geotechnical Unit G1 (0 to 24.1 mbsf)

Because of poor core recovery, the lower boundary of this unit is not well defined, but is tentatively placed in accordance with lithologic Unit I (see "Lithostratigraphy and Sedimentology" section), immediately above the top of the first recovered harder interval. Core 119-739C-3R has fossils ranging from late Pliocene to Holocene in age (see "Biostratigraphy" section), thereby defining rough age brackets for the unit. The recovered part of this unit has about 20% water content, an average 41% porosity, and an average 2 g/cm^3 bulk density (only five data points, from the upper 5 m). Compressional-wave velocity varies from 1780 to 2490 m/s over the interval measured. The velocities are, however, measured in a core disturbed during retrieval because of a broken liner, and the lowest velocities could be ascribed to disturbance. Velocities of about 2000 m/s are not untypical for this type of firm diamicton, even if it is normally consolidated (Solheim and Pfirman, 1985). Vane and fall cone shear strengths range between 5 and 63 kPa, reflecting the normally consolidated but disturbed character of the recovered unit G1 material.

Geotechnical Unit G2 (24.1 to 170.5 mbsf)

Geotechnical unit G2 covers most of lithologic Unit II, which is a massive, structureless diamicton (see "Lithostratigraphy and Sedimentology" section) of a late Miocene to Pliocene age (see "Biostratigraphy" section). Because of the low core recovery in the upper 100 m of sediment, the character of this part of the unit is poorly defined. However, the overall appearance is that of relatively constant low values of water content and porosity, averaging 12.5% and 27%, respectively. There is a slight trend of higher values between 130 and 160 mbsf, with a peak at 142 mbsf, decreasing toward the lower boundary of the unit. Bulk density shows similar trends, but with a considerable scatter seen in both the gravimetrically measured values and in the GRAPE data. The average densities are 2.37 and 2.30 g/cm^3, respectively, with a low value that corresponds to the water content and porosity high between 130 and 160 mbsf.

Pocket penetrometer undrained shear-strength values are at the upper boundary of the measurable range for this instrument, at about 800–900 kPa. The sediment is rather sandy, and the measured shear-strength values are uncertain. However, the high readings confirm the visual appearance of a highly overconsolidated sediment.

Compressional-wave velocities average about 2340 m/s, except for the uppermost part (Core 119-739C-4R), which has a velocity of 2100 m/s. Because this is a noncemented sediment, the high velocities provide additional evidence of its highly compacted state. The travel distance for the compressional waves is typically 3–6 cm, so the large scatter can be accounted for by clasts within the samples. Most of the scatter is on the high side of the general trend, up to 2830 m/s.

Geotechnical Unit G3 (170.5 to 198.2 mbsf)

Geotechnical unit G3 corresponds roughly to lithologic Subunits IIIA and IIIB, a stratified diamicton showing diffuse bedding and slickensides on fractures and a diatomaceous sandy, silty claystone of early Oligocene to late Eocene age (see "Lithostratigraphy and Sedimentology" and "Biostratigraphy" sections). The latter material was recovered in Core 119-739C-27R, which has a recovery of only 0.95 m. Most of the sediment was broken through drilling and subsequent splitting, but individual pieces showed densely spaced fracture planes.

Unit G3 is characterized by an increase in water content from 14% to 22% and in porosity from 31% to 42%. Bulk density decreases from 2.35 to 2.09 g/cm^3. Compressional-wave velocity decreases from a peak of 2537 m/s to a distinct low, confirmed by several data points, with a minimum of 2078 m/s. Despite the tendency toward lower velocity and higher porosity, shear strength was not measurable in this unit (i.e., it was above the upper limit of the pocket penetrometer, 900 kPa).

Geotechnical Unit G4 (198.2 to 255.5 mbsf)

Geotechnical unit G4 approximates most of lithologic Subunit IIIC, a stratified diamictite showing wispy bedding, slump and load structures, bioturbation, faults with slickensides, and minor rhythmically laminated horizons (see "Lithostratigraphy and Sedimentology" section). All of the unit appears to be of early Oligocene–late Eocene age (see "Biostratigraphy" section).

After a jump (in a region of poor core recovery) back to low water content and porosity and high bulk density, geotechnical unit G4 has another increase and decrease in these respective parameters. The trend is similar to that observed in geotechnical unit G3. The water content of unit G4 varies from 11.36% to 32.87%, porosity from 25.42% to 57.5%, and gravitationally measured bulk density from 1.80 to 2.48 g/cm^3. Similar values are found for the GRAPE densities, although the maximum GRAPE value is only 2.32 g/cm^3. Compressional-wave velocity varies between 2739 and 1887 m/s, averaging 2254 m/s. The values around 2000 m/s near the lower unit boundary are the lowest below unit G1. Undrained shear strength appears to be too high for the shipboard pocket penetrometer.

The changes in measured values in unit G4 appear to be somewhat different from the overlying units, showing a stepwise character, with relatively constant values in the upper and middle parts of the unit. This is particularly evident in the water content and porosity plots.

Geotechnical Unit G5 (255.5 to 310.5 mbsf)

Geotechnical unit G5 includes the lowermost part of lithologic Subunit IIIC and most of Unit IV, the latter being an essentially massive, structureless diamictite (see "Lithostratigraphy and Sedimentology" section) of probable early Oligocene to late Eocene age, although the age is poorly constrained (see "Biostratigraphy" section).

Unit G5 shows an overall change back to low water content and porosity and high bulk density. The variable values at the

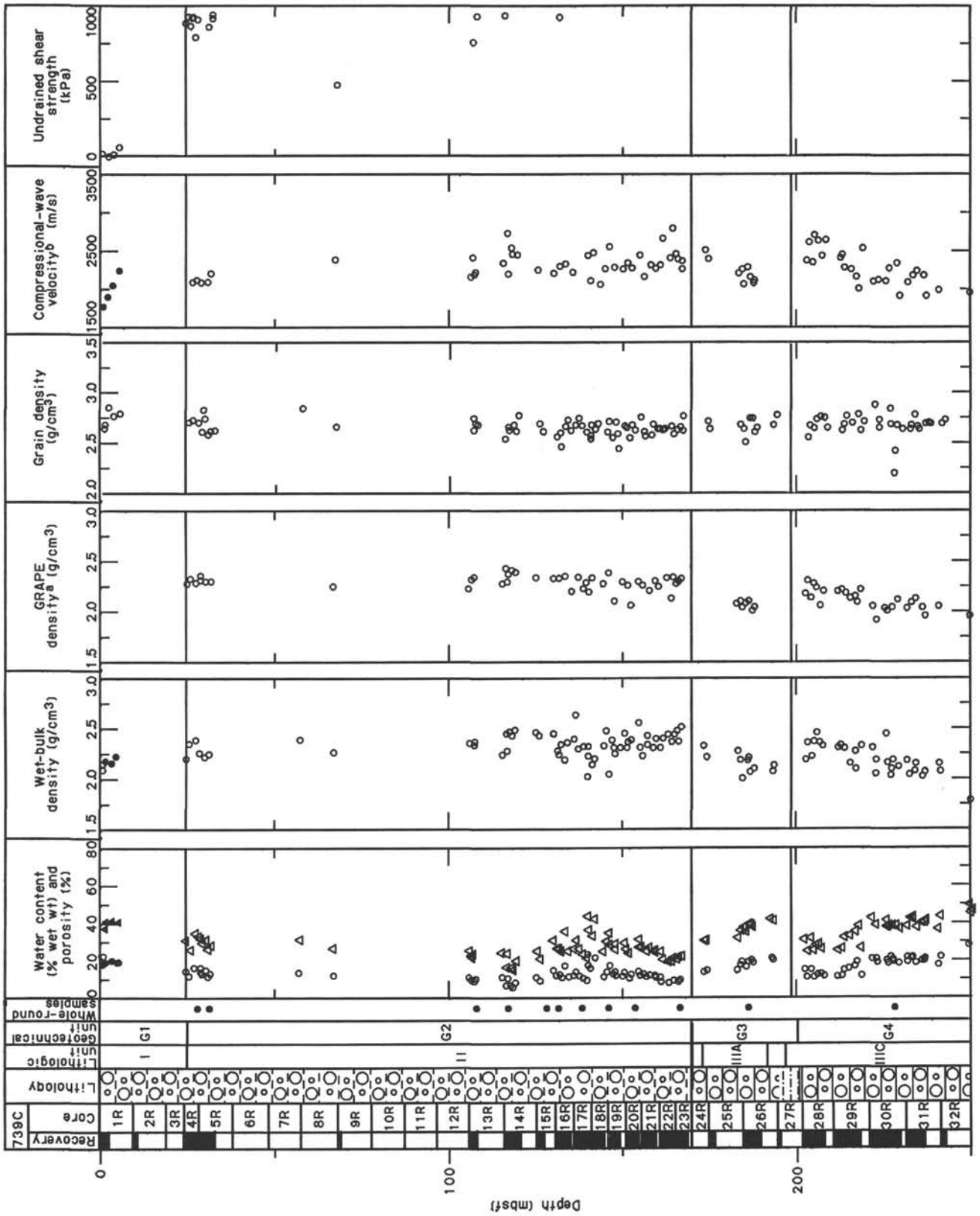
739C
Recovery
Core
Lithology
Lithologic unit
Geotechnical unit
Whole-round samples
Water content (% wet wt) and porosity (%)
Wet-bulk density (g/cm3)
GRAPE densitya (g/cm3)
Grain density (g/cm3)
Compressional-wave velocityb (m/s)
Undrained shear strength (kPa)
Depth (mbsf)
I
II
IIIA
IIIC
G1
G2
G3
G4

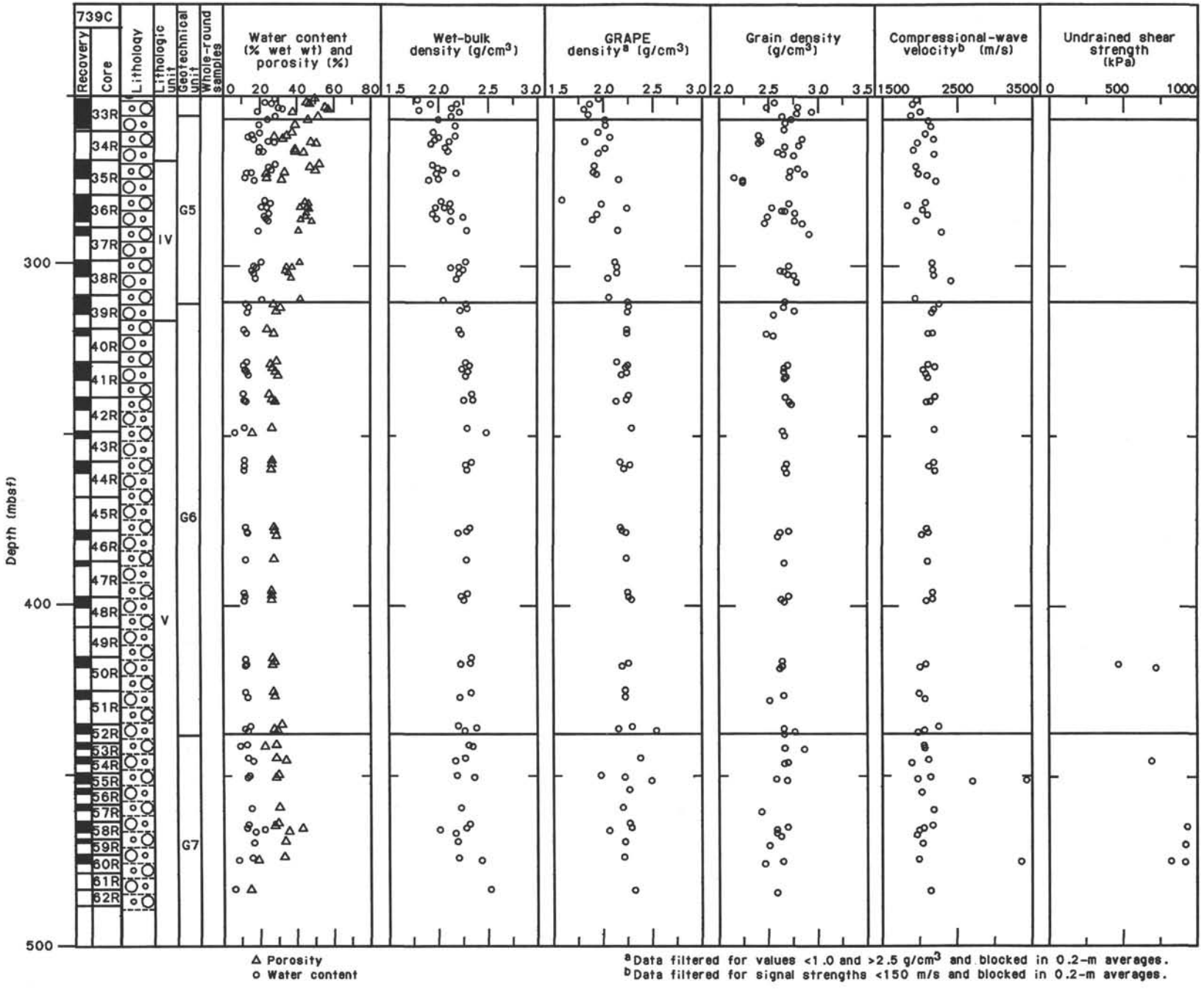

Figure 21. Physical-property profiles, Site 739. Data from both Holes 739A and 739C are included, but only four data points in the upper 5 m of the sediment column are from Hole 739A.

Table 10. Physical-properties data, Site 739.

Core, section, interval (cm)[a]	Depth (mbsf)	Water content (% wet wt)	Porosity (%)	Wet-bulk density (g/cm^3)	Dry-bulk density (g/cm^3)	Grain density (g/cm^3)	GRAPE density (g/cm^3)	Undrained shear strength[b] (kPa)	Compressional-wave velocity[c] (m/s)
119-739A-									
1H-1, 60	0.60	18.50	37.28	2.17	1.77	2.66		23 W	1782.6
1H-2, 70	1.92	19.70	40.93	2.20	1.77	2.87		5 W	1912.4
1H-3, 60	3.32	20.57	41.60	2.18	1.73	2.79		15 W	2066.1
2H-1, 40	5.00	19.67	40.49	2.24	1.80	2.82		63 W	2263.2
119-739B-									
1H-1, 65	0.65	21.77	43.62	2.09	1.63	2.82		11 W	2490.2
1H-1, 65	0.65							15 F	
1H-1, 136	1.36							24 F	
119-739C-									
1R-1, 100	1.00	22.83	43.96	2.10	1.62	2.69			
4R-1, 20	24.30							890 P	
4R-1, 80	24.90	14.68	31.56	2.22	1.90	2.72		930 P	
4R-1, 120	25.30						2.29	870 P	
4R-2, 20	25.80							925 P	
4R-2, 40	26.00	11.88	26.63	2.37	2.08	2.74	2.34		2106.0
4R-2, 70	26.30							930 P	
4R-2, 110	26.70							795 P	
4R-3, 20	27.30							915 P	
4R-3, 50	27.60	16.88	35.20	2.41	2.01	2.72	2.30		2140.6
4R-4, 20	28.80	16.50	33.76	2.28	1.90	2.62	2.32		2106.7
5R-1, 30	29.00	14.85	32.74	2.38	2.03	2.84	2.37		2099.0
5R-1, 88	29.58	13.69	30.09	2.44	2.11	2.76			
5R-2, 24	30.44	15.54	31.90	2.24	1.89	2.59	2.31	863 P	2113.0
5R-2, 104	31.24	12.40	26.79	2.48	2.17	2.63			
5R-2, 120	31.40							945 P	
5R-3, 10	31.80	13.35	28.63	2.27	1.97	2.64	2.31		2229.0
5R-3, 30	32.00							916 P	
8R-CC, 2	57.62	14.02	31.48	2.41	2.07	2.86			
9R-CC, 8	67.38	12.44	27.21	2.29	2.01	2.67	2.26	480 P	2411.0
13R-1, 47	106.37	11.32	25.77	2.38	2.11	2.76	2.24	760 P	2173.0
13R-1, 87	106.77	10.33	23.03	2.37	2.12	2.64			2431.0
13R-1, 131	107.21	9.59	22.03	2.39	2.17	2.71	2.33		2208.0
13R-2, 13	107.53	10.49	23.74	2.36	2.11	2.70	2.35	935 P	2234.0
14R-1, 20	115.70	11.48	24.64	2.26	2.00	2.56	2.29	940 P	2365.4
14R-1, 139	116.89	7.10	16.74	2.47	2.29	2.67	2.44		2760.0
14R-2, 9	117.09	10.99	24.28	2.30	2.04	2.64	2.31		2215.4
14R-2, 91	117.91	7.08	16.77	2.49	2.32	2.69	2.39		2561.4
14R-3, 8	118.58	6.43	15.08	2.45	2.29	2.63	2.42		2487.0
14R-3, 81	119.31						2.41		2482.4
14R-3, 96	119.46	8.52	20.37	2.51	2.29	2.79			
15R-1, 30	125.50	11.42	25.59	2.48	2.20	2.71	2.35		2274.0
15R-1, 118	126.38	9.47	21.31	2.45	2.22	2.63			
16R-1, 10	130.40	15.14	31.21	2.47	2.10	2.58	2.34		2232.0
16R-1, 64	130.94							930 P	
16R-1, 128	131.58	12.57	26.99	2.30	2.01	2.61			
16R-2, 15	131.95	13.06	26.78	2.26	1.96	2.47	2.35		2324.5
16R-2, 108	132.88	11.50	25.52	2.36	2.09	2.68			
16R-3, 26	133.56	17.37	36.18	2.21	1.82	2.74	2.36		2351.8
16R-3, 121	134.51	11.62	25.41	2.38	2.11	2.63			
17R-1, 65	135.65						2.21		2235.3
17R-1, 116	136.16	12.08	26.66	2.42	2.13	2.69			
17R-2, 33	136.83	14.34	31.22	2.66	2.28	2.76			
17R-2, 117	137.67	12.15	26.70	2.32	2.04	2.68	2.35		
17R-3, 107	139.07	10.83	23.88	2.34	2.09	2.62	2.24		2506.4
17R-4, 50	140.00	9.94	21.87	2.34	2.11	2.58			2466.7
18R-1, 23	140.23	23.91	44.16	2.04	1.55	2.55	2.30		
18R-1, 55	140.55	18.03	36.81	2.25	1.84	2.69	2.20		2132.0
18R-2, 15	141.65	16.33	33.72	2.16	1.81	2.65	2.35		2500.0
18R-2, 88	142.38	21.86	42.73	2.22	1.74	2.71			
18R-3, 40	143.40								2075.3
19R-1, 16	144.86	11.58	25.24	2.35	2.08	2.62	2.29		2287.6
19R-1, 100	145.70	14.23	30.72	2.50	2.14	2.72			
19R-2, 13	146.33	17.61	35.03	2.06	1.70	2.56	2.40		2584.0
19R-2, 94	147.14	13.30	29.00	2.41	2.09	2.72			
19R-3, 10	147.80	13.94	29.31	2.34	2.01	2.60	2.11		2306.2
19R-3, 60	148.30	12.95	26.40	2.27	1.98	2.45			
20R-1, 49	150.19	11.99	26.44	2.33	2.05	2.68	2.31		2281.5
20R-1, 114	150.84	14.00	29.94	2.48	2.13	2.67			
20R-2, 20	151.40	12.58	26.65	2.33	2.04	2.56	2.27		2361.7
20R-2, 100	152.20	10.94	24.54	2.39	2.13	2.69			
20R-3, 1	152.71	12.80	27.57	2.41	2.10	2.64	2.07		2297.9

Table 10 (continued).

Core, section, interval (cm)[a]	Depth (mbsf)	Water content (% wet wt)	Porosity (%)	Wet-bulk density (g/cm^3)	Dry-bulk density (g/cm^3)	Grain density (g/cm^3)	GRAPE density (g/cm^3)	Undrained shear strength[b] (kPa)	Compressional-wave velocity[c] (m/s)
119-739C-									
21R-1, 47	154.77	14.54	31.71	2.58	2.20	2.77	2.31		2467.0
21R-1, 118	155.48	12.74	27.32	2.33	2.04	2.62			
21R-2, 28	156.08	13.17	27.79	2.25	1.96	2.58	2.27		2181.1
21R-2, 140	157.20	11.79	25.39	2.36	2.08	2.59			
21R-3, 68	157.98	12.54	27.49	2.45	2.14	2.69	2.22		2336.1
21R-3, 117	158.47								
22R-1, 24	159.54	11.92	26.06	2.33	2.05	2.65	2.32		2291.7
22R-1, 77	160.07	11.31	24.97	2.43	2.16	2.65			
22R-2, 15	160.95	11.45	25.16	2.33	2.06	2.64	2.26		2335.1
22R-2, 65	161.45	9.23	20.95	2.42	2.20	2.65			2693.2
22R-3, 127	163.57	8.64	19.89	2.47	2.25	2.67	2.35		2428.6
23R-1, 41	164.41	8.96	20.09	2.39	2.18	2.60	2.14		2830.0
23R-1, 131	165.31	9.51	21.48	2.46	2.23	2.64	2.35		2490.0
23R-2, 37	165.87	9.28	21.19	2.50	2.27	2.67	2.29		2414.8
23R-2, 117	166.67	9.97	22.36	2.40	2.16	2.64	2.32		2389.3
23R-CC, 20	167.03	9.80	22.91	2.54	2.29	2.78	2.34		2281.4
25R-1, 28	173.88	14.29	30.94	2.35	2.02	2.73			2536.9
25R-1, 99	174.59	14.89	31.37	2.24	1.91	2.65			2422.7
26R-1, 19	183.39	15.19	32.22	2.30	1.95	2.69	2.09		2224.9
26R-1, 108	184.28	17.92	36.32	2.21	1.81	2.65	2.11		2273.5
26R-2, 10	184.80	19.78	37.99	2.02	1.62	2.52	2.05		2077.6
26R-2, 113	185.83	16.97	35.68	2.21	1.84	2.76	2.09		2301.5
26R-3, 46	186.66	19.69	40.02	2.23	1.79	2.76	2.11		2176.6
26R-3, 113	187.33	20.47	39.90	2.09	1.66	2.62			
26R-3, 134	187.54						2.03		2097.3
26R-CC, 27	187.97	19.26	38.47	2.12	1.71	2.66	2.05		2127.8
27R-1, 17	193.07	21.79	42.51	2.09	1.64	2.69			
27R-1, 70	193.60	20.78	41.91	2.15	1.71	2.79			
28R-1, 30	202.80	15.45	31.64	2.21	1.87	2.57	2.19		2392.5
28R-1, 108	203.58	11.44	25.42	2.38	2.10	2.68	2.32		2637.3
28R-2, 50	204.50	15.48	32.41	2.24	1.89	2.66	2.15		2373.2
28R-2, 135	205.35	11.36	25.73	2.39	2.12	2.75	2.29		2739.4
28R-3, 79	206.29	12.75	28.46	2.48	2.17	2.77	2.25		2664.7
28R-4, 27	207.27	13.15	29.11	2.38	2.07	2.76	2.07		2460.0
28R-4, 128	208.28	12.25	26.76	2.35	2.06	2.66	2.21		2674.6
29R-1, 33	212.53	11.97	26.05	2.34	2.06	2.63	2.21		2444.4
29R-1, 103	213.23	12.14	26.90	2.35	2.06	2.70	2.23		2472.0
29R-2, 33	214.03	15.11	32.77	2.33	1.98	2.78	2.19		2303.1
29R-3, 41	215.61	16.00	33.69	2.18	1.83	2.71	2.14		2281.3
29R-4, 55	217.25	16.84	35.79	2.29	1.91	2.80	2.16		2178.8
29R-4, 132	218.02	19.69	38.82	2.11	1.69	2.63	2.10		2026.8
29R-5, 84	219.04	12.12	26.98	2.35	2.07	2.72	2.23		2559.8
30R-1, 30	222.10	21.20	43.40	2.33	1.84	2.89	2.06		2120.8
30R-1, 139	223.19	21.20	39.40	2.07	1.63	2.66			
30R-2, 21	223.51	19.41	39.37	2.21	1.78	2.74	1.92		2136.4
30R-3, 95	225.75						2.04		2124.0
30R-3, 150	226.30	20.41	41.90	2.47	1.96	2.86			
30R-4, 38	226.68	19.06	38.53	2.18	1.76	2.70	2.02		2290.0
30R-4, 109	227.39	22.17	38.31	2.05	1.60	2.21			
30R-5, 13	227.93	21.07	39.03	2.11	1.67	2.43	2.05		
30R-5, 58	228.38	19.69	39.35	2.21	1.78	2.69			
30R-5, 123	229.03								2362.3
30R-6, 48	229.78	18.78	37.67	2.14	1.74	2.65	2.13		1926.3
31R-1, 68	232.08	19.58	38.89	2.20	1.77	2.65	2.04		2113.7
31R-1, 136	232.76	22.25	43.12	2.06	1.60	2.69			
31R-2, 66	233.56	21.75	43.42	2.09	1.64	2.80	2.10		2193.4
31R-2, 110	234.00	22.10	42.74	2.09	1.62	2.67			
31R-3, 25	234.65	19.06	38.10	2.17	1.76	2.65	2.14		2260.9
31R-4, 88	236.78	20.45	40.68	2.04	1.63	2.71	2.05		2205.9
31R-4, 145	237.35	20.46	40.75	2.09	1.67	2.72			
31R-5, 19	237.59	21.31	42.01	2.09	1.64	2.71	1.96		1923.1
32R-1, 18	241.28	18.14	37.15	2.17	1.77	2.71	2.06		2000.0
32R-1, 92	242.02	22.54	44.04	2.09	1.62	2.74			
33R-1, 44	251.14	28.60	50.36	1.80	1.29	2.57	1.96		1962.4
33R-1, 144	252.14	23.18	45.48	2.20	1.69	2.81			
33R-2, 19	252.39	26.72	47.23	1.93	1.41	2.49	1.87		1911.8
33R-2, 146	253.66	30.39	55.95	2.15	1.49	2.95			
33R-3, 40	254.10	32.87	57.50	1.82	1.22	2.80	1.81		2011.1
33R-3, 126	254.96	19.03	38.01	2.23	1.80	2.65			
33R-4, 20	255.40						1.85		1887.0
33R-4, 88	256.08	28.76	52.13	2.14	1.52	2.74			
33R-5, 44	257.14	24.71	46.43	2.02	1.52	2.68	2.03		2124.1
33R-6, 68	258.88	20.18	39.89	2.18	1.74	2.67	2.03		2165.6
34R-1, 42	260.82	20.40	37.80	1.97	1.57	2.41	1.95		2085.7
34R-1, 130	261.70	16.10	35.00	2.19	1.84	2.85			

Table 10 (continued).

Core, section, interval (cm)[a]	Depth (mbsf)	Water content (% wet wt)	Porosity (%)	Wet-bulk density (g/cm^3)	Dry-bulk density (g/cm^3)	Grain density (g/cm^3)	GRAPE density (g/cm^3)	Undrained shear strength[b] (kPa)	Compressional-wave velocity[c] (m/s)
119-739C-									
34R-2, 37	262.27	14.20	28.30	2.02	1.73	2.43	2.07		2196.9
34R-2, 80	262.70	17.10	32.90	1.98	1.64	2.41			
34R-3, 10	263.50	24.94	48.04	2.13	1.60	2.82	1.82		1969.4
34R-3, 48	263.88	28.53	51.29	1.94	1.39	2.68			
34R-4, 59	265.49	20.27	39.54	2.09	1.67	2.61	2.03		1915.3
34R-4, 130	266.20	20.11	39.75	2.11	1.68	2.66			
34R-5, 25	266.65	22.52	44.27	2.12	1.64	2.77	1.96		2214.3
35R-1, 32	270.32	29.00	53.04	1.96	1.39	2.81	1.92		1964.6
35R-1, 116	271.16	25.41	47.86	2.01	1.50	2.73			
35R-2, 50	272.00	26.43	50.56	2.07	1.52	2.89	1.91		1988.2
35R-2, 122	272.72	16.13	33.96	2.20	1.85	2.72			
35R-3, 1	273.01	12.89	23.92	2.00	1.74	2.16	1.94		2110.1
35R-3, 123	274.23	12.63	24.27	2.02	1.77	2.25			
35R-4, 19	274.69	17.65	32.27	1.92	1.58	2.25	2.16		2233.9
36R-1, 108	280.78	23.31	44.91	2.05	1.57	2.72	1.59		2089.1
36R-2, 60	281.80	26.02	46.98	2.14	1.58	2.55	1.99		1843.4
36R-2, 147	282.67	21.87	42.23	1.99	1.56	2.65			
36R-3, 20	282.90	24.60	46.31	2.08	1.57	2.68	2.25		2059.0
36R-3, 85	283.55	24.88	47.54	2.15	1.62	2.78			
36R-4, 47	284.67	25.59	45.92	1.96	1.46	2.50	1.95		2114.5
36R-4, 140	285.60	23.38	45.50	2.27	1.74	2.78			
36R-5, 54	286.24	23.77	43.21	2.00	1.52	2.47	1.90		1968.7
36R-5, 98	286.68	25.07	48.55	2.15	1.61	2.86			
37R-1, 30	289.60	19.75	41.50	2.31	1.85	2.93	2.16		2309.2
38R-1, 8	298.98	21.42	42.23	2.30	1.81	2.72	2.13		2186.4
38R-1, 145	300.35	17.35	35.18	2.15	1.78	2.63			
38R-2, 14	300.54	18.88	38.10	2.23	1.81	2.68	2.15		2197.5
38R-2, 96	301.36	16.31	34.19	2.27	1.90	2.71			
38R-3, 5	301.95	17.20	36.18	2.23	1.85	2.77	2.15		2210.5
38R-3, 60	302.50								
38R-4, 20	303.60	17.99	37.67	2.21	1.82	2.80	2.06		2442.8
39R-1, 25	308.85						2.07		1954.4
39R-1, 121	309.81	21.80	42.39	2.07	1.62	2.68			
39R-2, 30	310.40						2.26		2280.9
39R-2, 108	311.18	12.85	27.92	2.30	2.00	2.67			
39R-3, 46	312.06	14.60	31.88	2.31	1.97	2.78			
39R-3, 58	312.18						2.27		2203.6
39R-3, 148	313.08	14.22	29.52	2.24	1.92	2.57	2.26		2180.5
40R-1, 50	318.70	11.80	24.60	2.23	1.97	2.49	2.26		2188.5
40R-1, 127	319.47	13.40	28.00	2.25					2125.6
41R-1, 24	328.04	13.60	29.70	2.30	1.98	2.71	2.15		2126.1
41R-1, 123	329.03	11.90	26.20	2.34	2.06	2.68	2.26		2222.2
41R-2, 60	329.90	12.70	27.60	2.26	1.97	2.67	2.24		2066.9
41R-3, 16	330.96	13.30	29.00	2.32	2.01	2.70	2.25		2102.2
41R-3, 107	331.87	14.30	30.60	2.30	1.97	2.68	2.20		2123.2
42R-1, 22	337.72	11.60	25.90	2.36	2.09	2.69	2.27		2229.3
42R-1, 146	338.96	12.18	27.14	2.37	2.08	2.73	2.25		2161.5
42R-2, 46	339.46	13.04	28.88	2.28	1.99	2.75	2.14		2106.5
43R-1, 18	347.28	12.24	26.76	2.31	2.03	2.66	2.30		2212.8
43R-CC, 14	348.74	6.86	16.26	2.51	2.34	2.68			
44R-1, 44	357.24	12.38	27.28	2.36	2.06	2.70	2.18		2215.4
44R-2, 3	358.33	12.35	27.07	2.30	2.02	2.68	2.28		2140.8
44R-2, 117	359.47	12.07	26.71	2.31	2.03	2.70	2.22		2219.9
46R-1, 38	376.58	12.85	28.30	2.34	2.04	2.72	2.19		2112.4
46R-1, 131	377.51	13.41	28.62	2.31	2.00	2.63	2.21		2147.8
46R-2, 45	378.15	13.82	29.22	2.22	1.92	2.61	2.24		2048.2
47R-1, 22	386.12	13.04	28.33	2.31	2.01	2.68	2.25		2125.0
48R-1, 15	395.75	12.15	26.98	2.32	2.04	2.72	2.27		2200.0
48R-1, 118	396.78	12.50	27.10	2.26	1.98	2.65	2.28		2188.0
48R-2, 33	397.43	12.30	27.00	2.28	2.00	2.67	2.30		2109.5
50R-1, 29	415.19	12.70	27.50	2.36	2.06	2.65			
50R-1, 80	415.70							476 P	
50R-1, 134	416.24	13.20	28.40	2.35	2.04	2.65	2.27		2102.2
50R-2, 33	416.73							727 P	
50R-2, 53	416.93	12.64	27.28	2.25	1.97	2.63	2.20		2020.2
51R-1, 26	424.76	12.72	27.69	2.35	2.05	2.67	2.24		2008.8
51R-2, 14	426.14	13.86	28.65	2.24	1.93	2.53	2.24		2091.8
51R-2, 36	434.56	15.34	32.30	2.22	1.88	2.67	2.30		2282.1
52R-1, 120	435.40	12.51	28.09	2.41	2.11	2.78	2.17		2081.6
52R-2, 22	435.92	14.17	30.26	2.29	1.96	2.67	2.56		1990.0
53R-1, 94	440.14	13.47	29.11	2.33	2.01	2.68	2.26	696 P	2076.2
53R-CC, 10	440.59	9.63	23.19	2.37	2.14	2.88	2.25		2090.4
54R-1, 25	444.15	13.55	29.45	2.29	1.98	2.71	2.39		2133.3
54R-1, 104	444.94	16.75	34.63	2.19	1.83	2.67			1902.7
55R-1, 29	449.19	14.77	30.69	2.21	1.89	2.60	1.99		2161.7

Table 10 (continued).

Core, section, interval (cm)[a]	Depth (mbsf)	Water content (% wet wt)	Porosity (%)	Wet-bulk density (g/cm^3)	Dry-bulk density (g/cm^3)	Grain density (g/cm^3)	GRAPE density (g/cm^3)	Undrained shear strength[b] (kPa)	Compressional-wave velocity[c] (m/s)
119-739C-									
55R-1, 98	449.88	13.57	29.43	2.39	2.07	2.70	2.23		1981.9
55R-2, 22	450.62						2.50		2727.9
55R-2, 25	450.65								3476.7
56R-1, 13	453.63						2.28		2036.1
57R-1, 25	458.75	15.67	30.89	2.25	1.90	2.44	2.21		2204.3
58R-1, 15	463.35							940 P	
58R-1, 30	463.50	14.02	30.31	2.34	2.01	2.71	2.28		2192.4
58R-1, 109	464.29	13.40	28.40	2.30	1.99	2.60	2.30		2069.9
58R-2, 45	465.15	22.90	43.30	2.03	1.57	2.60	2.07		2007.1
58R-2, 130	466.00	17.87	36.15	2.19	1.80	2.64			1977.3
59R-1, 40	468.60							925 P	
59R-1, 55	468.75	17.18	33.97	2.21	1.83	2.52	2.23		2053.6
60R-1, 35	473.25							830 P	
60R-1, 47	473.37	16.09	33.39	2.23	1.88	2.66	2.22	925 P	2004.3
60R-1, 130	474.20	8.94	19.28	2.46	2.24	2.47			3401.6
62R-CC, 4	482.64	6.49	15.06	2.55	2.38	2.60	2.33		2163.8

[a] Interval in which measurement was made never exceeds 10 cm.
[b] Instrument used: F = fall cone aparatus; P = pocket pentrometer; W = Wykeham-Farrance motorized vane.
[c] Measured normal to bedding (A direction).

Table 11. Physical-properties minimum, mean, and maximum values for the geotechnical units of Site 739.

Geotechnical unit		Water content (% wet wt)	Porosity (%)	Wet-bulk density (g/cm^3)	GRAPE density (g/cm^3)	Compressional-wave velocity (m/s)	Undrained shear strength[a] (kPa)
	minimum	18.50	37.28	2.09	No	1783	5
G1	mean	20.50	41.31	2.16	data	2103	22
	maximum	22.83	43.96	2.24		2490	63
	minimum	6.43	15.08	2.04	2.07	2075	480
G2	mean	12.53	27.04	2.37	2.30	2343	868
	maximum	23.59	44.16	2.66	2.44	2830	945
	minimum	14.29	30.94	2.09	2.03	2078	
G3	mean	18.28	37.03	2.18	2.08	2248	
	maximum	21.79	42.51	2.35	2.11	2537	
	minimum	11.36	25.42	1.80	1.81	1887	
G4	mean	19.08	38.02	2.19	2.09	2254	
	maximum	32.87	57.50	2.48	2.32	2739	
	minimum	12.63	23.92	1.92	1.59	1843	
G5	mean	21.31	41.11	2.10	2.01	2106	
	maximum	29.00	53.04	2.31	2.25	2443	
	minimum	6.86	16.26	2.22	2.14	2009	476
G6	mean	12.77	27.69	2.31	2.24	2149	602
	maximum	15.34	32.30	2.51	2.30	2282	727
	minimum	6.49	15.06	2.03	1.99	1903	696
G7	mean	14.18	29.74	2.30	2.27	2236	863
	maximum	22.90	43.30	2.55	2.56	3476	940

[a] Measured normal to bedding (A direction); no data indicates sediment too stiff to measure.

lower boundary of the unit average about 20% water content, 38% porosity, and 2.25 g/cm^3 bulk density. Undrained shear strength is too high to be measured by shipboard instruments. Compressional-wave velocity increases from about 2000 to about 2200 m/s.

Within the overall trend, this unit displays a cyclic trend that does not appear random, particularly in the upper part. The small-scale variations are confirmed by more than one data point, reducing the probability that they are the result of erroneous measurement. A good high-resolution record is, however, severely hampered by an uneven recovery that averages $<60\%$ in this interval.

Geotechnical Unit G6 (310.5 to 435 mbsf)

The upper boundary of geotechnical unit G6 roughly corresponds to the upper boundary of lithologic Unit V, a structureless diamicton that is heavily broken by drilling effects (see "Lithostratigraphy and Sedimentology" section). Lithologic Unit V extends to total depth at 486.8 mbsf. The age is uncertain, but may range from pre-early Oligocene to late Eocene (see "Biostratigraphy" section).

This unit shows a distinctly different trend from the cyclic changes in physical properties observed in the overlying units. Most of the properties stay relatively constant throughout the unit, with averages of 12.77% water content, 27.69% porosity, and 2.31 g/cm^3 bulk density. Compressional-wave velocity shows a slight downward decrease in the unit of approximately 100 m/s. The material of unit G6 appears to be less competent than the sediment of the preceding units. It is more disturbed by drilling, and individual pieces were more easily broken during the sawing of samples for velocity and index-properties measurements. However, only two shear-strength measurements were obtained, in

Core 119-739C-50R, and their different results (727 and 476 kPa) make their value dubious.

Recovery became increasingly poor in this unit, averaging only 24%. Hence, an "aliasing" effect cannot be excluded as at least a part of the reason for the smoothness of the graphs in this interval.

Geotechnical Unit G7 (435 to 486.8 mbsf)

Average values of the physical properties do not change significantly in geotechnical unit G7, but the scatter is larger. Cementing effects are seen in thin layers, and the varying degree of cementation could be the main reason for the variation. The two velocities between 3400 and 3500 m/s were measured on intervals of well-cemented diamictite. Pocket penetrometer shear-strength values obtained from this unit vary between 700 and 940 kPa. However dubious the values, that penetration was at all obtainable indicates a less competent sediment (with the exception of the cemented intervals) than the overlying units.

Summary and Discussion

The physical properties of the glacial sediments at Site 739 show the effects of variations in glacial coverage and a post-depositional history of excess loading. Values in the uppermost part of the drilled sequence are typical for normally consolidated ice-proximal glacial diamictons (Solheim, in press). These values change to values clearly indicative of overconsolidation (low porosity and high shear strength) within the upper 24 mbsf. As a result of poor core recovery, the change from normally consolidated to overconsolidated sediments cannot be resolved in greater detail. On an average for Hole 739C, water content and porosity remain low, whereas seismic velocity, shear strength (a few measurements), and bulk density are high. Grain density stays relatively constant at about 2.7 g/cm^3, indicating a siliciclastic composition throughout, which is in accordance with smear slide descriptions (see "Lithostratigraphy and Sedimentology" section) and serves to control the quality of the other index-property measurements. Within the overall trend, the downhole physical-property profiles show frequent, significant variations, and seven geotechnical units have been defined, based mostly on intervals of decreasing, increasing, or constant values.

Particularly the middle part of the drilled section (geotechnical units G3 to G5) shows a sequence of alternating increasing and decreasing trends, including downhole velocity reversals. Within the environmental framework presented by the geographical location and cored sediment type, the most probable explanation for the cyclicity is the effect of glacial-interglacial cycles. Fluctuating glaciers may have caused (1) erosion of previously deposited sediments, particularly glaciomarine sediments deposited since the previous period of expanded ice, (2) a varying degree of overconsolidation, both owing to ice loading and erosion and to lithologic variations in the deposited sediments with varying distance to the grounding line. Preliminary results of post-cruise grain-size analyses indicate a close correlation between the physical properties and grain-size distribution, with increasing mud (<63 μm) proportional to increasing water content and porosity and inversely proportional to bulk density and velocity.

The lithologic description indicates only one unit of lodgement till (Unit II; "Lithostratigraphy and Sedimentology" section) and hence, only one period of ice-loading and glacial erosion. The nature of compaction should thus imply a decreasing degree of overconsolidation with depth, which is also indicated in the physical-properties profiles. However, both biostratigraphy and logging results indicate previous periods of erosion/nondeposition (see "Biostratigraphy" and "Logging" sections) and, therefore, more than one period of excess loading, at stratigraphically lower intervals than lithologic Unit II. Although this could also cause fluctuations in the physical-properties profiles, a differentiation of compaction from grain-size effects is impossible at this stage. Consolidation can be only quantitatively treated through laboratory tests. Previously published empirical functions relating the state of consolidation to undrained shear strength, effective overburden pressure, and plasticity index (Skempton, 1954, 1970; Andresen et al., 1979) are not considered adequate here because they are based on well-sorted clays from shallower burial depths. Furthermore, to use undrained shear strengths quantitatively, more accurate measurements simulating *in-situ* conditions are necessary. The use of the pocket penetrometer in this study was with a relatively inaccurate instrument, involved only a small and possibly unrepresentative volume of sediment, and obtained measurements that were near the upper limit of the instrument range.

The grain-size distribution will reflect the distance to the grounding line, with an increasing fine fraction implying a more distal environment. Hence, units G3 to G5 in particular record significant fluctuations in the grounding line position. Variations on a smaller scale, such as in the lower part of unit G2 and the upper part of unit G5, may have a similar origin. Recovery varied significantly throughout Hole 739C, and even if a relatively dense sampling program had been performed, aliasing effects would have still severely hampered resolution in the physical-properties profiles. Thus, the exact shape of the individual cycles may not be recorded correctly. Because of the poor biostratigraphic control, the number and relative size of the hiatuses are uncertain. Therefore, parts of the stratigraphic record may be missing. Distal glaciomarine sediments would have been particularly susceptible to erosion during subsequent advances of grounded ice.

Geotechnical unit G6 (and possibly below) marks an apparently different environment than that of the units above. The smooth shape of the curve may indicate a stable position of the grounding line over a relatively long time span. However, diagenetic effects influencing the physical properties cannot be excluded at this depth. Smear slide sediment descriptions indicate micrite-bearing sediments in a few discrete, thin intervals from approximately 300 mbsf, but on average, this seems to be a minor component (see "Lithostratigraphy and Sedimentology" section). The chemical analyses of the carbonate content performed on core catchers and physical-properties samples from 200 mbsf indicate a carbonate content generally less than 2% (see "Organic Geochemistry" section), with the exception of two peak values of 18% and 23%. More detailed sedimentologic analyses are necessary for resolution.

A composite plot of laboratory and downhole logging results of velocity and porosity (Fig. 22; see "Logging" section) shows that all of the main trends are defined by both methods. There is a distinct discrepancy between the laboratory and downhole velocities from approximately 300 mbsf. This may be due partly to increased drilling disturbance, causing laboratory values to be too low, in addition to a rebound effect resulting from bringing the samples to the surface. Downhole porosity is calculated from resistivity, and the fact that it is significantly lower than the laboratory values throughout the hole indicates that the constants used in the calculations may be inadequate for the present sediment type.

Despite the uncertainties, the physical-properties data indicate a thin cover of normally consolidated glacigenic sediments covering a thick sequence of overconsolidated sediments. The upper 310 mbsf bears evidence of glacial oscillations, recorded as cyclic variations in physical properties. This sequence is underlain by sediments that apparently experienced a relatively stable grounding line position over an unknown, but probably considerable, time interval. Although the sedimentology of the recovered intervals shows no unambiguous evidence of ground-

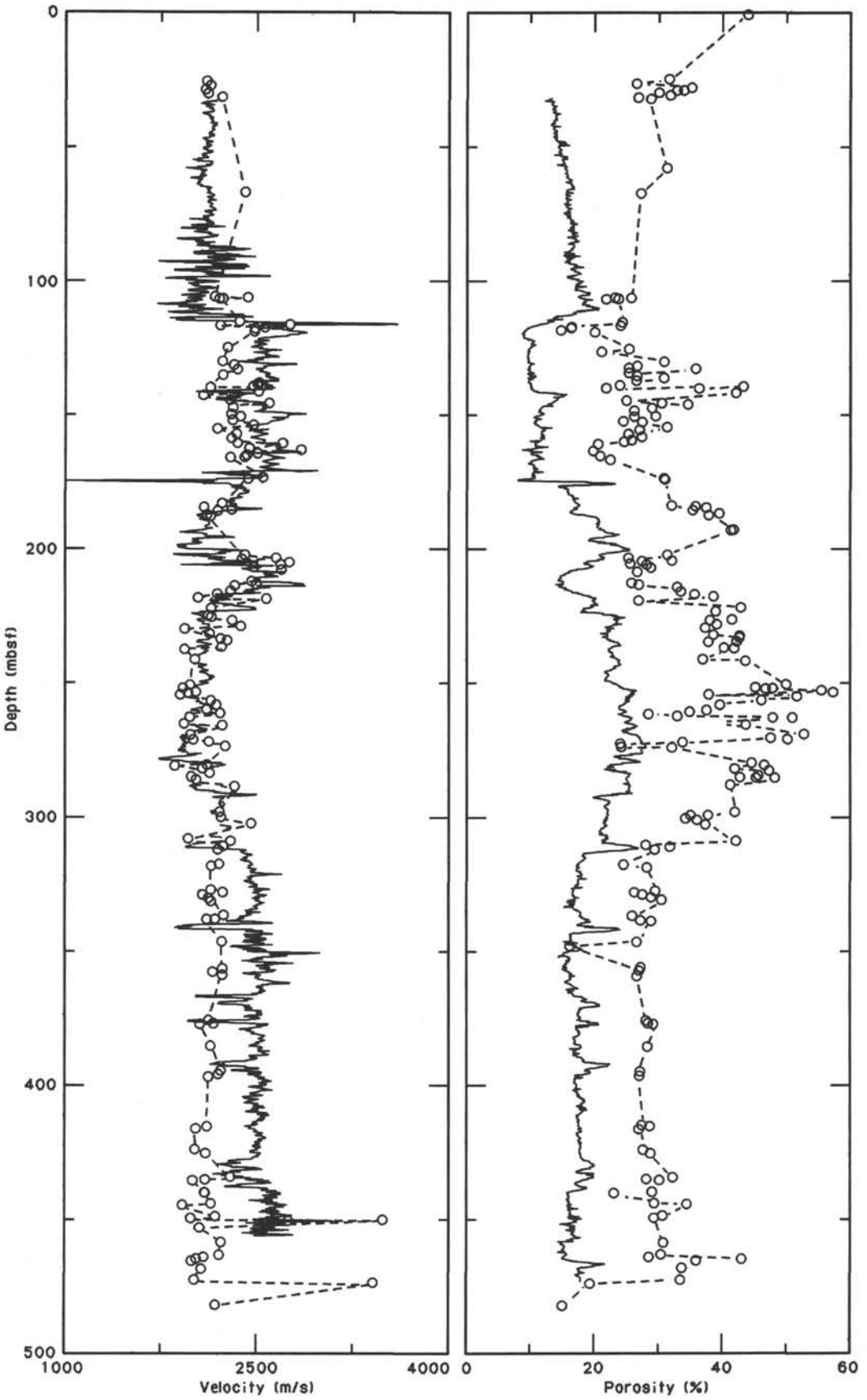

Figure 22. Comparison of downhole (solid line) and laboratory measurements (circles) of velocity and porosity for the logged interval from 32 to 450 mbsf, Site 739.

ing of glaciers at the site (see "Lithostratigraphy and Sedimentology" section), overcompaction resulting from glacial loading and erosion is not excluded as a partial reason for the observed variations. Site 739 shows that important information about the history of the East Antarctic ice sheet is recorded in and can be interpreted from the sediments' physical properties.

LOGGING

Operations

One logging run was completed in Hole 739C using the seismic stratigraphic combination (see "Logging" sections, "Site 737" and "Site 738" chapters, and "Explanatory Notes" chapter, this volume). The hole conditions in Hole 739C were excellent, owing to the consolidated pebbly mudstones (diamictites). The hole was filled with mud composed of 25% prehydrated gel and 75% seawater with a density of 1.7 lb/bbl. The pipe was left at 55 mbsf during the logging and was pulled up to 25 mbsf when the logging tool reached the pipe.

The seismic stratigraphic combination was rigged at 1830 hr on 22 January, and the logging run ended at 2330 hr. The total logged interval corresponds to 443 m between 25 and 468 mbsf.

Log Quality

The five logging parameters (formation spontaneous potential, resistivity, sonic velocity, natural radioactivity, and hole diameter) recorded with the seismic stratigraphic combination in Hole 739C are, for the most part, of good quality. Replicability of results is good in the section recorded twice between 468 and 412 mbsf.

The logging curves are presented in Figures 23 through 27. Because the caliper did not work properly between 145 and 355 mbsf, a synthetic caliper curve will be computed from the sonic log transit times in order to accurately correct the other logs for the borehole geometry effect.

The sonic velocity record (Fig. 24) shows very high and/or low values corresponding to cycle skipping or noise during acquisition (see "Logging" section, "Site 737" chapter) in three depth intervals, 75–80, 210–225, and 440–455 mbsf. Incorrect values were eliminated from the sonic log with the algorithm used for Site 645 (Shipboard Scientific Party, 1987). The corrected sonic curve for Site 739 is shown in Figure 24.

The formation spontaneous potential (SP) measurement is the electrical potential difference that spontaneously exists between an electrode in the borehole and a remote reference electrode. The SP is a good indicator of porous and permeable beds. However, the SP is a very small potential, on the order of millivolts, which is usually difficult to measure aboard a drillship because electric noise on the surface can easily interfere with recording. Such noises were not detected at Site 739 where the variations of the SP curve are in good agreement with the variations of the porosity curve. Where the porosity increases the SP shows a negative deflection, and where the porosity decreases the SP shows a positive deflection (Fig. 23).

Porosity Log

In-situ porosities were not measured directly (neutron and density tools) at Site 739. A porosity curve was calculated using Archie's (1942) law, an empirical formula relating resistivity and porosity:

$$R_t = aR_w q - m,$$

where R_w is the resistivity of the water contained in the pore structure, R_t is the bulk resistivity of the rock, q is the porosity, and a and m are parameters for which values are assigned arbitrarily to make the equation fit a particular group of measurements. For Hole 739C, a values of 0.62 and 1.72 were chosen for a and m, respectively, which correspond to values commonly used for moderately well-cemented sedimentary rocks, including sandstones and limestones, with a porosity range from 18% to 35%. The calculated porosity log from the resistivity logging record is presented in Figure 23. The porosity calculated from the resistivity log is about 10% lower than the porosity values proposed from the physical-properties measurements on cores, but the two measurements (Figs. 24 and 27) show the same variations.

Lithologic Estimation

Because core recovery was poor parts in Hole 739C, the lithology for the missing intervals has been interpreted from the logging records (Fig. 25). The presumed lithologies were determined on the assumption that quartz, clays, and detrital terrigenous minerals are the main components of the formations. The lithology proposed in Figure 25 remains questionable, particularly because accurate information about the kind and the quantity of clay minerals was not available, and also because no density log was recorded.

The main lithology recovered for the drilled section consists of pebbly mudstones (diamictites) that are fairly constant in their facies, which suggests a uniform glacial sequence. The logging parameters (Fig. 25), however, show several unexpected deflections, attesting to the existence of major changes in the physical characteristics of the diamictites and/or in the lithology of the unrecovered sections. Within depth intervals where the porosity values and the velocity values remain constant, gently decrease, or gently increase with increasing depth, diamictite lithology usually is extrapolated to those sections without recovery. For example, between 32 and 80 mbsf only one core (119-739C-5R, from 28.7 to 38.7 mbsf) was recovered that corresponds to a diamictite. The logging curves are very flat along the depth interval from 32 to 80 mbsf and indicate only a slight increase in porosity, from 12.6% to 16.5%, with increasing depth. We do not consider this slight change in the logging characteristics to correspond to an important change in the lithology; thus, the diamictite described in Core 119-739C-5R was extrapolated to the entire interval from 32 to 80 mbsf.

Several peaks on the logging records occur in the diamictites (Fig. 25), corresponding to layers from 1 to 3 m thick. The peaks are mainly below 250 mbsf (312, 341, and 375 mbsf) and correspond to low-velocity and high-porosity intervals. An abrupt negative deflection of the SP at these layers confirms their high porosity and attests to their permeability (see the preceding discussion on log quality). Between 250 and 350 mbsf, the gamma-ray tool response corresponds to peaks of low radioactivity for the porous layers. High-porosity beds with low radioactivity in a siliciclastic sedimentary environment are usually related to sand or gravel layers. Below 350 mbsf the gamma-ray tool gives a peak of increasing radioactivity for each porosity peak. A high radioactivity value for a porous clastic layer can be interpreted as a sand with radioactive minerals, such as potassium feldspar or zircon. The low recovery in the interval where porous layers occur (290–450 mbsf) may be due to sand layers interbedded in the diamictite.

Between 75 and 105 mbsf the caliper curve shows an alternation of caved and noncaved zones about 2 to 4 m thick, indicating hard strata interbedded in softer material (see Fig. 26). Caved zones correspond to low radioactivity values and noncaved zones to high radioactivity values. The SP log and the velocity log also attest to the existence of alternations of hard/soft or fine/coarse material in the interval from 75 to 105 mbsf. In the noncaved zones, the sonic, resistivity, and radioactivity values are close to those of the surrounding diamictites, suggesting that the non-

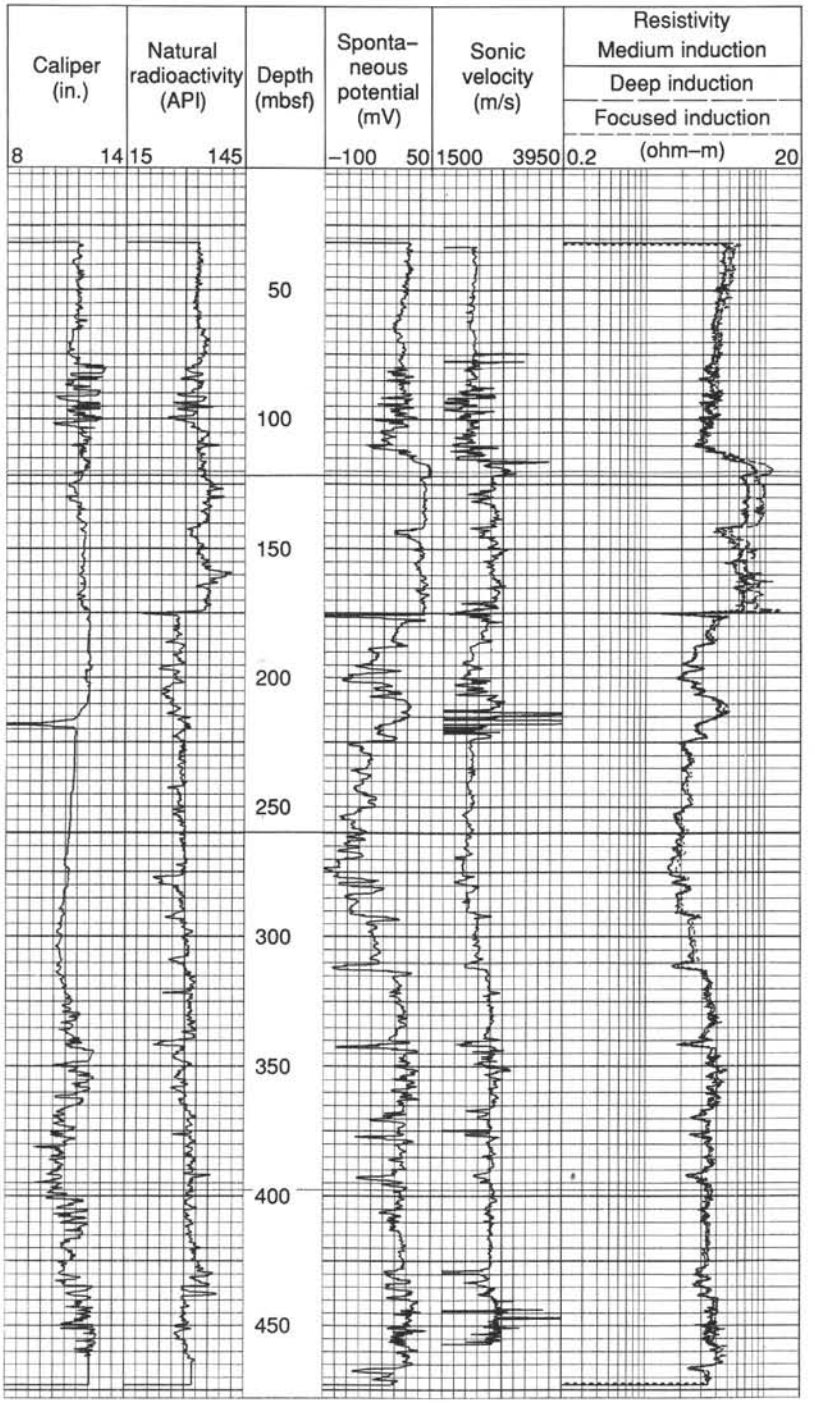

Figure 23. Downhole logs for the seismic stratigraphic combination: caliper, gamma ray, spontaneous potential, sonic velocity, and medium, deep, velocity and focused resistivity for the interval from 32 to 465 mbsf, Hole 739C.

caved intervals also correspond to diamictites. Interbedded caved zones with low radioactivity, low resistivity, and low sonic values might consist of sandy sediment.

Logging Units

Four units were identified in Hole 739C on the basis of the logging records (Fig. 25). No coarsening- or fining-upward sequences were identified in the cores, and cemented diamictites were found at only a few intervals; consequently, for each lithology we assumed that the porosity variations were related to only the compaction effect.

Logging Unit 1 (32 to 110 mbsf)

Logging unit 1 is characterized by relatively low porosity values that decrease from 12.6% at 32 mbsf to 21% at 110 mbsf (Fig. 25). The actual "low porosity" of the diamictites probably results from an initial low porosity at the time of deposition, which is typical for coarse detrital sediments. On the other hand,

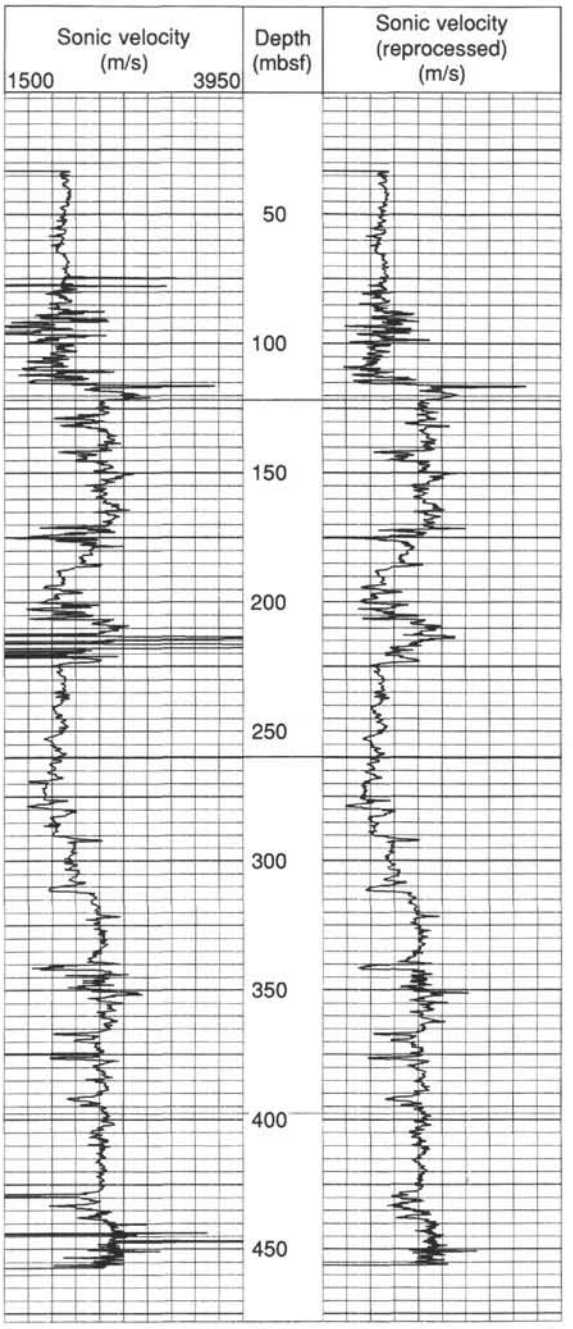

Figure 24. Comparison of observed (left) and corrected (right) velocity logs, Hole 739C.

the loading of the sedimentary section by a thick ice sheet during the last glacial period is an additional explanation for the low porosities. Two lithologies occur in logging unit 1: a diamictite from 32 to 80 mbsf and a lower sandy sediment interbedded with diamictite layers.

Logging Unit 2 (110 to 175 mbsf)

An abrupt change in the logging values occurs between logging units 1 and 2. Within 10 m, the porosity decreases from 21% to 9%, the velocity increases from 1867 to 2847 m/s, the natural radioactivity increases from 54 to 106 API units, and a positive deflection of 75 mV is measured on the SP log. This deflection corresponds to the unit 1/unit 2 boundary. Within logging unit 2, the porosity does not change with depth. Logging unit 2 consists of highly compacted (only 9% porosity) diamictites. A thin (5-m-thick) bed of porous material, probably sand or gravel, is in the middle of the unit (Fig. 25). The abrupt increase in the compaction rate between logging units 1 and 2 is probably the result of cycles of glacial loading, compaction, and erosion of the upper part of unit 2 prior to the deposition of unit 1.

Logging Unit 3 (175 to 275 mbsf)

A high-amplitude narrow peak on all logging records and an abrupt decrease in the radioactivity value occur at the boundary between logging units 2 and 3 (Fig. 25). The boundary is a major unconformity between upper Miocene and underlying lower Oligocene glacial sediments (see "Biostratigraphy" section). The peak corresponding to the boundary is a porous layer (24% porosity), interpreted as a sand layer in the "Physical Properties" section. The lithology of logging unit 3 is described in the "Lithostratigraphy and Sedimentology" section as a stratified diamictite that is commonly contorted. As in logging unit 1, the porosity increases with increasing depth, but it is more variable. In particular, a thick bed at 200 to 225 mbsf corresponds to a well-consolidated diamictite with a minimum porosity of 9%. The depth interval from 200 to 225 mbsf was nearly completely recovered by coring, but no lithologic variation was observed; thus, the decrease in porosity could not be explained by a change in the rock composition (see "Lithostratigraphy and Sedimentology" section). As in logging unit 2, an erosional event occurring after an initial compaction by ice loading is probably the best explanation for the presence of a highly compacted layer within logging unit 3. A high rate of sedimentation, which is usual during glacial stages, would explain the increase of porosity with depth in unit 3. The abrupt decrease in radioactivity from 104.5 to 69 API units between logging units 2 and 3 is possibly the result of a change in the source of the sediments. However, the difference in compaction between the two units could also explain the higher concentration of radioactive minerals in unit 2 than in unit 3.

Logging Unit 4 (275 to 474 mbsf)

The first porosity decrease with depth in Hole 739C is found in logging unit 4, increasing from 27% at 275 mbsf to 20% at 350 mbsf. In the lower part of logging unit 4, the porosity remains fairly constant from 350 to 474 mbsf. Unit 4 corresponds to a poorly recovered interval. As discussed previously, the logging parameters suggest that the lithology consists of sand layers interbedded in the diamictites. An increase in compaction with depth and the occurrence of sand layers within the unit attest to a change in the sedimentation conditions from logging units 3 to 4. Unlike for the overlying units, the sedimentation conditions of the unit 4 deposits probably allowed water to escape more easily, possibly due to the presence of permeable layers.

Results

The preliminary interpretation of the logging records at Site 739 suggests the following:

1. Diamictites have a relatively low porosity resulting from an initial low porosity and ice-loading processes.
2. Porosity decreases with depth below 275 mbsf, possibly because of the presence of permeable layers that allow water to escape.
3. Two highly compacted units located between 110 and 175 mbsf and between 200 and 225 mbsf result from a process of overcompaction, probably related to strong glacial-loading erosional events.

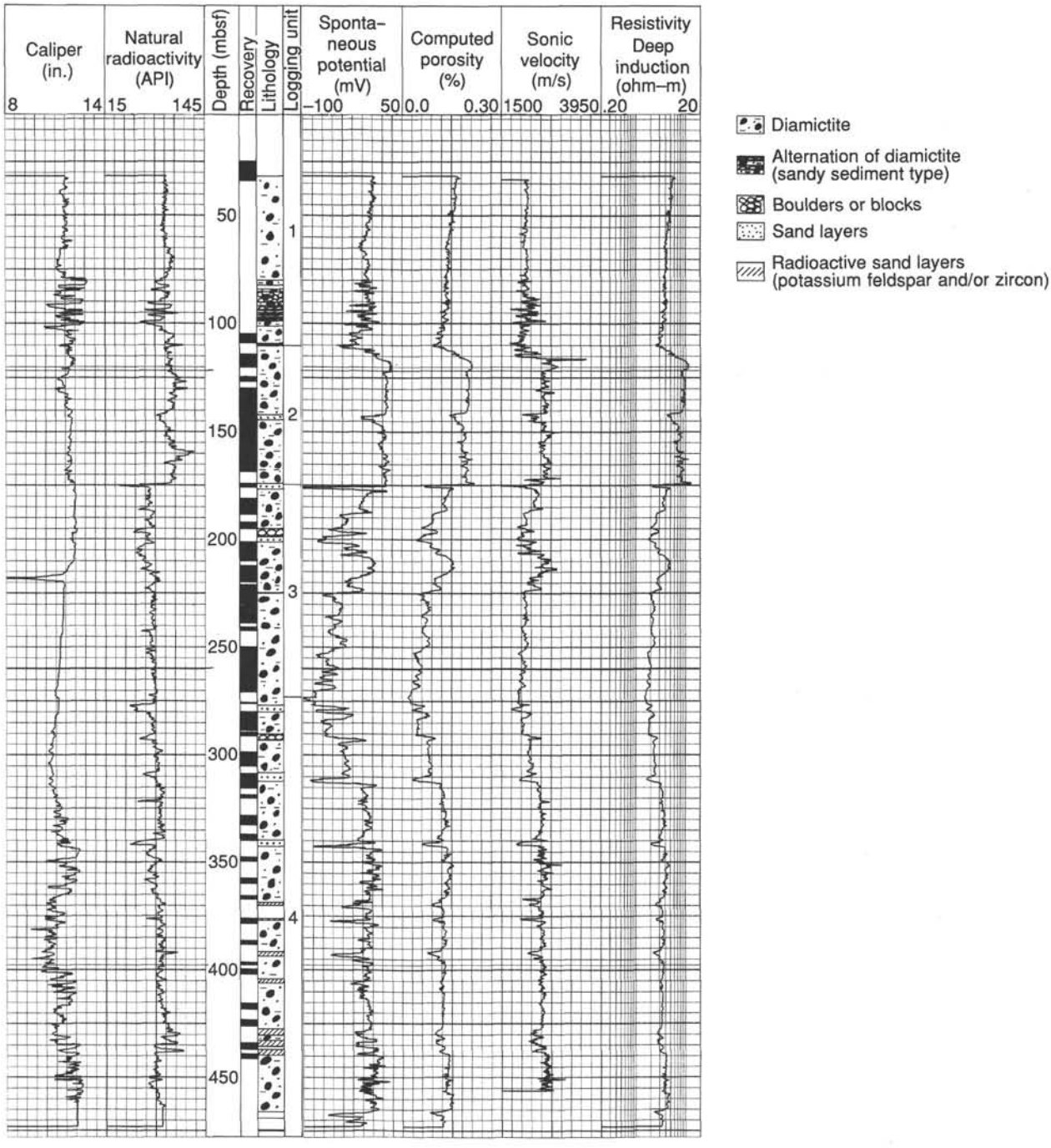

Figure 25. Summary compilation of downhole logs, intervals of core recovery, lithology, and downhole logging units at Site 739. Lithology is based on coring results and also inferred from logging results.

4. The increase in porosity with depth in logging unit 2 is the result of a high rate of sedimentation.

5. The existence of a sandy sediment interbedded in the diamictites between 80 and 100 mbsf.

6. The occurrence of quartzitic and radioactive sand layers in the lower part of the drilled section.

Synthetic Seismogram

A synthetic seismogram was computed for Site 739 to accurately tie the drilled sequence in the hole to seismic-reflection data over the site (Fig. 27). The seismogram covers the logged interval from 30 to 455 mbsf (a few meters above the bottom of the hole at 467 mbsf).

Values from the long-spacing sonic velocity log (long-spacing = 3.5 m), which was post-processed to remove intervals with noisy data, were used to compute the acoustic impedance, assuming an arbitrary constant density of 1 g/cm^3. A constant density was used because downhole density logs were not recorded and laboratory density measurements were too sparse to yield a reliable synthetic seismogram. The use of velocity information, without density, for the synthetic seismogram gives a good approximation to the observed seismic data based on the

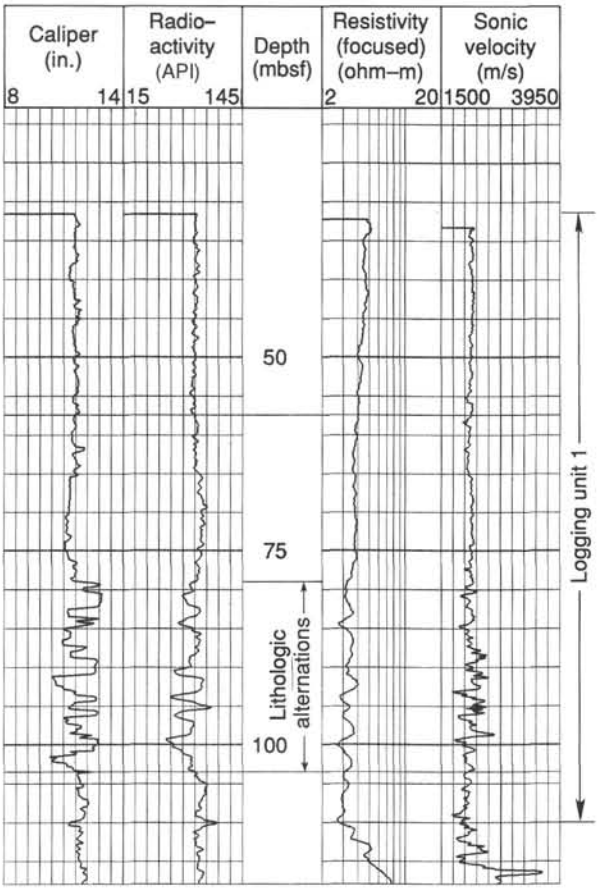

Figure 26. Downhole caliper, gamma ray, focused resistivity, and sonic velocity logs for the interval from 32 to 125 mbsf, Hole 739C.

results of Sites 737 and 738 for this leg. The impedance and synthetic seismogram are shown in Figure 28. The correlation of the synthetic trace with the seismic-reflection profile over Site 739 is given in Figure 29. A velocity of 2.0 km/s was assumed for the interval from 0 to 30 mbsf to shift the synthetic seismogram to the proper initial depth on the seismic profile.

Hole 739 was drilled into a glacial marine sequence composed of flat (to 170 mbsf) and seaward-prograding (below 170 mbsf) strata that have a complex acoustic signature in reflection profiles (Fig. 27). Shipboard visual inspection of cores from these sequences indicates a mostly uniform lithology (diamictite), yet the downhole logs show great diversity (see the preceding text). The synthetic seismogram (Figs. 28 and 29) also shows the complexity recorded by the downhole measurements. Several observations from the synthetic trace (Fig. 28) are noteworthy:

1. The complexity of the seismic trace results principally from abrupt, rather than broad, variations in the *in-situ* velocity (e.g., lithology or compaction) throughout the sedimentary section.
2. Significant geologic hiatuses and layers can be identified in the reflection data only if they are associated with large velocity (or density) changes.
3. The amplitudes of the seismic reflections are highly variable: large amplitudes result principally from large isolated changes in velocity (110 and 205 mbsf) and also from the constructive interference of small, nearby variations in velocity (305 to 385 mbsf).
4. The polarity of the velocity change (i.e., lithologic variation) causing the reflection cannot be determined solely from the reflection data, because of intervals of large velocity variability (e.g., the entire section beneath Site 739).
5. Intervals with small reflection amplitudes are characterized by relatively uniform velocity (i.e., lithology—230–270 and 30–80 mbsf).
6. Velocity variations that occur over broad intervals, such as those resulting from gradual lithologic changes or compaction, cannot be uniquely identified in the synthetic seismic trace.

Accurate correlation of the synthetic seismogram with vertical-incident seismic-reflection data recorded over Site 739 (Fig. 28) is predicated on the assumption that the seismic-reflection profile was recorded directly above the drilling site, as shown. Location errors of up to 50–100 m (2 to 4 shotpoints) are probable because of uncertainties in beacon location on the seafloor relative to reflection-recording geometry (see "Explanatory Notes" chapter). The Site 739 location is placed at reflection shotpoint 952, or 8 shots from the point of beacon deployment.

Reasonable correlation of the synthetic trace with the seismic profile is possible, with exception of the interval from 30 to 100 mbsf. The correlation is tied primarily to (1) locations of two high-amplitude peaks at 113 and 170 mbsf that occur at major unconformities, (2) locations of four high-amplitude peaks within the prograding wedge and deeper (210, 240, 315, and 350 mbsf), and (3) the breadth of a low-amplitude peak at 400–420 mbsf.

A few general interpretations of the rocks comprising the sedimentary section beneath Site 739 can be made by extrapolating the downhole logging results onto the seismic-reflection profile (Fig. 30).

1. 0–110 mbsf: High-frequency, discontinuous reflections characterize this interval in the seismic profile. The total lack of coherent reflections is due, in part, to the superposition of the water gun bubble pulse, the high- and low-frequency diffractions from seafloor irregularities, and the weak primary reflections. The synthetic data show one large and two small reflections, which cannot be seen in the seismic profile. The lack of lateral reflection continuity for this interval indicates that the small velocity variations observed in the downhole logs probably do not continue laterally over distances of more than 25–50 m, or otherwise, traceable reflections would be expected.
2. 110–170 mbsf: High-amplitude reflections occur at the top and bottom of this interval and are separated by negative amplitude reflections. The synthetic trace shows that the high-amplitude reflections are caused by abrupt velocity changes (1.9 to 2.5 to 2.0 km/s). The central part of the unit has high velocities that continue, with minor variations, laterally for tens of kilometers away from Site 739, at least to Site 742.
3. 170–310 mbsf: This interval is characterized by distinctly dipping reflections that, individually, continue laterally for 150 to 400 m. In the seismic profile, the reflectors abruptly change dip, terminate, and change waveform shape, suggesting highly variable lithologies over short distances. The downhole velocity data show thick (60 m) and thin (5 m) variations of up to 0.5 km/s within the unit, indicating that the prograding wedge of reflections results from diverse velocities (lithologies).
4. 310–467 mbsf: Reflections within this interval are continuous over distances of several kilometers or more, indicating a different depositional environment than the overlying unit. The synthetic seismogram shows that the strong reflections are caused by low-velocity layers, 2 to 5 m thick, that are probably unconsolidated sands (see the preceding text). These sand layers are of relatively uniform thickness seaward of Site 739, based on the uniform shape of the reflection. Landward of Site 739, however, the reflections become wider and contorted, indicating a change in layer thickness or a change in lithology.

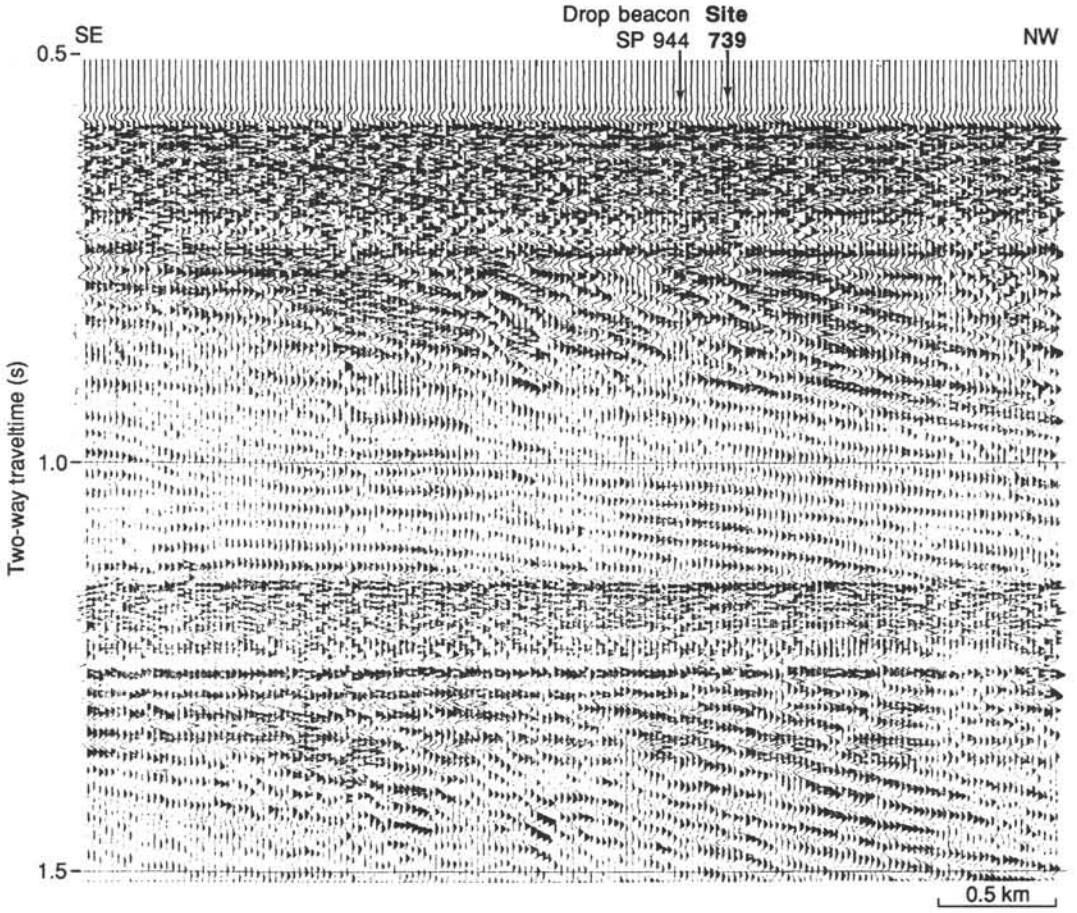

Figure 27. Seismic-reflection profile across Site 739.

Summary

In summary, six downhole logs were successfully recorded on one logging run at Site 739, leading to the identification of four logging units (Fig. 25). These units indicate that major fluctuations occur in porosity, velocity, resistivity, and spontaneous potential values at depth. The large logging variations are probably the result of different degrees of compaction and dewatering caused by intermittent periods of loading by grounded ice sheets on glacially derived sediments. These sediments were deposited on, and directly in front of, the continental shelf edge.

Comparison of the synthetic seismogram derived from downhole logs with seismic-reflection profiles across Site 739 (Figs. 29 and 30) indicates that large velocity variations (up to 0.5 km/s) occur at unconformities or at thin layers (most less than 5 m thick) and that these variations are the principal cause of observed reflections. Within the prograding sediment wedge (170 to 310 mbsf) discontinuous reflections (150–400 m long) result from both high- and low-velocity layers. Below 310 mbsf, however, the reflections that are continuous over several kilometers are caused principally by 2–5-m-thick low-velocity horizons, which are probably unconsolidated sands.

SEISMIC STRATIGRAPHY

Overview—Prydz Bay Seismic Stratigraphy

The seismic stratigraphy of Prydz Bay has been described by Stagg (1985), based on six-channel seismic-reflection profiles recorded across the 200-km-wide Prydz Bay shelf by the Australian Bureau of Mineral Resources (BMR). BMR recorded several long, parallel profiles, but did not run cross lines to tie reflectors between the profiles. The only other seismic data were a single six-channel profile recorded across the outer Prydz Bay shelf (Mizukoshi et al., 1988). During Leg 119, a seismic-reflection profile was recorded across the entire Prydz Bay shelf during transits between the drilling sites. The seismic stratigraphy that is described for the Prydz Bay drilling Sites 739–743 is based on a regional interpretation of this transect. At each site, the acoustic units are described and are tied, where possible, to other drilling sites.

The Leg 119 seismic transect is close to BMR seismic line PB-21, along which the proposed drilling sites had been selected. The new transect provided greater resolution of seismic reflectors than PB-21, because a smaller seismic source yielding higher frequencies was used. The two small (80-in.^{3}) water guns provided adequate energy to penetrate the sedimentary section above the first water-bottom multiple, which is the deepest level penetrated by all existing seismic data (other than sonobuoy-seismic data). In several places, the greater resolution (and absence of data-processing artifacts) of the Leg 119 data gave a different picture of detailed subsurface structure and stratigraphy, providing information needed for the selection of the drill sites. The regional picture of reflector geometry described by Stagg (1985) remains nearly unchanged.

The general acoustic stratigraphy of Prydz Bay (Fig. 31) is characterized by sequences of reflectors that dip seaward on the inner and outer parts of the shelf and lie nearly flat beneath the central shelf. Dipping sequences on the inner shelf are uni-

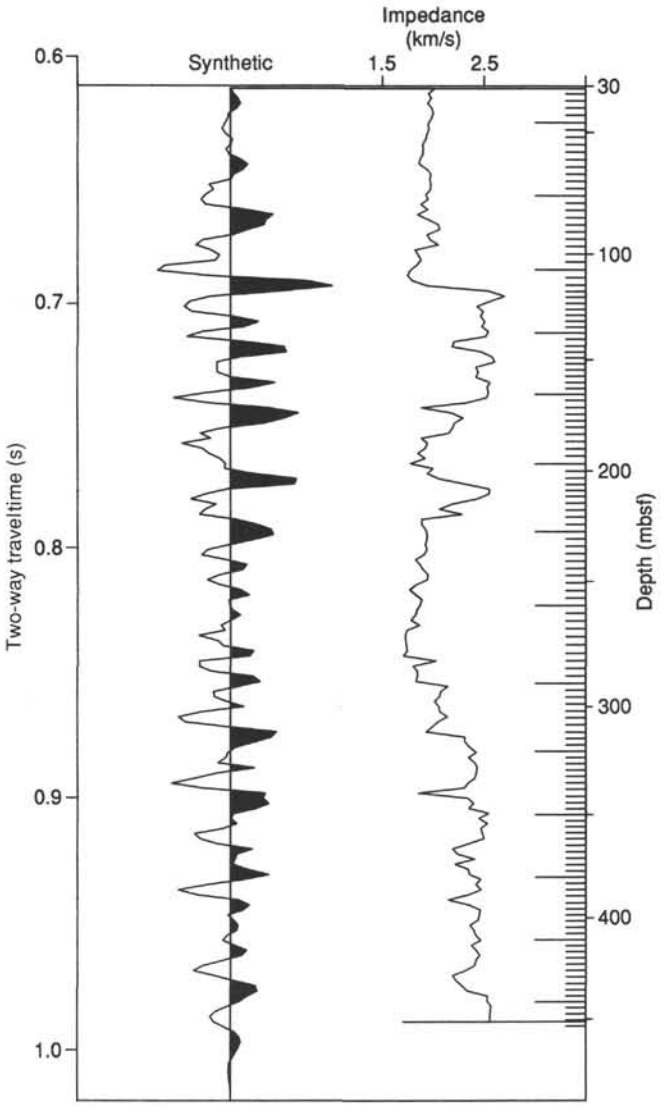

Figure 28. Synthetic seismic trace computed from downhole velocity log. The impedance is velocity at an assumed density of 1 g/cm^3. Reflection time is from sea level.

formly layered whereas those of the outer shelf dip more steeply and form wedges of prograding strata. These dipping sequences are truncated(?) and overlain by flat-lying reflectors within 30 to 150 ms of the seafloor. The Leg 119 data confirmed that the dipping sequences of the inner and outer shelf are homoclinal or regionally dipping sequences, because seismic lines oriented nearly perpendicular to the inferred bedding dips show apparently flat-lying reflectors over distances of up to 10 km. The acoustic character of strata is highly variable beneath the shelf, and the probable explanations for this, based on core data and downhole logging at Sites 739 and 742, are discussed in the site chapters.

Sources of Seismic Noise

The seismic interpretations are, in places, adversely affected by poor data quality resulting principally from geologic (e.g., glacially related), rather than instrumental, noise. The most insidious problem encountered was severe seafloor multiple reflections that not only limited the seismic penetration but also resulted in acoustically disrupted records, because of large noise levels in the water column. Rapid (9-s) seismic shot intervals were used on Leg 119 to get high-resolution images of seismic structures; however, in some areas of hard seafloor, the multiple reverberations in the water column did not fully dissipate before the following shot. The seafloor-multiple problem was more severe during the survey of the inner part of Prydz Bay, where seas were glassy or calm. The glassy seas provided a good upper reflection surface, enhancing multiples from the primary as well as the sea-surface "ghost" reflections.

Another severe source of noise was small irregularities on the seafloor (probably iceberg gouges) that produced diffractions observed not only along the seafloor reflector, but also randomly throughout the seismic data. The random events (e.g., side-swipe) were occasionally severe and easy to identify, but more commonly were relatively weak, and disrupted otherwise continuous reflectors. Seafloor diffractions also occurred as steeply dipping reflections, of high and low frequency, that appeared to offset reflections. Consequently, the acoustic character of seismic units beneath Prydz Bay is, in places, variable because of factors (e.g., diffractions and internal and seafloor multiples) other than *in-situ* rock properties. This problem is more severe in Prydz Bay than elsewhere because of major episodes of grounding and "ploughing" of the Amery Ice Sheet and individual icebergs.

In the Leg 119 analog seismic profiles, reflections within 70–80 ms (about 75–85 m) of the seafloor cannot be resolved. This depth corresponds to the effective width of the water gun seismic pulse. The high velocity of the seafloor (2.0–2.2 km/s) in Prydz Bay produces a strong reflector (70–80 ms long) that masks lower-amplitude reflections that might be present.

Introduction—Site 739

Site 739 is in northern Prydz Bay about 30 km from the continental shelf edge and 200 km from the Antarctic coast. This site is the most seaward of the Prydz Bay shelf drill sites, 29 km northwest of Site 742.

Site 739 lies above a sequence of seaward-dipping reflections that comprise the prograded sedimentary units underlying the outer Prydz Bay shelf. The reflectors beneath Site 739 are part of Stagg's (1985) unit PS-2, which he identifies under the entire central and outer Prydz Bay shelf. On ODP line 119-08 (Fig. 31), three seimic units are recognized within the glacial diamictons encountered throughout Hole 739C: (1) an upper unit (0–175 mbsf) of flat-lying, high-amplitude reflections; (2) an intermediate unit (175–310 mbsf) of steeply dipping and semicontinuous reflections; and (3) a lower unit (310–487 mbsf) of gently dipping, weak, continuous reflections. The continuity and amplitude of reflections is strongly controlled by downhole variations in lithology and degree of compaction in the omnipresent glacial diamictons.

Seismic Units

Seismic Unit I (0–175 mbsf) consists of high-amplitude reflections that are highly disrupted within 70–80 mbsf but become more continuous, and higher in amplitude, at 80–170 mbsf. Two high-amplitude, continuous reflections occur at 120 and 170 mbsf, and a subtle negative, continuous reflection is seen at 100 mbsf (Fig. 31). The great variability in reflection character of seismic Unit I results from the large fluctuations of *in-situ* velocity and density, as measured by downhole logging and confirmed by a synthetic seismic study (see "Logging" section). Reflections are discontinuous in intervals of uniform, or highly variable, velocities, and continuous reflections occur only at abrupt changes in velocity.

The two high-amplitude reflections at 120 and 170 mbsf are of such uniform thickness and amplitude over large distances that they might be considered internal multiple reflections or

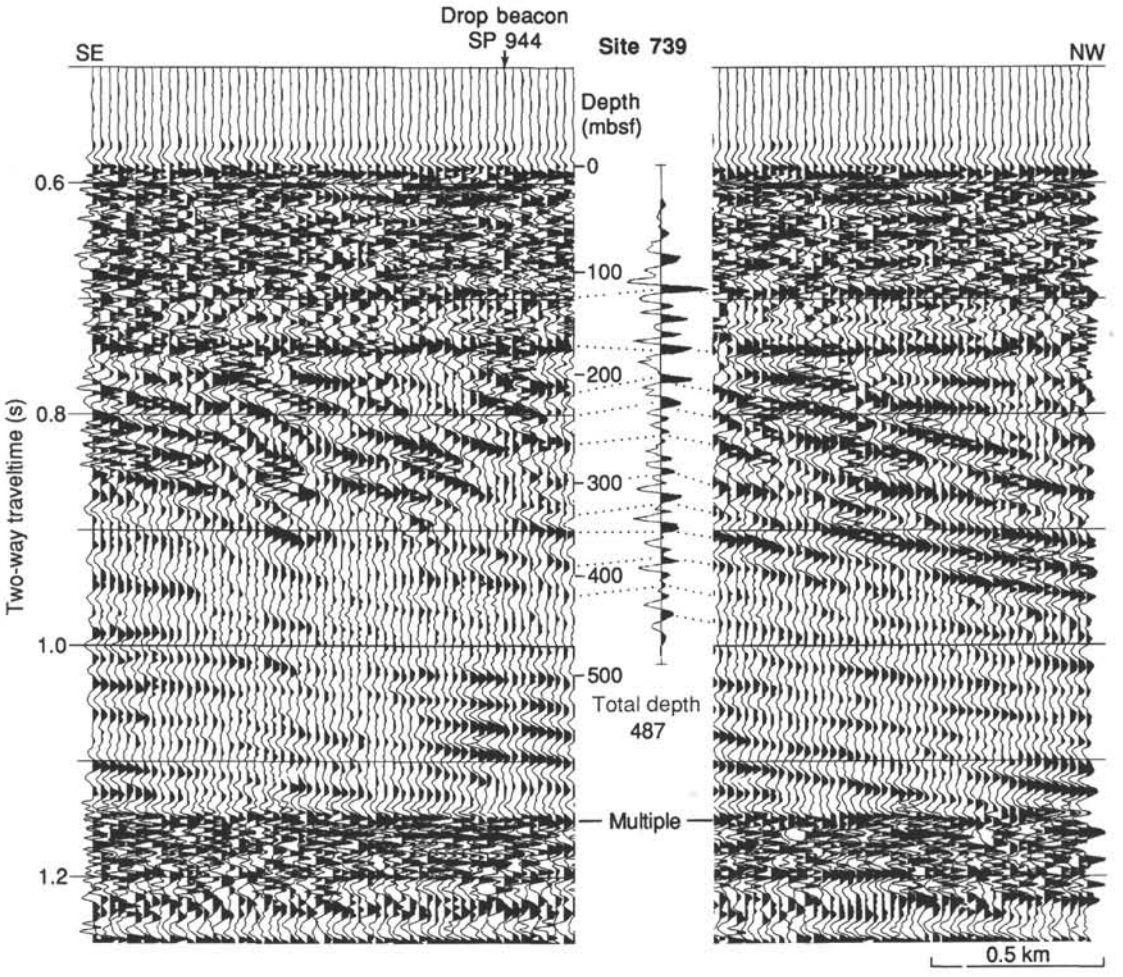

Figure 29. Comparison of vertical-incident seismic-reflection data recorded over Site 739 with a synthetic seismic-reflection trace computed from downhole velocity measurements.

seismic-source reverberations. The downhole logging and synthetic seismic study clearly show that the reflections occur at the top and bottom of a uniformly thick layer of high-velocity (2.4–2.6 km/s), massive diamicton. A hiatus between late Miocene and late Eocene to Oligocene times is placed at the bottom of this high-velocity layer. Early Pliocene age diatoms are found directly above this massive diamicton, within a low-velocity layer marked by a semicontinuous reflector. The reflectors in seismic Unit I trace layers with uniform lithology or compaction, as evidenced by downhole logging, and may approximate time boundaries within the unit.

Seismic Unit II (175–310 mbsf) is characterized by a seaward-dipping sequence, or wedge, of reflections that show high variability in reflection amplitude, continuity, reflector dip, and internal deformation (Fig. 31). The appearance of the unit, in the shipboard analog seismic record, is more uniform and continuous than in the full-waveform processed data. In the digitally processed data, the variations in reflection amplitudes caused by velocity, density (i.e., compaction), and layer-thickness changes are more clearly visible than in the analog data. High-amplitude reflections with positive and negative polarity are commonly seen over only 8–20 traces (0.2–5 km), and some of the amplitudes attenuate rapidly into diffractions. The reflections are irregular in overall shape and the constituent waveforms are commonly complex and change shape over short (a few traces) distances. In other parts of the unit, reflections are low amplitude or are disrupted.

The diverse acoustic character of seismic Unit II indicates great variability in the continuity of strata, the uniformity of lithology, and/or the degree of lithification of the diamictons that comprise the wedge. The short, irregular-shaped reflections with diffractions and the complex reflection waveforms indicate rapid lateral changes in layer thickness and lithology. Such changes are more easily explained by rapid input of sediments or by sediment slumping than by the effects of differential ice-loading compaction, post-depositional faulting, or secondary cementation. The large variability of the *in-situ* velocities and densities (see "Logging" section) and in the character of the diamictons (see "Lithostratigraphy and Sedimentology" section) is consistent with the large variability in the character of reflections. The seismic profiles indicate that the variability extends laterally throughout the dipping reflection wedge, and thus, the variability is probably a primary depositional feature and not a secondary glacial-loading effect.

Seismic Unit III (310–467 mbsf) is characterized by a sequence of generally low-amplitude reflections that, near Site 739, are relatively continuous and dip gently seaward (Fig. 31). To the southeast (updip and landward), seismic Unit III increases in thickness and the reflections become semicontinuous to discontinuous. The unit consists of slightly indurated but fri-

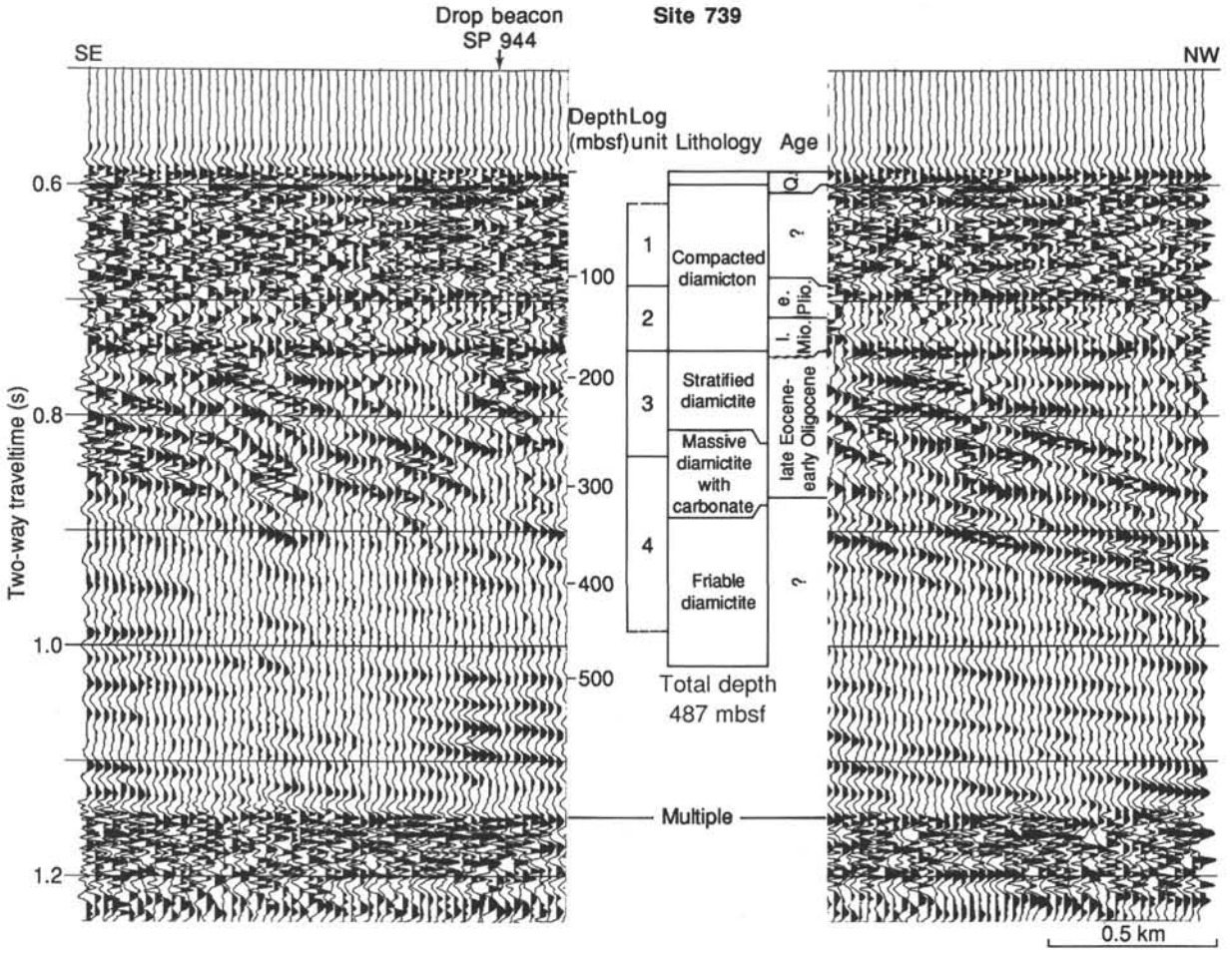

Figure 30. Seismic-reflection data over Site 739 showing depths to logging units, major lithologic boundaries, unconformities, and ages. Depths are from synthetic seismic traces of Figure 29.

able diamictites of possible middle Eocene to Oligocene age (378 mbsf; see "Biostratigraphy" section). Reflection amplitudes increase at depths greater than 550 mbsf, below the bottom of Hole 739C, and these reflections can be traced for 10–20 km landward. The abrupt change in reflection character from seismic Units II to III can be explained by downhole and physical-properties measurements that show a distinct difference in the velocity-depth profiles for the two units. The highly variable character of seismic Unit II changes to one that displays, in seismic Unit III, uniformly increasing velocities with depth. The character of seismic Unit III suggests a sedimentary section undergoing normal burial compaction (see "Physical Properties" section).

Reflections in the upper part of seismic Unit III appear, from downhole logs and synthetic seismic studies, to result principally from low-velocity layers, 2–5 m thick, that are probably composed of unlithified sands (see "Logging" section). These layers can be traced as continuous reflectors for distances up to 10–15 km. Similar reflectors (low-velocity sands?) below Hole 739C can be traced up to 25 km. The good continuity, low dip, and minimal widening (i.e., layer thickening) of the high-amplitude reflectors suggest that the lower part of seismic Unit III was deposited in a relatively stable depositional environment, probably on the outer continental shelf. A slight seaward shift occurs in the location of high amplitudes, along continuous reflections, at progressively shallower depths.

Seismic Stratigraphy of Outer Prydz Bay Shelf

Site 739 lies on the inner edge of a relatively steeply dipping sequence, or prograding wedge, of reflectors that underlie the outer 30 km of the continental shelf (Fig. 32). The acoustic stratigraphy, in conjunction with drilling data from Site 739, place some constraints on the relative timing and age of depositional events for these sequences.

Several general observations can be made from the seismic profile across the prograding wedges (Fig. 32):

1. The seafloor is relatively flat, with exception of iceberg gouging, and deepens landward from the shelf edge. This reverse deepening is characteristic of Antarctic shelves and is due principally to ice loading of the continent.

2. Reflections within 0.08–0.23 s of the seafloor are nearly flat, with a slight seaward dip that implies seaward thickening of the uppermost layers. These high-amplitude reflectors represent the glacial topset beds of the prograding wedge and, where traced seaward to their apparent termination, define the outer paleoshelf edge. The deepest topset bed can be traced seaward to a point about 10 km from the present shelf edge, where the bed terminates (Fig. 32, A). The next stratigraphically deeper, topset bed termination lies about 2 km southwest of Site 739, or about 40 km from the present shelf edge (Fig. 32, B). The apparently abrupt, large shift (30 km) in shelf edge topset reflectors could

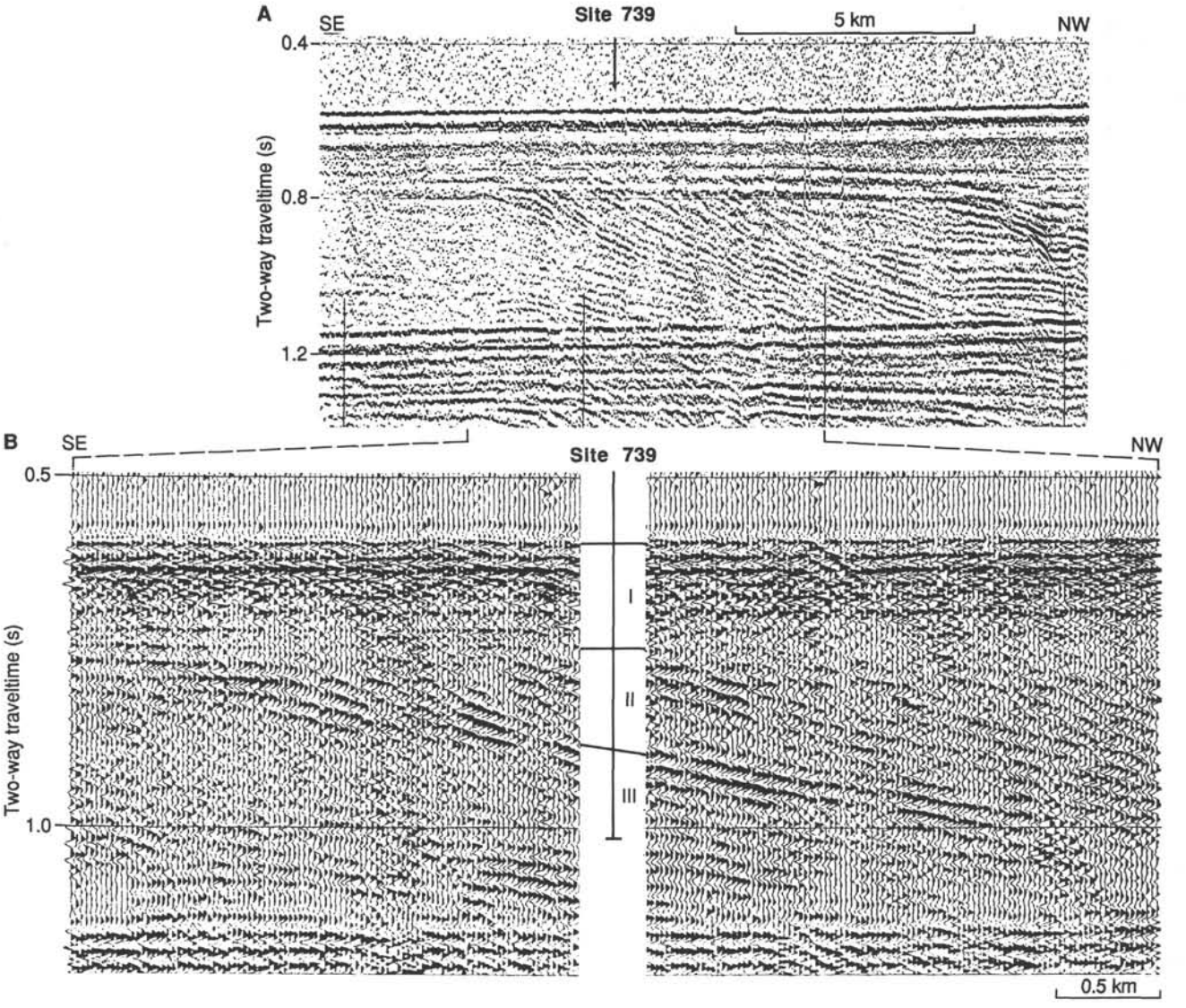

Figure 31. Seismic-reflection profiles (ODP line 119-08) across Site 739. **A.** Analog. **B.** Digital, with seismic units labeled.

be explained by (a) a period of rapid deposition that caused the shelf edge to prograde 30 km seaward or (b) periods of erosion that have removed evidence for the history of seaward shelf prograding.

3. The dipping sedimentary sequences drilled at Site 739 can be reliably traced seaward no more than 5–6 km, where they enter the seafloor multiple. The top of the seaward-dipping reflections is the regionally flat, high-amplitude reflector at 170 mbsf, which corresponds to the base of a high-velocity layer.

4. At least four distinct packets of reflections, with angular discordance between the packets, can be identified within 12 km seaward of Site 739. Farther seaward, the steep reflection dips appear concordant.

5. Near Site 739, topset beds lie within the upper 0.04–0.06 s of the prograding wedge. These nearly flat reflections lie directly below the high-velocity late Miocene age unit, and they can be traced about 0.5–1.5 km seaward of Site 739, where they dip down and into the prograding wedge. From drilling, the glacial diamictons within the prograding wedge (seismic Unit II) are of late Eocene to early Oligocene age. The seismic stratigraphy indicates that the shallowest rocks of this age may extend no farther than about 0.5 to 1.5 km seaward of the drill site, where they dip into the wedge. All reflector packets seaward of about 5 km of Site 739 would thus be younger than late Eocene to early Oligocene. Even allowing for erosion of topset beds and the uncertainty in resolution of the seismic reflections, the small thickness of the topset beds suggests that they do not continue far from Site 739 before entering the prograding wedge.

The age of the more seaward prograding deposits beneath the shelf is unknown by drilling. However, recovery of upper Miocene rocks from the high-velocity layer that can be traced as a strong reflector to within 10 km of the shelf edge (point A, Fig. 32) suggests that the outermost 10 km of the prograding shelf wedge could be late Miocene and younger. The abrupt increase in dips of the prograding shelf deposits about 12 km from Site 739 and the abrupt seaward shift of the paleoshelf edge (see the preceding second item) probably signal a major increase in sedimentation rates, possibly as a result of late Cenozoic increased glaciation. The Quaternary rocks recovered from

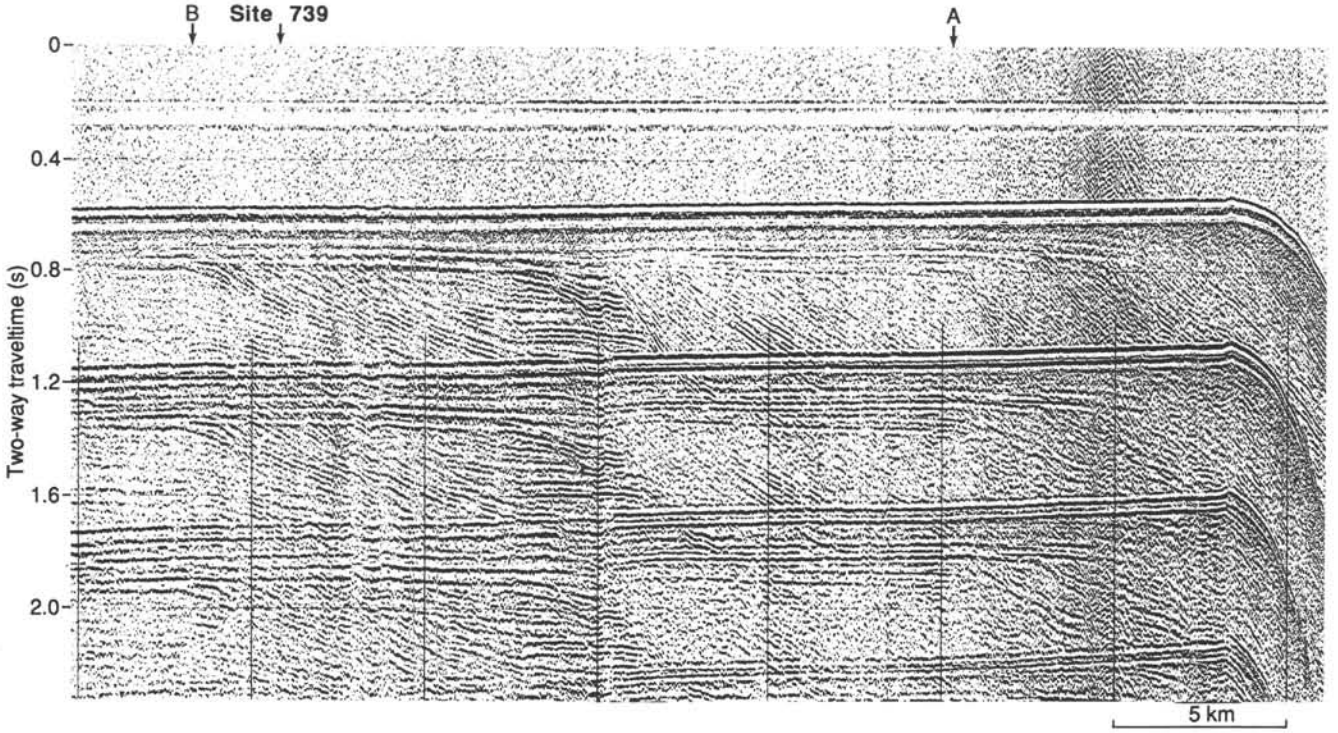

Figure 32. Analog seismic-reflection profile (ODP line 119-08) across Site 739 and the outer edge of the Prydz Bay continental shelf illustrating the thick prograding sedimentary wedges underlying the outer shelf. A = seaward limit of strong reflector correlated with upper Miocene rocks at Hole 739C; B = termination point of next stratigraphically deeper topset bed.

the topmost 100 mbsf at Site 743, on the upper continental slope, indicate that the ice front probably reached the shelf edge in Quaternary time.

Summary

Seismic Unit I (0–175 mbsf) is nearly flat lying and contains high-amplitude reflections as a result of glacially overcompacted (high-velocity) and normally consolidated (low-velocity) layers of Quaternary to late Miocene age. Seismic Unit II (175–310 mbsf) consists of highly variable and complex seaward-dipping reflections that form a prograding wedge of late Eocene to early Oligocene age. Seismic Unit III (310–467 mbsf) is characterized by weak but continuous reflections (near Site 739) that result from low-velocity layers within normally compacted friable diamicton.

The great variability in reflection character at Site 739 results from large, and commonly abrupt, variations in velocity and density at depth, as observed from downhole logging. The high-velocity layers in seismic Unit I are continuous across broad areas and are clearly related to compaction by grounded ice sheets. The great lateral variation in reflection amplitude, continuity, and structure in seismic Unit II attests to a complex and unstable depositional environment that is probably dominated by rapid deposition and slumping. In contrast, seismic Unit III is characterized by normally compacted sediments that suggest deposition of a possible regressive sequence on a stable continental shelf.

The ages of sedimentary wedges beneath the outer Prydz Bay shelf are unknown from drilling, but seismic evidence suggests that the shallowest late Eocene to early Oligocene age topset strata drilled at Site 739 do not extend more than 0.5–1.0 km seaward of the drill site before dipping into the prograding wedge. Late Miocene age rocks drilled at Site 739 may extend to within 10 km of the shelf edge, suggesting that most of the outer, and more steeply dipping, parts of the sedimentary sequences may be of late Cenozoic age. The outermost rocks are of Quaternary age, based on Site 743 drilling.

SUMMARY AND CONCLUSIONS

Site 739 is 30 km from the shelf edge, and represents the most seaward of the sites drilled on the Prydz Bay shelf. The water depth is 412.4 m, and the distance from land near Davis Station and from the Amery Ice Shelf is 140 km. Because the Lambert Graben, which has probably existed since Permian or Early Cretaceous time, drains 22% of the East Antarctic Ice Sheet, we expected that sites in Prydz Bay would provide a record of the initiation of the ice sheet and its long-term development.

Seismic data of Stagg (1985) suggested that beneath a 100-m-thick cover of presumed Pliocene-Pleistocene glacial sediments lay a seaward-dipping prograding sequence at the mouth of the broad Prydz channel, and it was inferred that the oldest part of the prograding sequence would mark the time when grounded glaciers reached the shelf edge. Site 739 was expected to pass through this prograding sequence into strata of more shallow dip and dating from preglacial time. However, the less inclined strata also proved to be glacial. An onsite geophysical survey revealed that the base of the glacial sequence was at an estimated depth of 600 m. Therefore, although total depth was 486 mbsf, the base of the glacial sequence was not reached at this site.

A long record of glacial history is recorded at Site 739, but a detailed chronology is not possible because core recovery averaged only 35%. Indeed, in the interval from 38 to 106 mbsf, recovery was negligible, but downhole logging results provide insight as to the composition of the missing lithologies.

The sequence has been divided into five lithologic units. Unit I (0–24.1 mbsf) is Quaternary normally consolidated massive diamicton. Unit II (24.1–173.6 mbsf) is late Miocene to early Pliocene or younger massive diamictite (indurated diamicton) where recovered, although in the unrecovered upper part (about 38–106 mbsf) it is probably bouldery diamictite with sand, according to downhole logging results and drilling characteristics. Unit III (173.6–267.2 mbsf) consists of two stratified diamictite horizons with diatoms, separated by a thin diatomaceous sandy silty claystone, of late Eocene to early Oligocene age. Unit IV (267.2–315.7 mbsf) is a massive, slightly indurated but friable diamictite, also of late Eocene to early Oligocene age. Unit V (315.7–486.8 mbsf) is similar to Unit IV, but is mainly unfossiliferous and of uncertain age, although a middle Eocene age is possible from sparse calcareous nannofossils.

Site 739 is thus dominated by diamicton and diamictites of various types and attests to glacial sedimentation almost without interruption on the basis of recovered core. However, at least some nonglacial sediments are probably represented by the nonrecovered intervals.

The sedimentary sequence can be considered principally in terms of deposition close to and immediately seaward of the grounding line of an extended Lambert Glacier, probably close to the shelf edge. Probably little or no land was exposed during periods of till deposition over the site, and the bulk of the sediment was derived subglacially, modified by transport at the base of the sliding ice mass. Overall, there appears to have been little if any reworking by fluvial processes, but unrecovered intervals of sand could have been formed by such processes. Clast composition indicates that the bulk of the detritus was derived from the nearby granite-gneiss basement, with only minor contributions from sedimentary cover sequences. However, the high content of ferrugineous type III organic matter in the lower part of lithologic Unit II indicates a substantial amount of erosion of carbonaceous sediments of a type similar to those near the base of Site 741.

The sequence is remarkable for its apparent uniformity, especially the homogeneity of the hundreds of meters of massive diamictite. This can be explained only if the grounding line was in a relatively stable position, or if interbedded lodgement tills and glaciomarine sediments were removed by subsequent glacier advances or were not recovered. The loading history of the sediment indeed suggests a more complex history of glacial advances and retreats than that indicated by the recovered facies.

In general, tidewater glaciers are characterized by rapid fluctuations in grounding line and snout positions, and they are highly sensitive to climatic change. However, stable grounding-line positions may arise if there is a sharp break in the submarine slope, such as a shelf edge, beyond which grounding would require a vastly increased supply of ice. This situation may have prevailed at Site 739 for much of the time represented by the recovered section below 175 m (while each massive diamictite unit accumulated), a view supported by the nature of seaward-dipping seismic reflectors suggesting an old shelf break near this point. Landward of the grounding line, lodgement tills would have been deposited, but they are not represented at Site 739 below 175 mbsf. Above this depth, although mainly unrecovered, they may form the bulk of the sequence, built up on the shelf after the prograding wedge had extended beyond Site 739. More distal glaciomarine facies are only evident in lithologic Unit III, and the greater part of the nonglacial history is missing.

This stratigraphic succession that developed from waxing and waning ice records in detail, for the first time, a shelf marginal succession dominated for a prolonged period by a major glacier complex, which may be typical of the majority of the Antarctic continental margin.

Biostratigraphic age constraints on these sediments are generally poor. Factors contributing to the poor stratigraphic resolution include several broad intervals characterized by a lack of microfossils, poor core recovery, absence of zonal marker species, and the occurrence of reworked specimens. Of the fossil groups examined, diatoms are the most abundant and persistent. They provide most of the age estimates, suggesting that the upper two-thirds of the recovered sequence is of late Eocene–early Oligocene to Quaternary age, with a hiatus representing much of late Oligocene and early and middle Miocene time. Rare calcareous nannofossils support a middle Eocene to early Oligocene age for the lower lithologic unit. Planktonic foraminifers were not observed below 38 mbsf, and benthic foraminifers are very rare throughout. Radiolarians were observed only in the upper 5 mbsf, and no palynomorphs were discovered.

It was not possible to achieve a magnetic stratigraphy for this site because the random orientation of the gravelly and sandy units that dominate the succession is unsuitable for establishing a reversal stratigraphy. However, long-term oscillations in NRM intensity were found to follow the same trend as magnetic susceptibility, providing strong evidence that the magnetic intensity fluctuates according to the abundance of magnetic minerals in the rock, rather than from changes in the Earth's magnetic field.

Measurements of physical properties (index properties, undrained shear strength, and compressional-wave velocity) provide constraints on the main events recorded by the core, in particular the nature of the complex loading history to which the sediments were subjected at different times. Seven geotechnical units were recognized: unit G1 (0–24 mbsf) has characteristics typical of normally consolidated ice-proximal glacial diamictites and is partly equivalent to lithologic Units I and II. Unit G2 (24–170 mbsf) is characterized by overconsolidated diamictites typical of sediments loaded by ice or sediment and is approximately equivalent to lithologic Unit II. Units G3 through G5 (170–310 mbsf) show alternations of increasing and decreasing trends in physical properties of stratified and massive diamictites, representing grain-size distribution variations superimposed on varying degrees of overconsolidation, both bearing evidence of several fluctuations of the grounding line of a glacier back and forth over the site; these units equate approximately with lithologic Units III and IV. Units G6 and G7 (310–486 mbsf) lack any evidence of major ice-loading events. The diamictites apparently are not overconsolidated; thus, these units correspond approximately to lithologic Unit V.

On the basis of downhole logging, four units were defined according to major fluctuations in porosity, velocity, resistivity, and spontaneous potential. These changes reflect differences in the degree of compaction. These parameters have been used to infer the lithologic characteristics of the unrecovered intervals. In particular, lithologic Unit II was subdivided into logging units 1 (32–110 mbsf) and 2 (100–175 mbsf); the former is the unrecovered interval that is interpreted as a sequence of bouldery diamictites (also suspected from drilling characteristics). Logging unit 3 approximately matches lithologic Unit III, and logging unit 4 matches lithologic Units IV and V. The intervals of nonrecovery in these lower units are probably sand layers.

Seismic data obtained near the site are part of a continuous transect from inner Prydz Bay to the shelf edge, which will be helpful in making correlations between the sites, especially for Sites 739 and 742. Three seismic units have been distinguished at Site 739. Seismic Unit I (0–175 mbsf) shows flat-lying, high-amplitude reflections. This great variability in reflection character results from large fluctuations of *in-situ* velocity and density measured during the downhole logging. Two high-amplitude reflections at 120 and 175 mbsf coincide with the top and bottom

of a massive diamictite (the main part recovered in lithologic Unit II), and the lower boundary also corresponds with the paleontologically determined early Oligocene to late Miocene age hiatus. Seismic Unit II (175–310 mbsf) is characterized by a seaward-dipping sequence of high variability, reflecting marked changes in the continuity, uniformity, and degree of lithification of the sedimentary facies. This unit is equivalent to the mixed massive and stratified diamictites of lithologic Units III and IV. Seismic Unit III (310–467 mbsf) shows near-continuous, gently seaward-dipping, low-amplitude reflections that have a relatively uniform increase in velocity with depth, characteristic of burial compaction. Relatively low-velocity layers match the sands inferred from the downhole logging, but not recovered by drilling.

Site 739 has provided considerable new information concerning the timing and nature of the initiation of the Antarctic Ice Sheet, which has been the subject of considerable discussion in recent years. Prior to Leg 119, the earliest known unequivocal Cenozoic glacial sediments were discovered in an early Oligocene age sequence in the Ross Sea (Barrett et al., in press), at 78°S latitude. Glacial deposits of Eocene age were reported from the South Shetland Islands (62°S latitude) by Birkenmajer (1986), but proved difficult to link with other evidence for glaciation in West Antarctica. Ice-rafted quartz grains of Eocene age were reported on the slender evidence of grain textures and were considered by Kennett (1982) to be inconclusive with regard to glaciation. The earliest ice-rafted sediments reported by ODP Leg 113 (Weddell Sea) were of early Oligocene age (Leg 113 Shipboard Scientific Party, 1987). The Ross Sea record is the most complete and records an early Oligocene phase of limited glaciation down to the coast, although perhaps of local extent only, and a late Oligocene phase of ice several times more extensive than that of the present day. The former was tentatively attributed to local glaciation of the Transantarctic Mountains, the latter to full-scale development of an East Antarctic Ice Sheet.

The main conclusion concerning Site 739 is that a major glacier complex (see Drewry, 1983, for present configuration) reached Prydz Bay as early as late Eocene or early Oligocene time, and that the outer limit of the ice front was beyond that of the present day by at least 140 km. This suggests that the early Oligocene glaciation of the Ross Sea extended beyond the limits of the Transantarctic Mountains and indicates that full-scale ice-sheet development took place over East Antarctica by early Oligocene time and possibly earlier. The major series of late Oligocene ice advances in the Ross Sea may be matched, in part, by events in Prydz Bay, if we assume that ice advanced beyond Site 739, removing sediment and creating the late Oligocene to middle Miocene age hiatus. Because of the sparse occurrence of datable material and incomplete sedimentary record, we cannot determine the full glacial chronology for the site at present. It is, however, clear that the glacial depositional record extends through early Oligocene, late Miocene to early Pliocene, and Quaternary time. At no time represented by the recovered material was ice far removed from the site—probably grounded nearby most of the time—but intervals of nonrecovery and hiatuses may hide greater fluctuations, or even disappearances, of the ice sheet.

REFERENCES

Anderson, J. B., Clark, H. C., and Weaver, F. M., 1977. Sediments and sediment processes on high latitude continental shelves. *Proc. Annu. Offshore Technol. Conf.*, 9:Pap. 2738:91–96.

Anderson, J. B., Kurtz, D. D., Domack, E. W., and Balshaw, K. M., 1980. Glacial and glacial marine sediments on the Antarctic continental shelf. *J. Geol.*, 88:399–414.

Andresen, A., Berre, T., Kleven, A., and Lunne, T., 1979. Procedures used to obtain soil parameters for foundation engineering in the North Sea. *Nor. Geotech. Inst. Publ.*, 129:1–18.

Archie, G. E., 1942. The electrical resistivity log as an aid in determining some reservoir characteristics. *J. Pet. Technol.*, 5:1–18.

Backman, J., 1980. Miocene-Pliocene nannofossils and sedimentation rates in the Hatton-Rockall Basin, NE Atlantic Ocean. *Stockholm Contrib. Geol.*, 36:1–91.

Barrett, P. J., Hambrey, M. J., and Robinson, P. R., in press. Cenozoic glacial and tectonic history from CIROS-1, McMurdo Sound. *Antarct. Earth Sci. Pap. Int. Symp., 5th.*

Birkenmajer, K., 1986. Geochronology of Tertiary island-arc volcanics and glacigenic deposits, King George Island, South Shetland Islands (West Antarctica). *Bull. Pol. Acad. Sci., Earth Sci.*, 34:257–273.

Clukey, E. C., Nelson, H., and Newby, J. E., 1978. Geotechnical properties of northern Bering Sea sediments. *Open File Rep. U.S. Geol. Surv.*, 78–408.

Drewry, D. J. (Ed.), 1983. *Antarctica: Glaciological and Geophysical Folio: Sheet 2, The Surface of the Antarctic Ice Sheet*: Cambridge (Scot. Polar Inst.).

Fenner, J., 1978. Cenozoic diatom biostratigraphy of the equatorial and southern Atlantic Ocean. *In* Supko, P. R., Perch-Nielsen, K., et al., *Init. Repts. DSDP*, Suppl. to Vols. 38, 39, 40, and 41: Washington (U.S. Govt. Printing Office), 491–623.

Fryxell, G. A., 1988. Polymorphism in relation to environmental conditions as exemplified by clonal cultures of *Thalassiosira tumida* (Janisch) Hasle. *In* Mann, E., and Stoermer, E. (Eds.), *Proc. Int. Diatom Symp.*, 9:61–73.

_____, in press. Antarctic marine phytoplankton at the Weddell Sea ice edge: seasonal changes at the specific level. *Polar Biol.*

Gombos, A., Jr., and Ciesielski, P., 1983. Late Eocene to early Miocene diatoms from the southwest Atlantic. *In* Ludwig, W. J., Krasheninnikov, V. A., et al., *Init. Repts. DSDP*, 71: Washington (U.S. Govt. Printing Office), 583–634.

Hajos, M., 1976. Upper Eocene and lower Oligocene Diatomaceae, Archaeomonadaceae, and Silicoflagellatae in southwestern Pacific sediments. *In* Hollister, C. D., Craddock, C., et al., *Init. Repts. DSDP*, 35: Washington (U.S. Govt. Printing Office), 817–883.

Hayes, D. E., Frakes, L. A., et al., 1975. *Init. Repts. DSDP*, 28: Washington (U.S. Govt. Printing Office).

Kennett, J. P., 1982. *Marine Geology*: Englewood Cliffs, NJ (Prentice-Hall).

Kurtz, D. D., Anderson, J. B., Balshaw, K. M., and Cole, M. L., 1979. Glacial marine sedimentation: relationship to distribution of sediment geotechnical properties on high latitude continental margins. *Proc. Annu. Offshore Technol. Conf.*, 11:683–688.

Leg 113 Shipboard Scientific Party, 1987. Glacial history of Antarctica. *Nature*, 328:115–116.

Mizukoshi, I., Sunouchi, H., Saki, T., Sato, S., and Tanahashi, M., 1988. Preliminary report of geological and geophysical surveys off Amery Ice Shelf, East Antarctica. *Mem. Nat. Inst. Polar Res. Spec. Issue (Jpn.)*, 43:48–61.

Quilty, P. G., 1985. Distribution of foraminiferids in sediments of Prydz Bay, Antarctica. *Spec. Publ. S. Aust. Dept. Mines Energy*, 5:329–340.

Schrader, H. J., and Fenner, J., 1976. Norwegian Sea diatom biostratigraphy and taxonomy. *In* Talwani, M., Udintsev, G., et al., *Init. Repts. DSDP*, 38: Washington (U.S. Govt. Printing Office), 921–1098.

Schwab, W. C., and Lee, H. J., 1983. Geotechnical analysis of submarine landslides in glacial marine sediment, northeast Gulf of Alaska. *In* Molnia, B. F. (Ed.), *Glacial Marine Sedimentation*: New York (Plenum Press), 145–184.

Shipboard Scientific Party, 1987. Site 645. *In* Srivastava, S. P., Arthur, M. A., et al., *Proc. ODP, Init. Repts.*, 105: College Station, TX (Ocean Drilling Program), 61–418.

Skempton, A. W., 1954. Discussion of the structure of inorganic soil. *Proc. Am. Soc. Civil Eng.*, 80:19–22.

_____, 1970. The consolidation of clays by gravitational compaction. *J. Geol. Soc. London*, 125:373–411.

Solheim, A., in press. The depositional environment of surging subpolar tidewater glaciers: a case study of the morphology, sedimentation and sediment properties in a surge affected marine basin outside Nordaustlandet, northern Barents Sea. *Skr. Nor. Polarinst.*

Solheim, A., and Pfirman, S. L., 1985. Sea-floor morphology outside a grounded, surging glacier, Braasvellbreen, Svalbard. *Mar. Geol.*, 65: 91–95.

Stagg, H.M.J., 1985. The structure and origin of Prydz Bay and MacRobertson Shelf, East Antarctica. *Tectonophysics*, 114:315–340.

Stumm, W., and Morgan, J. J., 1981. *Aquatic Chemistry*: New York (Wiley).

Tappan, H., 1980. *The Paleobiology of Plant Protists*: San Francisco (W. H. Freeman).

Udinstev, G. B. (Ed.), 1975. *Geological-Geophysical Atlas of the Indian Ocean*: Moscow (Akad. Nauk. SSSR).

Vorren, T. O., Lebesbye, E., Andreassen, K., and Larsen, K.-B., 1989. Glacigenic sediments on a passive continental margin as exemplified by the Barents Sea. *Mar. Geol.*, 85:251–272.

Ms 119A-107

Summary Log for Hole 739C

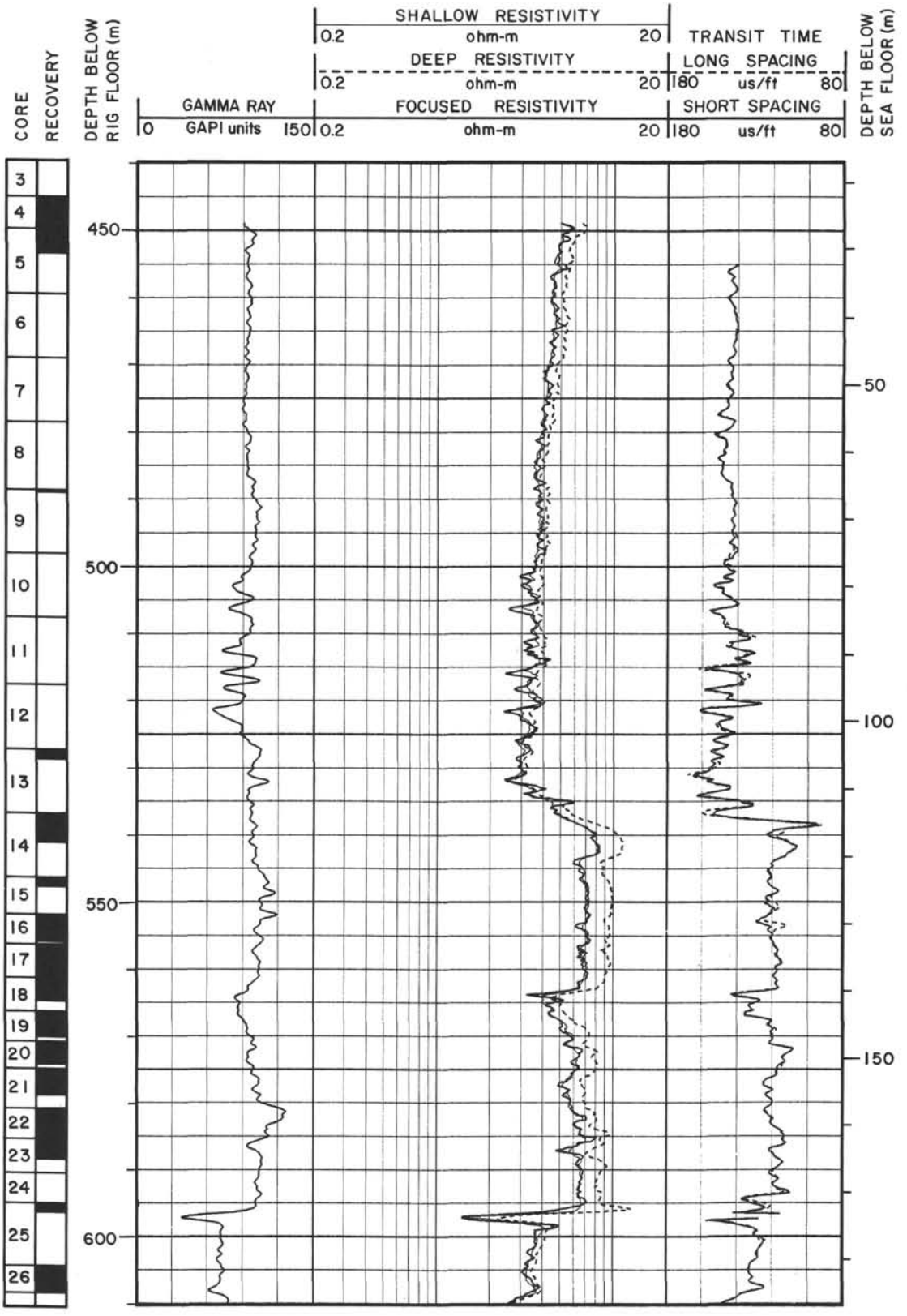

Summary Log for Hole 739C (continued)

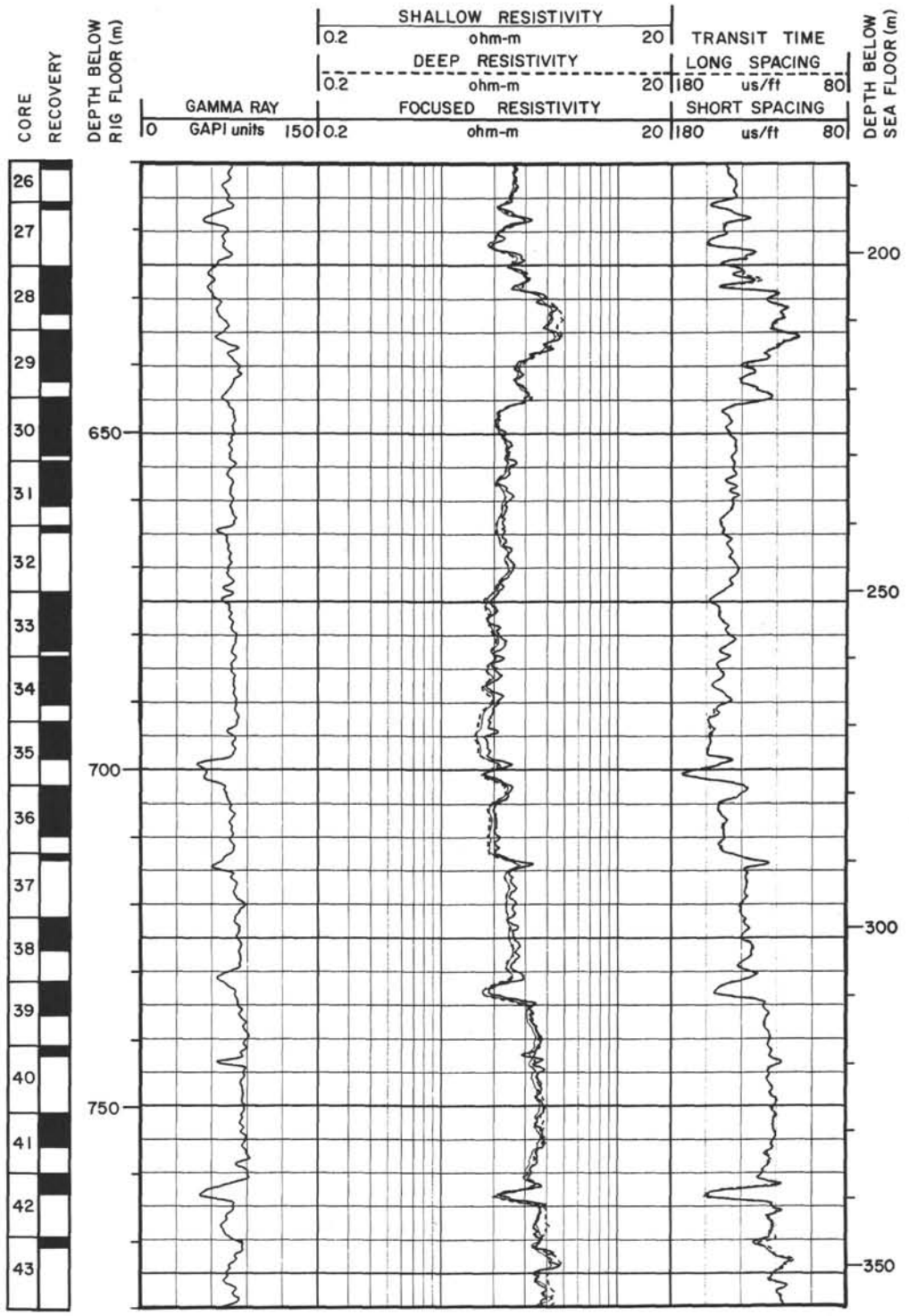

Summary Log for Hole 739C (continued)